Master in Molecular Biology and Biomedicine

"The ASO Nusinersen ameliorates motor function and prevents Cajal body disassembly and abnormal poly(A) RNA distribution in motor neurons from a Spinal Muscular Atrophy mouse model"

Author

Luz Almudena Medina Samamé

Directors

Prof. Miguel Lafarga

Dra. Olga Tapia

Santander, 2020

This Master's Thesis work was supported by grants from:

- Health Research Institute Valdecilla IDIVAL (NVAL17/22)
- Centro de Investigación Biomédica en Red sobre Enfermedades Neurodegenerativas (CIBERNED; CB06/05/0037)

ABSTRACT

Spinal muscular atrophy (SMA) is a devastating autosomal recessive neuromuscular disease characterized by degeneration of spinal cord alpha motor neurons (αMNs). It is caused by the homozygous deletion or mutation of the survival motor neuron 1 (SMN1) gene, resulting in reduced expression of SMN protein, which leads to αMN degeneration and muscle atrophy. A second gene, SMN2, contains a mutation that promotes exclusion of exon 7 and causes the SMN2 transcripts to generate a truncated, nonfunctional, form of SMN: the SMNΔ7 protein. A recent treatment with antisense oligonucleotides (ASOs) has been developed for SMA – Nusinersen (Spinraza, BIOGEN), which works by promoting the inclusion of exon 7 in SMN2 transcripts.

In this work, we used the αMNs of the SMNΔ7 mouse model of SMA to study the effects of Nusinersen in the behavior of Cajal bodies (CBs) and the cellular distribution of polyadenylated mRNAs. CBs are nuclear structures involved in RNA metabolism that can be disrupted in response to cellular stress in SMA αMNs. Moreover, an abnormal accumulation of polyadenylated mRNAs in nuclear granules (PARGs) have been previously shown in αMNs from the SMNΔ7 mouse model of SMA. Notably, in our study we demonstrate that the treatment with Nusinersen, administered via intracerebroventricular injection, rescues growth curve and improves motor behavior in these mice. Importantly, Nusinersen also recovers the number of canonical CBs and reduces the abnormal accumulation of polyadenylated RNAs in nuclear granules or PARGs. Furthermore, the treatment with this ASO normalizes the expression of the pre-mRNAs encoding chondrolectin and choline acetyltransferase, two key factors for αMNs homeostasis.

In light of these results, we propose that the mechanism of action of Nusinersen is partially mediated by the rescue of both CB biogenesis and the normal processing and distribution of polyadenylated mRNAs. It also becomes apparent that the rescue of SMN levels in the spinal cord has a beneficial effect on αMNs and skeletal myofibers, but the rescue of SMN expression in muscle is needed for the complete recovery of motor function.

PREFACE

In the interest of giving context to the work here presented, I would be remiss not to mention the events of March 2020. This academic year has been truncated by the virus SARS-CoV-2, which has caused a global pandemic and forced schools and universities to close their doors shortly after the beginning of the second semester of classes. At the time, many students in the master's program in which this thesis was developed were forced to interrupt the experimental portion of their work.

I was lucky enough, however, to have already been integrated by then in the group I was working with. I have done two separate internships with them in my time as an undergrad, spanning 5 months in total, in which I had been able to contribute to their works. When I started the first semester of classes in the master, I was able to join right back at the beginning of October, thus granting me almost half a year more of time to produce the results discussed in this work. Thus, while I have not been working in the laboratory after March 2020, I have been able to produce a master's thesis modeled after a published paper in which I am one of the authors.

After completing this work, I have nothing but respect toward the people who work in research, and I could not leave without thanking my supervisors, Dr. Olga Tapia Martínez and Dr. Miguel Lafarga Coscojuela, as well as Dr. María Teresa Berciano Blanco and Alba Puente Bedia, for everything they have taught me, and all the thoughtful guidance and companionship they have provided me with as I wrote this thesis.

Olga – thank you. You have shown me more patience than I ever had with myself, and I'm not sure I would have managed to write something I can be proud of without your constant support. I hope you know that your warm welcome into the world of scientific research has meant everything to me.

Last, but in no way least, I want to thank my family. Mom, dad, Julio – you have been there for me when I felt empty, believed in me when I couldn't, and I wish I could articulate better just how much I've needed that. Inés, my otherself – thank you for being my reality check all this time.

TABLE OF CONTENTS

ABBREVIATIONS

3'ss / 5'ss – 3' splicing site / 5' splicing site

AAV – Adeno-associated Viruses

ASO – Antisense Oligonucleotides

BBB – Blood Brain Barrier

CARM1 – Coactivator Associated Arginine Methyltransferase 1

CBs – Cajal Bodies

ChAT – Choline Acetyltransferase

Chodl – Chondrolectin

CNS – Central Nervous System

ESE/ESS – Exonal Splicing Enhancer / Exonal Splicing Silencer

Exint – Extended inhibitory context

FF motor unit – Fast, fatigable motor unit

FFR motor unit – Fast, fatigue-resistant motor unit

FISH – Fluorescence *in situ* hybridization

GAPDH – Glyceraldehyde 3-phosphate dehydrogenase

ICV – Intracerebroventricular

ISS-N1 / ISS-N2 – Intronic Splicing Silencer N1 / N2

ISTL1 – Internal-Stem formed by LDI 1

MND – Motor Neuron Disease

NMJ – Neuromuscular Junction

PARGs – Polyadenylated RNA Granules

PBS – Phosphate Saline Buffer

PFA – Paraformaldehyde

qRT-PCR – Quantitative reverse transcription polymerase chain reaction

RNPs – Ribonucleoproteins

- **scaRNP** – small Cajal Body-specific ribonucleoprotein
- **snoRNP** – small nucleolar ribonucleoprotein
- **snRNP** – small nuclear ribonucleoprotein

SDH – Succinate Dehydrogenase

SFR motor unit – Slow, fatigue-resistant motor unit

SIM – SUMO-interacting motif

SMA – Spinal Muscular Atrophy

SMN protein – Survival Motor Neuron protein

***SMN1/SMN2* genes** – Survival Motor Neuron 1/2 genes

TA muscle – *Tibialis anterior* muscle

TSL1/TSL2 – Terminal Stem Loop 1/2

URC – U-rich clusters

USPL1 – Ubiquitin-Specific Protease-Like 1

WT animal – Wild Type animal

αMNs – Alpha Motor Neurons

γMNs – Gamma Motor Neurons

INTRODUCTION

1. Spinal muscular atrophy

1.1. Introduction

Spinal muscular atrophy (SMA) is an autosomal recessive neuromuscular disease, currently considered as the leading genetic cause of infant mortality. It is characterized by reduced levels of the Survival Motor Neuron (SMN) protein that lead to alpha motor neuron (αMNs) degeneration and death and, consequently, muscle atrophy [1–4]. The αMNs are located in the anterior horn of the spinal cord, and they innervate muscle myofibers (**Figure 1**). Muscle atrophy leads to SMA's characteristic clinical symptom – generalized progressive muscular weakness (**Figure 1**). This weakness is more pronounced in proximal muscles and, in severe SMA patients, intercostal muscles are weaker than the diaphragm which in most cases leads to respiratory complications leading to death [5].

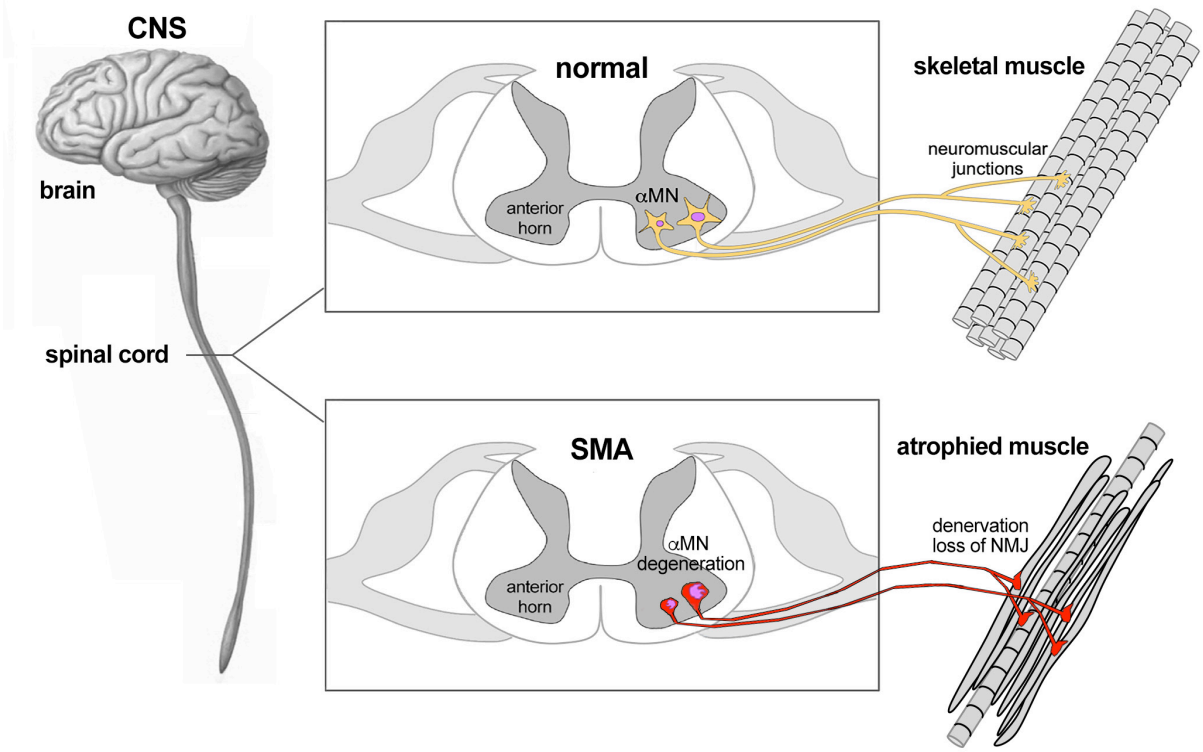

Figure 1. Distribution of the CNS (left), divided in bran and spinal cord. Cross-section of the spinal cord (middle) showing the localization of the αMNs in the anterior horn. On the top, the yellow αMNs innervate the muscle fibers properly, maintaining the neuromuscular junctions. On the bottom, illustrating the SMA situation, the red αMNs are degenerated, and loss of the neuromuscular junction leads to denervation and atrophied muscle.

Despite αMNs being especially affected in SMA, SMN protein is ubiquitously expressed in all somatic cells with multitude of housekeeping and tissue-specific functions. Therefore, while the selective

vulnerability of αMNs is a predominant feature in SMA, SMN deficit has been shown to also affect other organs such as skeletal muscle, liver, pancreas, spleen, blood vessels, and heart [6]. Despite SMA being a systemic disease and involving several organs, the predominant clinical feature is the range of mobility a patient has, and the age of onset. Based on these criteria, the clinical spectrum ranges from early infant death to mild weakness in adulthood [7].

SMN is a well conserved protein encoded by the Survival Motor Neuron 1 gene (*SMN1*) [2,3]. Most vertebrates maintain a similar sequence, with a C-terminal YG box as the most conserved motif, from yeast to humans [2]. This has permitted the use of various animal models in research, such as *Drosophila melanogaster, Caenorhabditis elegans*, zebrafish (*Danio rerio*), and mouse (*Mus musculus*) [2,4]. In all organisms, total loss of SMN causes lethality, although the point of death depends on the amount of maternal SMN that each embryo receives. Thus, oviparous animals have more SMN left over from the mother and, therefore survive for slightly longer [4]. Working with different models has the advantage of being able to identify both specific functions affected by specific mutations in animal SMA models like *Drosophila*, but also be able to see the systemic effect of those mutations in other animals like zebrafish or the mouse [4].

1.2 Epidemiology and clinical features

SMA was first described by Guido Werdnig (1844–1919) and Johann Hoffmann (1850–1919), but it wasn't until 1995 that the genetic cause of SMA, the *SMN1* gene deletion or mutation, was identified by Dr. Judith Melki and her team [8,9]. SMA has a prevalence of about 1 case per 6000-10000 live births, and a carrier frequency of 1:35 to 1:50, depending on ethnicity. In humans, *SMN1* gene has a paralogue, the *SMN2* gene, that due to natural specific point mutations is not able to fully compensate for the loss of *SMN1* [10,11]. The number of copies of *SMN2* that any patient has, will determine disease severity. Clinically, SMA has been divided in five categories, according to the age of onset and the clinical course (Table **1**) [5,7,12].

Spinal muscular atrophy classification

Type	Age of onset	Highest motor function reached	Age of death	SMN2 gene copy number
0	Prenatal	Breathing dysfunction	<1 month	1
I	0-6 months	Cannot sit	<2 years	2
II	<18 months	Cannot stand	>2 years	3
IIIa	18 months – 3 years	Can walk	Adulthood	3, 4
IIIb	>3 years	Can walk	Adulthood	3, 4
IV	>21 years	Can walk	Adulthood	4 or more

Table 1. Spinal muscular atrophy classification. Based on Martínez, 2012 [5].

SMA Type 0: is the most severe type of SMA, if very uncommon. It is a prenatal form of the disease, and it is fatal *in utero* or shortly after birth (<1 month). This type is very rare, and it has been defined by the following clinical features: paucity of movement in limbs, face and trunk, no suck, muscle atrophy, areflexia, congenital contractures, and requirement for mechanical ventilation support at birth [12].

SMA Type I: also called the Werdnig-Hoffmann disease, is the severe form of SMA, and the most common. It starts shortly after birth. Children are never able to sit on their own, have impaired head control, weak cry and cough. The tongue may atrophy and show fasciculation. Muscle atrophy in the limbs and trunk is followed by atrophy in the intercostal muscles, leading to a bell-shaped trunk with chest wall collapse and abdominal protrusion. This all leads to early death around 6 months of age, associated with bulbar dysfunction and pulmonary complications. Three subtypes have been proposed: type Ia with neonatal onset, type Ib with post neonatal period onset, and type Ic, with later onset, and slightly milder symptoms during the first 6 months of life [7,9] (**Figure 2**).

SMA Type II: the intermediate form of SMA. It starts before 18 months of age, and the children are able to sit, sometimes independently. These children have delayed motor milestones, although they all can maintain a sitting position unsupported. They have bulbar weakness, so they struggle to eat and gain weight, cough, and clear tracheal secretion. They also have fine tremors in the hands and can develop kyphoscoliosis and joint contractures [7,9] (**Figure 2**).

SMA Type III: also called Kugelberg-Welander disease or juvenile SMA. These patients are affected after 2 years of age, and all achieve independent walking. Some then lose this ability, others maintain it. They can develop scoliosis, muscle ache and joint overuse symptoms, but swallowing difficulties, cough and nocturnal hypoventilation are less common. Within this group, some subclassifications have been proposed. Type IIIa patients have an age of onset before 3 years old, whereas type IIIb patients have their onset after that age. It is more common for type IIIa SMA patients to maintain the ability to walk past the age of 40 [7,9] (**Figure 2**).

SMA Type IV: adult-onset form of the disease, usually in the second or third decade of life. It presents mild proximal muscle weakness, without respiratory or gastrointestinal problems, and a normal life expectancy [7,9]

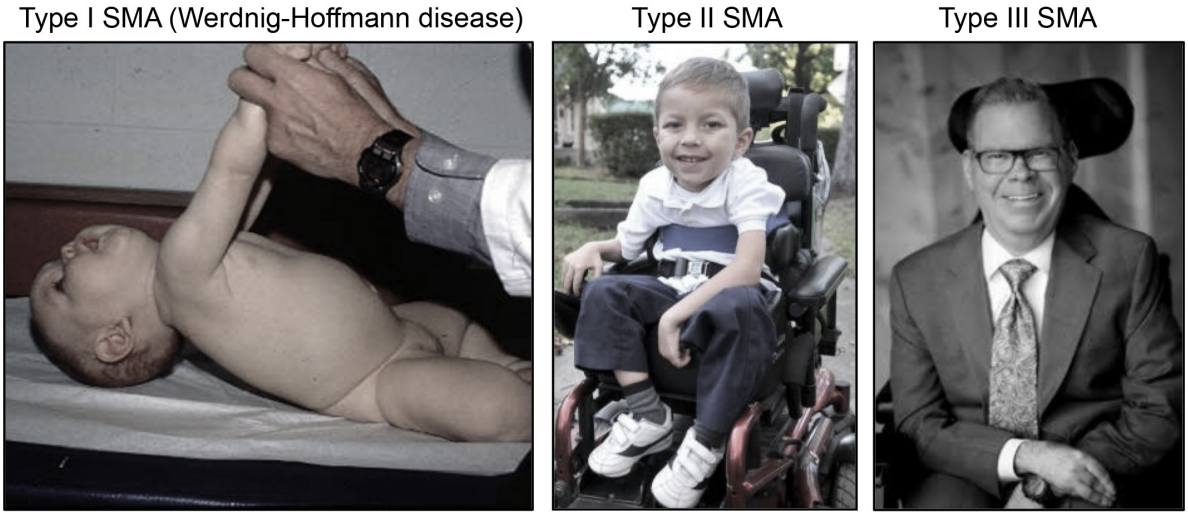

Figure 2. Photographs of SMA types I, II and III patients. In type I the child is seen unable to support themselves, and they exhibit a bell-shaped trunk with collapsed chest and protruding abdomen. In type II, the child is unable to walk, may have difficulty sitting. In type III, the symptoms are much milder, but the patient could still lose the ability to walk. Images were taken from fight-SMA.org

2. Molecular basis of SMA

2.1. The *SMN1* and *SMN2* genes

In 1995, Dr. Judith Melki and her team identified and determined the DNA sequence of the *SMN1* gene located in the long arm of chromosome 5 (5q11.2-p13.3) [13,14]. They demonstrated that, in 95% of the individuals with SMA, this gene was deleted or mutated [10]. Melki's team also identified that humans have a paralogue gene, *SMN2*, an inverted centromeric duplication of *SMN1* [15].

The *SMN1* and *SMN2* genes are nearly identical and encode a pre-mRNA composed of 9 exons, from which exon 8, the longest, is the 3' UTR. The rest, exon 1, 2A, 2B, 3, 4, 5, 6 and 7, code for the functional SMN protein [16]. However, *SMN2* and *SMN1* genes have an essential functional difference: a C-to-T (840C>T) silent point mutation, located in the +6 position of exon 7. This nucleotide change favors, in 90% of the cases, an alternative splicing of the *SMN2* pre-mRNA. As a result, the end product *SMN2* mRNA loses exon 7 during splicing events and is translated into a truncated non-functional isoform of SMN known as SMNΔ7 protein [4]. This truncated protein is unable to self-oligomerize, and is highly unstable in comparison to SMN, so it is degraded quickly by the proteasome [3] (**Figure 3**). In SMA, the low levels of SMN protein are due to the deletion or mutation in *SMN1* and, unfortunately, the presence of the *SMN2* gene cannot rescue the phenotype since only a small amount of functional SMN (10%) is produced by this gene. This is the main reason why the number of *SMN2* copies matters in terms of disease severity and clinical prognosis.

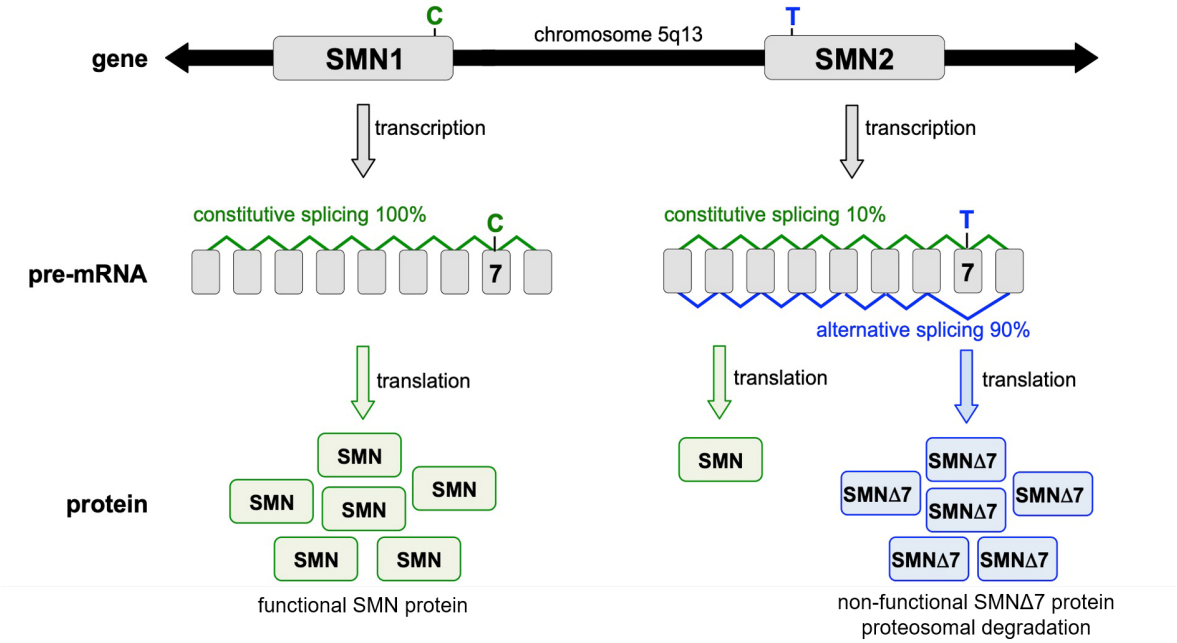

Figure 3. Comparative graphic of the full-length protein yield of genes *SMN1* vs *SMN2*. Due to a C-to-T mutation (reversed since SMN2 is an inverted copy), the pre-mRNA in SMA undergoes alternative splicing in 90% of the transcripts (blue). Thus, the main product after translation is the non-functional SMNΔ7, which becomes degraded quickly, while in the normal situation the constitutive splicing into functional SMN (green) is almost 100% of the yield. In SMA, the small amount of functional SMN, product of *SMN2,* is not enough to compensate for the loss of all SMN encoded by the *SMN1* gene. For this reason, patients with more than one copy of *SMN2* can have milder symptoms, leading to the different types of SMA patients described earlier.

2.2. Mechanisms of alternative splicing of the *SMN2* exon 7

Splicing is controlled by elements that can be located in the immediacies of their target genes. Cis-regulatory elements, often serve as binding sites for one or more factors, while Trans-regulatory elements can regulate distant genes. The specific sequence and location of cis-elements can have positive or negative effects depending on the specific factor bound and its splicing functional activity. Thus, exonic splicing enhancers (ESEs) are factors that stimulate splicing and are often required for efficient intron removal, whereas exonic splicing silencers (ESSs) inhibit splicing. In humans, the observed difference in exon 7 splicing between *SMN1* and *SMN2* is controlled by many cis-elements, with more than 40 splicing factors known so far. The preferential skipping found in *SMN2* seems to be the result of a combination of multiple negative interactions upon the 5´ and 3´ splicing sites [16].

In the case of *SMN2* exon 7 splicing, herein we will focus on those cis-regulatory elements that are located within exon 7, or in the immediately downstream intron. Thus, *SMN2* pre-mRNA contains, at the beginning of exon 7, an "Exint" (extended inhibitory) context. In particular, the C-to-T transition in the +6 position within *SMN2* exon 7 induces a terminal stem loop (TSL1) that has been proven to play an inhibitory role, preventing exon 7 inclusion by interfering with the binding of splicing factors at the 3´ splice site (3´ss) of exon 7 (**Figure 4**). At middle of exon 7, there are overlapping positive elements, while at the end, there is a cluster of negative cis-elements, including a second terminal stem loop (TSL2) near the 5´ splice site (5´ss) of exon 7 [16] (**Figure 4**).

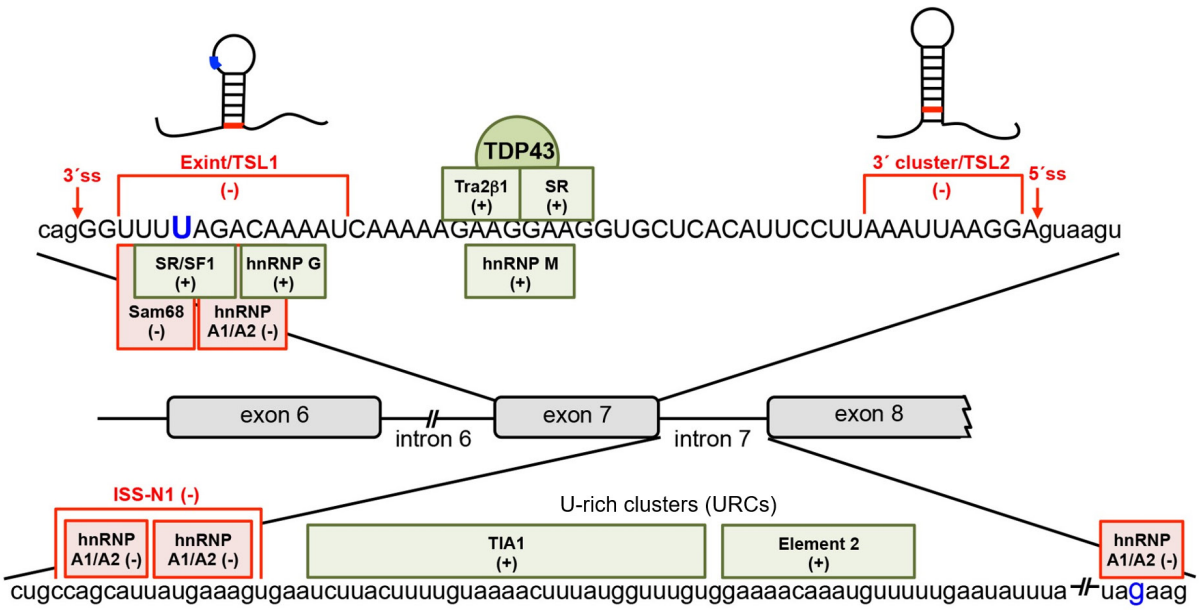

Figure 4. Scheme of exon 7 and intron 7's sequence in SMN2 pre-mRNA. Positive splicing elements in green and negative elements in red. Exonic and intronic sequences are written with uppercase and lowercase letters respectively. The blue U and g corresponds with the most common point mutation in SMA, that create additional binding sites for hnRNP A1/A2 (negative). Within the exon there are three regulatory elements: an extinct element (inhibitory), a cluster of positive overlapping elements, and the terminal stem-loop structure, TSL2, at the end (inhibitory). Within the intron, the ISS-N1 (silencer), contains two hnRNP A1/A2 binding sites, and URCs (positive). TIA1 interacts with the URCs and promotes exon 7 inclusion. Based on Singh and Singh, 2018 (Figs 2&3).

Located immediately downstream of exon 7 there is an intronic splicing silencer N1 (**ISS-N1**). ISS-N1, a 14 bp downstream of the 5´ss of exon 7 (positions 10th to 24th of intron 7), is a complex regulatory element encompassing overlapping negative motifs functionally implicated in the sequestration of the 5´ss. Other elements found within intron 7 are U-rich clusters (URCs), positive elements that bind **TIA1**, an RNA-binding protein that stimulates exon inclusion by recruiting U1 snRNP to the 5'ss (**Figure 4**).

In *SMN2* pre-mRNA, these URCs get sequestered into internal-stem structures formed through long-distance interactions. One of such structures known as ISTL1 has a 5' strand that overlaps with the 5'ss of exon 7 and the first position of ISS-N1, strengthening the TSL2, and a 3' strand that overlaps with another negative element (ISS-N2), located downstream in intron 7 [16-17].

2.3. The SMN protein and the SMN-complex

Human SMN is a protein with 294 amino acids and has several interacting motifs, including: a basic/lysine-rich domain, a Tudor domain, a proline-rich domain and a tyrosine/glycine-rich region or YG-box (**Figure 5A**) [3].

The basic/lysine-rich region is encoded by exon 2 and has been found to be the interaction site with RNAs, through a nucleic acid-binding domain. This N-terminal region is also the binding site with the Gemin-2 protein [3]. Through the highly conserved TUDOR domain, SMN binds to the RNA-binding proteins Sm, which are the major constituents of the spliceosome. The Tudor domain is also responsible for the interaction of SMN with coilin, the main structural protein of the nuclear Cajal bodies (CBs). Furthermore, the Tudor domain has a SUMO-interacting motif (SIM), whose non-covalent SUMOylation is key for Sm protein binding and for CB assembly [3]. These are ubiquitous structures in mammalian cells whose number correlate with cell body size and transcriptional activity. CBs are involved in the biogenesis of essential factors required for the processing of pre-mRNAs and pre-rRNAs [18]. At the C-terminal, the SMN protein has a proline-rich sequence that binds Profilin, a protein implicated in the regulation of actin dynamics, and the YG-box, a motif of 16 amino acids that facilitates SMN self-oligomerization, which is essential for protein stability and subcellular localization of SMN [2,19]. A recent study has demonstrated that monomeric SMN exposes a small degradation sequence – also called a degron – present within the YG box. This degron allows SMN binding to the SCF^{Slmb} ubiquitin E3 ligase prompting its degradation [20]. Deficit in SMN oligomerization directly correlates with the severity of SMA. Therefore, SMN is normally found as a homopolymer, complexed to the proteins Gemin2-8 and Unrip to form the so-called "SMN complex" [4] (**Figure 5B**).

Functional SMN protein, as part of the SMN complex, has essential housekeeping functions for cell survival. Among these, some functions have been proposed to have a bigger role in certain cell populations, such as MNs or myocytes, hence their specific affectation in SMA. Among its functions takes particular relevance the assembly of different categories of ribonucleoproteins (RNPs) (**Figure 5C**). The most well-studied, is its involvement in the assembly of spliceosomal snRNP, and since then it has been found that it participates in almost every step of mRNA metabolism [19] (**Figure 5D**). Overall, SMN main functions

include pre-mRNA splicing, histone mRNA 3´end processing, snoRNP biogenesis or mRNA transport that will be briefly described next. SMN has also been described to play a critical role in cytoskeleton homeostasis, including endocytosis and autophagy [2–4,8,21].

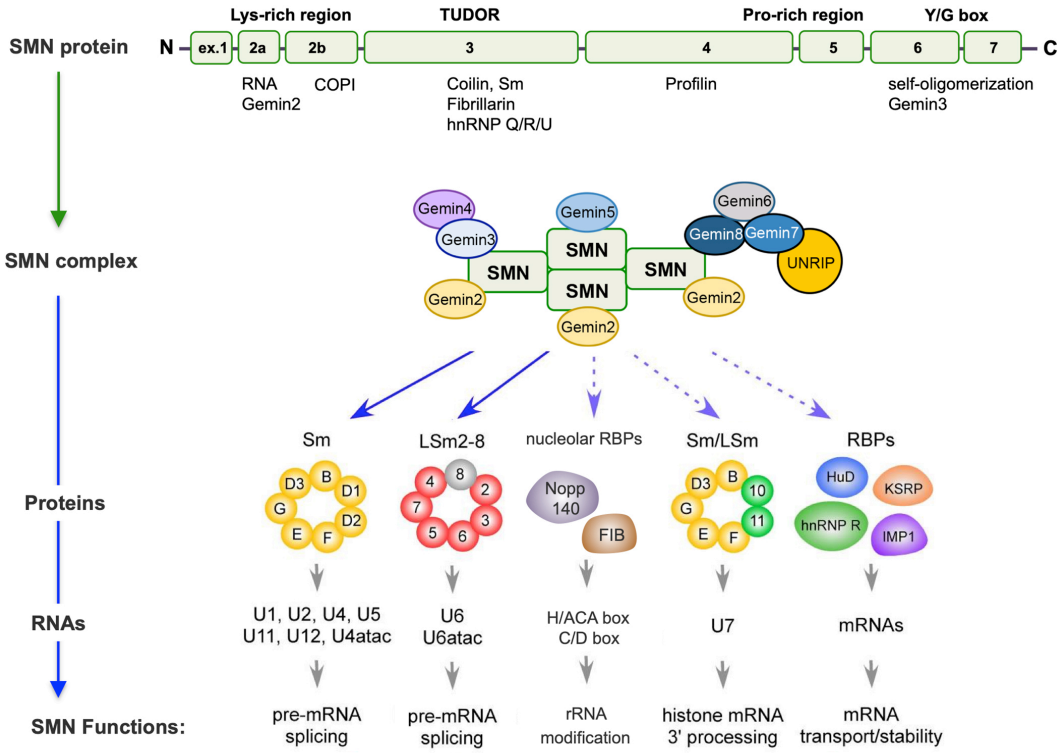

Figure 5. Overview of SMN protein's domains (A), which allow it to self-oligomerize and bind to other proteins, and its localization within the SMN complex (B), where it binds with the Gemin proteins and UNRIP. The SMN complex then goes on to bind a multitude of proteins and RNAs (C) as it facilitates their assembly into various elements of the protein synthesis machinery. This implicates SMN in many housekeeping functions, mostly related with mRNA homeostasis (D). Figure adapted from Li et al, 2014.

2.3.1. SMN Functions: Assembly of spliceosomal snRNPs and pre-mRNA splicing

Splicing, the process by which different proteins can be formed from a single mRNA transcript, is mediated by the function of spliceosomal snRNPs. These snRNPs are formed by a single U-rich small nuclear RNA (U1, U2, U4, U5, U11 or U12-snRNA), and a heptameric ring of Sm proteins, through a multi-step process mediated by the SMN complex (**Figure 5**) [19]. The U-snRNAs are a group of abundant, non-coding, non-polyadenylated transcripts that carry out their functions in the nucleoplasm [22]. They can be divided in two classes, Sm and Sm-like, depending on their sequence and the proteins with which they interact [22].

The SMN complex, binds to these U-snRNAs after they leave the nucleus, acting as a chaperone facilitating the binding of the U-snRNA to the specific Sm protein core [2,3]. The Sm core is not assembled previously, instead, the Sm proteins form heterodimeric or heterotrimeric subcomplexes. These then only bind to their RNA target in presence of SMN complex, which is thought to add specificity and act as a catalytic element for the reaction (**Figure 6**, **step 1**) [22]. The SMN complex stays with the snRNA while it

undergoes hypermethylation of its m7G cap, forming the TMG cap, and the trimming of its 3' end, processes required before entering the nucleus.

It is noteworthy that the SMN complex binds to the snRNA through the protein Gemin5, which recognizes the Sm site in the sequence. Gemin2, another member of the SMN complex, binds to five of the seven Sm proteins, helping them acquire the correct shape and orientation needed to assemble the snRNP [22] (**Figure 6, step 2**). Once assembled, the TMG cap of the U-snRNA and the SMN complex itself act as a nuclear import signal, and the whole snRNP gets reimported to the nucleus via interaction with importin-α [3] (**Figure 6, step 3**). Once in the nucleus, the SMN complex binds to the protein coilin, structural component of the CBs, to direct the localization of the snRNP to the interior of the CB. Here the U-snRNA will acquire snRNP-specific proteins and will be modified at nucleotide level. These modifications, guided by scaRNPs (small CB-specific RNPs), are essential maturation steps before the snRNP can become part of the spliceosome (**Figure 6**, **step 4**) [2,23].

Functional spliceosomes are large and complex molecular machine formed by five mature snRNPs and more than 80 RNA-binding proteins (**Figure 6, step 5**). During splicing, introns will be cleaved from a transcribed pre-mRNAs, and through combination of the exons a particular mRNA isoforms will be obtained [2–4,21]. Alternative splicing (the re-combination of different exons) is the major source of genetic diversity in eukaryotes.

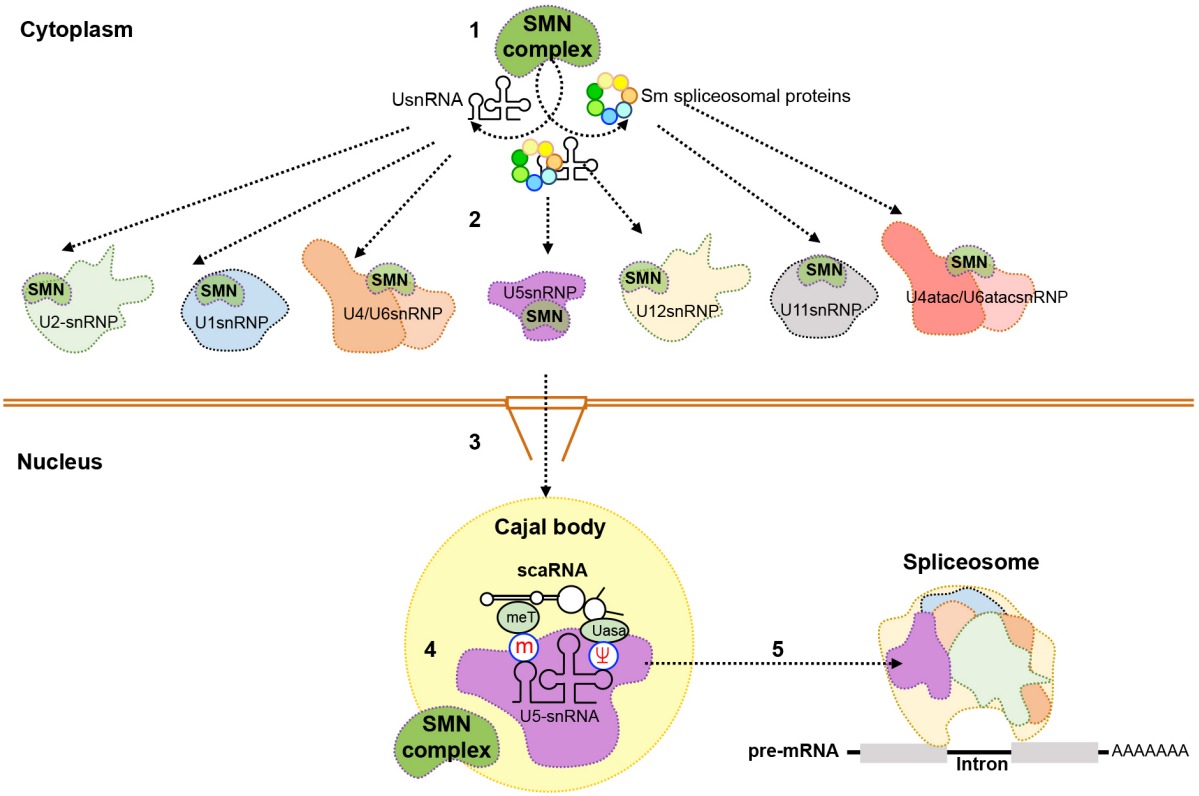

Figure 6. SMN's role in snRNP assembly. (1) The SMN complex binds to the U snRNA and the Sm ring once they are in the cytoplasm, (2) acting as a chaperone and facilitating their assembly into snRNPs that then (3) get reimported into the nucleus. (4) Once there they undergo more modifications in the CB, thanks to the scaRNAs, and the SMN complex dissociates from them. (5) Finally, the mature snRNPs become part of the spliceosome and are able to bind to pre-mRNAs.

2.3.2. SMN Functions: Biogenesis of snoRNPs and rRNA modification

Small nucleolar RNPs (snoRNPs) are a class of RNPs that are associated with the post-transcriptional processing of non-coding RNAs such as ribosomal RNAs through methylation and pseudourydilation [2,3]. They are formed by a small guide nucleolar RNA (snoRNA) and specific protein factors. Among these protein factors, some have been found to interact with SMN, such as GAR1 and Fibrillarin [2]. The snoRNAs can be separated into two categories. Depending on the motifs found in their sequences they can have a H/ACA box or a C/D box, which guide pseudouridylation and 2-O-methylation, respectively. Both of these types rely on their secondary structure to bring close together the different parts of their motifs (H box and ACA box, C box and D box). This structure is also required for them to interact with the protein components of snoRNPs, as well as their target rRNA [2].

Another subset of snoRNPs are the so-called scaRNPs. As mentioned before, they are located in CBs, where they guide the same post-translational modifications to target nucleotides within U-snRNAs. The CB localization signal present in scaRNAs is a CAB box sequence, which is specifically recognized by the WRAP53 protein. Moreover, both snoRNPs and scaRNPs are transcribed by the RNA polymerase II[23]. SMN has been shown to interact with WRAP53 and RNA pol II, further confirming that, in SMA, snoRNP localization can be impaired [2].

It has been proposed that CBs play a role in snoRNA and scaRNA maturation, since they are concentrated in CBs along with their associated proteins. It has also been observed that uncapped snoRNAs and scaRNAs may mature in CBs, though their transport into CBs remains unknown. In the case of scaRNAs, WRAP53 has being demonstrated to be involved in their transport to the CB [23]. It is particularly relevant, the fact that in SMA patients there is a strong depletion of scaRNPs which can in turn affect snoRNP biogenesis and therefore nucleolar dysfunction [2].

2.3.3. SMN Functions: Assembly of U7 snRNP and histone mRNA 3' processing

The 3' end of histone mRNAs requires a specific processing that is mediated by the U7-snRNP. U7-snRNP has a similar structure to spliceosomal snRNPs, however, instead of SmD1 and SmD2 proteins, its heptameric ring contains Sm-like proteins. The SMN complex that facilitates this snRNP assembly has been proposed to be slightly different. Therefore, in SMA, SMN deficiency would lead to accumulation of U7-snRNA unable to form the functional U7-snRNP, and to the incorrect processing of the 3'end of histone mRNAs, affecting in turn the structure of chromatin [2,3].

2.3.4. SMN Functions: mRNA transport and translation

SMN has been shown to interact with β-actin mRNAs in neuronal processes and growth cones [24]. As mentioned before, SMN forms the SMN complex with the Gemin proteins and Unrip. However, it has been found that, in motor axons, it does not fully co-localize with Gemin2, indicating that SMN protein

might be involved in functions unrelated to snRNP assembly [25]. In fact, SMN protein has been found to change its primary localization from mainly nuclear during development to cytoplasmic, and then axonal, suggesting a potential role for SMN in axons during axonal growth [26]. Using type I SMA mouse models, hnRNP-R has been studied in relation to axon growth. hnRNP-R is an RNA-binding protein that has been previously found to interact with the β-actin mRNA and with the SMN protein [24,27]. β-actin plays a main role in axonal growth, as it is part of the cytoskeleton, and its accumulation in the growth cone depends on its own mRNA correct transport. Interestingly, both β-actin and hnRNP-R expression have been found to be lower in SMN deficient neurons, correlating with a three times diminished growth cone area in cells isolated from the lumbar spinal cord [24]. On this basis, SMN is considered to be part of the regulation and localization of β-actin, as well as axonal growth in motor neurons [24].

SMN can also interact with other RNA-binding proteins that traffic proteins in MNs as HuD and IMP1. These two proteins have been found to transport more than 200 mRNAs that have been identified as potential targets for SMN trafficking [2]. In fact, in cultured cells from a severe SMA mouse model, overexpression of HuD and IMP1 rescues GAP43 mRNA and protein levels, and axon growth defects [28].

There is an increasing number of evidences that point toward SMN protein having a role in mRNA translation as well [3]. One proposed mechanism is that SMN has been shown to associate to polyribosomes. Using *in vitro* Luciferase reporter assays, it has being found that there was a dose-dependent reduction in translation efficiency directly related to SMN protein level [29]. Moreover, SMN may influence the Dicer-miRNA pathway, which is involved in nerve regeneration and axon outgrowth, as miRNAs, such as miR-9, are affected in SMA[30]. SMN may also control the mTOR pathway through its interaction with miRNAs, in particular miR-183 [2,31]. This has been studied both in the Taiwanese mouse model and in SMA patient-derived fibroblasts, where the pathway was knocked down [31]. Additionally, when a negative regulator of the mTOR pathway is knocked down, there is an increase in axonal growth and cell survival, and β-actin levels in the axon are restored [32]. Finally, an *in vivo* study that looked at the transcriptome versus the translatome with next-generation sequencing, has found that there are defects in the biogenesis of ribosomes, which could account for the defects in translation as well [3].

As a final note, the defects in translation are only amplified by the lack of RNA-binding proteins, and even properly translated proteins with other functions. For example, SMN regulates the translation of coactivator associated arginine methyltransferase 1 (CARM1), a protein implicated in transcription, splicing and autophagy [2]. CARM1 is consistently upregulated in SMA mouse models and SMA type I patients, since the lack of SMN increases CARM1 levels, and this in turn causes aberrant transcription of other proteins, such as the Ubiquitin-Specific Protease-Like 1 (USPL1) gene, a gene that shows an increased inclusion of exon 2 in its transcripts in SMA [2].

3. Neuromuscular pathophysiology of SMA

As mentioned before, SMA is a genetic disorder classified as a neuromuscular disorder and a motor neuron disease (MND). It is characterized by degeneration of **αMN** in the spinal cord that affects the control of voluntary muscle movement. However, the structural and functional cellular deficits that lead to the impairment of the neuromuscular system remain poorly defined.

3.1. The alpha motor neurons

Anatomically, the spinal cord is a cylindrical structure made of nervous tissue, located in the vertebral cavity. There are 31 pairs of spinal nerves come out of it to innervate skeletal muscle, smooth muscle, and glands. The spinal cord is enlarged at the cervical region, from which sensitivity and motor actions are signaled to the upper limbs, and at the lumbo-sacra region, responsible for sending the same information to the lower limbs. It maintains a continuous cross section along its length, formed by grey matter and white matter, arranged in a characteristic shape of a butterfly (grey matter) encased in the white matter around it. The anterior horns (ventral) are rounder and wider and contain the MNs [33,34] (**Figure 7**).

In humans, there are two types of motor neurons: **αMNs**, which have wider axonal diameter and innervate extrafusal fibers, and **γMNs**, which are thinner and innervate intrafusal fibers. The extrafusal fibers are the standard skeletal muscle fibers also known as **myofibers** that generate tension by contracting, which leads to movement. The connection of an αMN with the myofibers that it innervates is what is called a **motor unit** [35]. The intrafusal fibers are very small-diameter fibers that act as proprioceptors, detecting changes in muscle length (muscle tone). They are sheathed by connective tissue, apart from the rest of the fibers. They do not contract in the same way as extrafusal fibers, instead, the central part of them merely stretches when the two ends contract [33,35].

Both αMNs and γMNs have subtypes. For the γMNs, there are two types, differentiated by the effect they have on primary and secondary sensory endings, that is, whether they stimulate endings capable of sensing dynamic stimuli or static stimuli. In the case of αMNs, the differences stem from the resistance of the motor unit to fatigue, and the presence or absence of a "sag" in the tension generated under a continuous stimulus [36]. This leads to three types of motor units: (i) type FF (fast contracting fatigable motor units), which has big-diameter type IIb myofibers, the sag, and the highest number of myofibers per motor unit; ii) type FFR (fast contracting fatigue-resistant motor units), which has medium-diameter type IIa myofibers and the sag; and iii) type SFR (slow contracting fatigue-resistant motor units), which has small-diameter type I myofibers, no sag, and the lowest number of myofibers per motor unit.

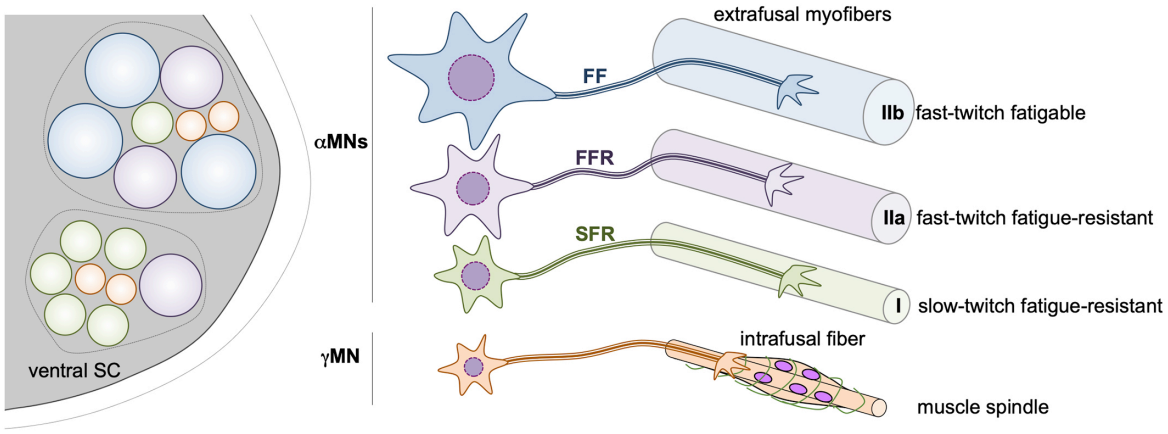

Figure 7. Types of MNs and the different fibers they innervate. αMNs innervate extrafusal myofibers, being differentiated in three subtypes depending on the resistance to fatigue and the presence of a sag in the depolarization response, which translates to a faster movement: Fast/fatigable fibers (blue), fast/fatigue-resistant fibers (purple), and slow/fatigue-resistant (green). αMNs innervate intrafusal fibers, acting as a propioceptor of the changes in length (muscle tone).

3.2. The skeletal muscle fibers

A skeletal muscle cell, as mentioned above commonly referred to as a **myofiber**, is a syncytium formed by the fusion of myoblasts to form a single one with multiple nuclei. A muscle is formed by these myofibers, held together by conjunctive tissue, the endomysium, which contains the nerve fibers and blood vessels [35].

Just like there are three types of motor units, there are also three types of myofibers: **Type I myofibers** or slow oxidative fibers. They are small in diameter, appear red, and have a high content of mitochondria, myoglobin and cytochrome complexes. They contract slowly and are fatigue resistant, though they generate less tension than the other types. **Type IIa myofibers** or fast glycolytic oxidative fibers, are the intermediate fibers seen in fresh tissue. They have many mitochondria and hemoglobin and high amounts of glycogen so they can go through anaerobic glycolysis. They contract quickly and are fatigue resistant. **Type IIb myofibers** or fast glycolytic fibers, are big, pale pink fibers. They have less myoglobin and mitochondria than the other types, but they store glycogen and show a high enzymatic glycolytic activity. They generate great muscular tension, but get fatigued quickly due to lactic acid production.[35]

The myofiber is composed of bundles of cylindrical myofibrils arranged in parallel to the longitudinal axis of the fiber. Myofibrils, in turn, are composed of myosin myofilaments (thick filaments) and actin myofilaments (thin filaments) which are spatially ordered in the A-band (anisotropic) and I-band (isotropic) forming a cross-striation pattern. Each I-band is bisected by a transverse line, the Z-disc, enriched in α-actinin. The segment of the myofibril between two successive Z-discs is called a sarcomere, which has typically 2-3 μm in length in a relaxed muscle and represents the functional unit of the myofiber (**Figure 8A**). The parallel and ordered disposition of the myosin and actin myofilaments in a myofiber produces transversal A- and I-bands which give the name of striated to the muscle, due to the dark and light band

pattern when observed by electron microscopy. A-bands are covered by both types of myofibrils and appear as dark highly electron-dense bands. I-bands are only covered by actin thin myofilaments (I band) and appear as lighter, less electron-dense bands. The A-band has a central sub-band only covered by myosin filaments during muscle relaxation called the H-band, which creates a thin linear density called the M-line at the middle of each A-band (**Figure 8**). During muscle contraction, both the I band and the H band become shorter, but the A band stays the same [35].

A recent study from our laboratory has demonstrated the precise localization of SMN in the human sarcomere [6]. Sarcomeric huSMN is localized to the titin-positive M-band and actin-positive I-band, and accumulates in SMN-positive granules that are flanking the Z-discs. Co-IP assays further revealed that SMN interacts with the molecular components of actomyosin filaments and with other sarcomeric proteins.

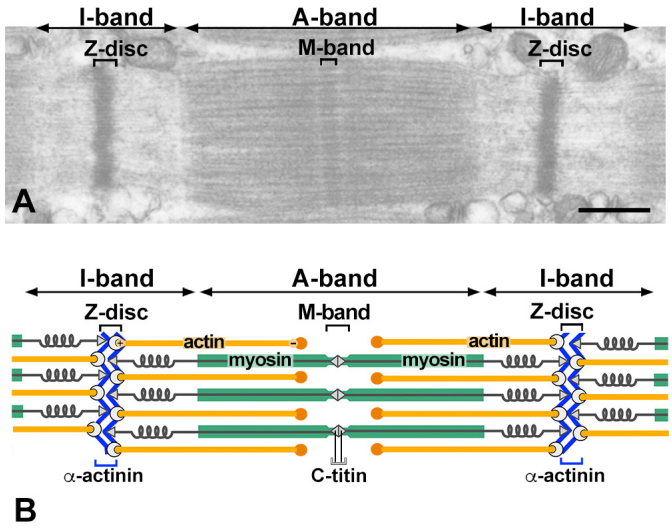

Figure 8. A. Electron microscopy image of a sarcomere, labeled with the position of the I and A bands, as well as the Z-disc and M-band in each respectively. The paralell distribution of the myofilaments is also visible. **B.** Graphic representation of the same structure, where the basic shape of the proteins can be seen. In green and yellow respectively, myosin and actin are represented. They are displayed parallel to one another and bound to the Z-disc, composed of α-actinin (blue). At the M-band the C-terminal region of titin is found (grey).

3.3. SMN-dependent mechanisms implicated in SMA pathogenesis

In αMNs under normal conditions, SMN localizes to the cytoplasm and the nucleus. In the cytoplasm it forms the SMN complex with other proteins, where it participates in the biogenesis of snRNPs and mRNA transport, among other functions. As we have previously mentioned, in the nucleus, the SMN complex accumulates in CBs, where is involved in the biogenesis of both snRNPs and snoRNPs. It also accumulates in coilin-negative gems (for Gemini of CBs), whose function is uncertain. SMN is also found in the MN axon and is an integral sarcomeric component within the myofibers (**Figure 9, left**) [37].

In type I SMA, approximately 65% of αMNs are lost, and the remaining ones show severe disruption of the protein synthesis machinery, showing chromatolytic somas and eccentric nuclei [37]. At nuclear level, the somas with eccentric nuclei often lack large CBs and, contrary to healthy αMNs, do not concentrate SMN, snRNPs nor snoRNPs [37] (**Figure 9, right**). The absence of nuclear SMN implicates potential defects in the maturation of spliceosomal snRNPs in CBs, which is one of the proposed SMA pathogenesis main mechanisms**: the SMN-dependent mRNA processing dysfunction** [9,38]. Nowadays, the dysfunction of

RNA metabolism has enabled to classify SMA as a **RNAopathy**, although it could also be considered a **spliceopathy** [39].

Beyond these nuclear defects, SMA αMNs receive fewer glutamatergic synaptic inputs from proprioceptive sensory neurons and interneurons [9]. The axon, as explained previously, presents outgrowth defects since the transport of one of its main components, β-actin mRNA, is impaired, as is the transport of many others mRNAs – thus impeding proper localization and translation of specific mRNAs [38]. Not only that, but the neuromuscular junction (NMJ) - the chemical synapse between an MNs and a muscle fiber - shows several defects. These include accumulation of presynaptic neurofilaments, reduced synaptic vesicle content, impaired synaptic transmission, alterations in intracellular calcium homeostasis, defective clustering of Cav2.2 channels in MN terminals, defective postsynaptic acetylcholine receptor clustering at the sarcolemma, and defective motor endplate development [9,40]. All of these defects in the NMJ lead to denervation of the myofiber causing muscular atrophy [9, 40] **(Figure 9)**.

At myofiber level, our own data suggest that SMN deficit causes primary effects independent of the neurogenic myopathy. Thus, in human type I SMA muscle low levels of SMN protein have a profound impact in the normal sarcomeric architecture, resulting in the disruption of myofibrils and overcontracted minisarcomeres in innervated hypertrophied myofibers [6].

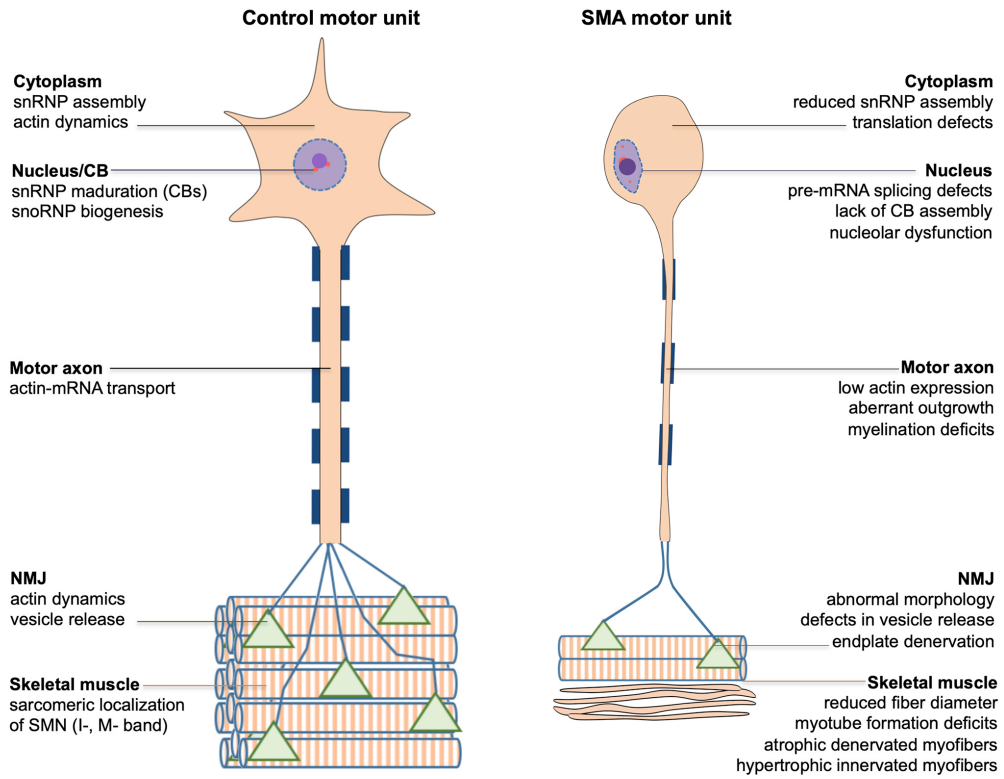

Figure 9. Functions of SMN within the motor unit. In a control motor unit, SMN has functions all across both cells involved, and within the NMJ. In a SMA motor unit, the lack of SMN protein leads to reduced ability to perform functional splicing and mRNA maturation, leading to abnormal expression of multiple proteins that affect translation, motor axon outgrowth (due to low actin expression), myelination deficits, abnormal NMJ morphology with defects in vesicle release, and denervation of the muscle fiber. As for the myofiber, the low levels of SMN lead to a reduced fiber diameter, and myotube formation deficits. Adapted from Boyer et al, 2010.

4. Current therapies for SMA

Because SMA is a monogenic disease, largely caused by the lack of SMN protein, the search for a cure has classically being focused on increasing protein levels to match the physiological ones. These can be done by improving full-length *SMN2* mRNA expression [21,41]. To do this, there have been various approaches, from activating enhancers, to increasing exon 7 inclusion, through stabilizing SMN protein or *SMN2* mRNA, and the gene therapy [21]. Each of these approaches have certain disadvantages, such as (i) the small window of action in the neonatal period, since treatment should be administer before the clinical symptoms of SMA appear; (ii) the difficulty of administering the treatment intrathecally (CNS), because of the restrictive properties of blood-brain barrier (BBB) and, (iii) the lack of SMN level recovery in the peripheral tissues, since the drug only reaches the CNS [42]. For all these reasons, classic approaches need to be accounted together with newer approaches.

4.1 Small molecules-based treatments

A series of small molecules, targeting the increase of *SMN2* gene expression, are being developed for SMA therapy. They are administered orally, which is an advantage over the other therapies, though it is possible that they might not be able to cross the BBB [21]. The first type identified were Quinazoline derivatives, which inhibit the RNA decapping scavenger enzyme DcpS, in turn activating *SMN2* expression [9]. However, they were found to only have moderate effects on SMA, so other alternatives have been sought. Currently, although their action mechanism is poorly understood, these small molecules seem to be highly specific to SMN [9]. These novel SMN-independent therapies are focused on complementing classic therapies during the later phases of the disease and can be divided into two categories [21]:

CNS-targeting molecules, as the cholesterol-like molecule called Olesoxime, the only one drug currently being tested in clinical trials. It acts on the outer mitochondrial membrane in response to oxidative stress. It is administered orally, and has been shown to have a neuroprotector effect; however, it has only managed to achieve stabilizing effects considering secondary objectives of treatment [21,41]. Other targets being considered for potential combinatorial therapies are the protein Chondrolectin (Chodl), a potential modifier of axonal integrity, and Stasimon (or Tmem41b in mammals), which has a role in synaptic transmission [41].

Non-CNS-targeting molecules are being tested since there is increasing evidences that SMA pathological mechanisms are not limited to αMNs. Therefore, therapies aimed exclusively toward the CNS might be insufficient, especially in type I SMA, where the SMN deficit is more pronounced [21]. So far, only targets in skeletal muscle are being studied, as this is the second most affected tissue in SMA. CK-2127107 is a drug already in phase 2 trials with SMA patients, which is a skeletal troponin activator. It has already been classified by the FDA as an orphan drug for SMA, despite the fact that it was developed for a rat model of heart failure, and tried in phase 1 as such [41]. Other targets that are being considered are the myostatin-follistatin pathway, and the actin dynamics regulation pathways [41]. Myostatin negatively regulates muscle growth, with follistatin inhibiting it, however, despite having several clinical trials in other diseases,

it is unclear whether it is affected in the same way in SMA yet. In the case of actin dynamic regulation pathways, both the ROCK-RhoA signaling and Plastin3 protein have been found to be involved in SMA pathogenesis, so those are also being considered as targets [41].

4.2. Gene therapy

SMA is an ideal candidate for gene therapy for a variety of reasons, among them: (i) type I SMA is lethal if left untreated, (ii) it has a specific genetic and cellular target (*SMN1* in the anterior horn of the spinal cord), (iii) SMN overexpression is well tolerated, (iv) there are animal and cellular models known well enough to be used in clinical trials, (v) the length of *SMN*'s cDNA can be used in vectors, and (vi) gene therapy can be used to alter SMN splicing and increase SMN levels [21]. The gene therapy focuses not on modifying the *SMN2* gene expression, but rather, in recovering the gene *SMN1*. To this effect, a copy of the *SMN1* human gene is introduced exogenously via a viral vector.

One example of viral vectors are the adeno-associated viruses (AAV), which have been "engineered from a nonpathogenic, naturally nonreplicating parvovirus" [43]. These vectors have been demonstrated to be safe in humans in the late 90s and have been used since for various diseases. They can show specific tropism to certain tissues, however, since they do not integrate with the host DNA, they are not ideal vectors for cells with high cellular turnover. In the case of SMA, however, and in other diseases with neurons, the effect of the vector has been shown to last for up to ten years [43].

AVXS-101, previously scAAV9.CB.SMN, carries DNA-encoding human SMN [43,44]. It has been through clinical trials in various models including large animals, and when tried in human patients, it has showed great improvements in motor milestones as well as survival. Moreover, the treatment seems safe, with rather occasional adverse events that are treatable [43,45]. The FDA has already classified it as an orphan drug for all types of SMA [43].

The main advantage of gene therapy is the administration method, as this only requires a single intravenous dose [21,44]. On the other hand, gene therapy runs the risk of the vector not being easy enough to produce at a large enough scale to treat patients efficiently [43]. Finally, as viral vectors are not yet commonplace as treatments, hospital staff might require specific training, and there might be safety concerns yet to be found [44].

4.3. ASOs-based therapies

Since all SMA patients keep at least one copy of *SMN2,* and the number of copies is inversely proportional to the severity of the disease, many types of therapies approaches have focused on increasing the expression of the functional isoform of the *SMN2* gene. One such approach is the use of antisense oligonucleotides (ASOs) to promote exon 7 inclusion [1,16,21].

ASOs are short, single-stranded, synthetic oligonucleotide chains, that can selectively bind to, and modify the expression of, its target pre-mRNA [21,43]. Nusinersen (Spinraza™, BIOGEN), approved by the FDA in December 2016, is an oligonucleotide which has chemical modifications – such as a

phosphorothioate backbone, and methoxyethyl modifications – to enhance its stability [16,43]. It binds to the *SMN2* pre-mRNA to match the ISS-N1 silencer in intron 7. In doing so, it displaces negative splicing factors such as hnRNP A1/A2, allowing the interaction with U1 snRNP, which promotes exon 7 inclusion, restoring the synthesis of full-length SMN protein (**Figure 10**) [42] [16].

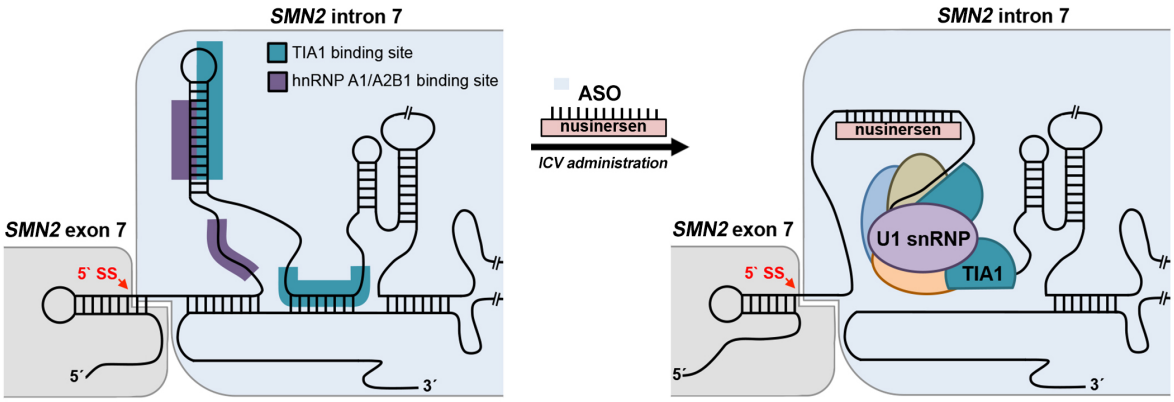

Figure 10. Method of action of Nusinersen (Spinraza™, BIOGEN) for exon 7 splicing correction. In SMN2 normally the ISS-N1 would be involved in sequestering the 5'ss of exon 7 (in red), impeding its inclusion. Nusinersen (in pink in the figure), once administered intracerebroventricularly binds to this silencer, causing structural rearrangements and displacing the negative factors that could previously bind to it (such as hnRNP A1/A2B1, in purple in the figure). This causes the disruption not only of ISS-N1, but also other elements such as TSL3 and ISTL1 (not shown). As a result of these rearrangements, binding of TIA1 (green) becomes accessible, which in turns increases the recruitment of U1 snRNP (light purple) to the 5'ss of exon 7, promoting its inclusion. Figure based in Singh and Singh, 2018.

ISS-N1 has become the most attractive target, as it is an accessible intronic sequence and thus will not cause interference with the protein coding transcript. Targeting it with ASOs has demonstrated its effectiveness even at very low doses, however, because ASOs cannot cross the BBB, it has to be administered intrathecally [16,43]. In clinical trials, Nusinersen has succeeded in improving life expectancy of the type I SMA patients – raising it by two years after treatment started, while untreated patients would have died before that. Moreover, Nusinersen improves motor function, reaching milestones typical of milder forms of SMA [42,43,46]. On top of that, ASOs are known to be stable inside the CNS for months, and have little to no toxicity [9]. However, Nusinersen has not achieved complete motor function, and there are several potential limitations to its use, such as the difficulty of administering the treatment to some patients with severe spine conditions, frequency of dosing, or the cost of the treatment itself [43]. There have been studies investigating whether administering the drug before symptom onset would help achieve even better results, but this has not been the case. While the newer treatment protocols of this drug may very well solve some of these problems – for example, if it became possible to administer intravenously [44] – this calls for the development of other therapies, whether SMN augmentation-based or not, in order to improve therapy outcomes [42].

All the three SMA therapy methods explained above have specific limitations, that can be summarized in the following **Table 2** [21,42].

	ASO-based therapy	Gene therapy	Small molecules
Administration	**Intratecal** •Higher cost •Might require multiple injections periodically •Some patients that are diagnosed late in life might not be able to receive this treatment.	**Intravenous** •More comfortable •Vector can access both the peripheral tissues and the CNS. •If multiple doses are required, it makes it simpler.	**Oral** •Requires no technical knowledge to administer •They can cross the brain blood barrier.
Drug distribution	Does not reach peripheral tissues.	Would have to be administered very early in life to be able to reach the CNS.	The action mechanism is not well known yet, might have off-target effects.
SMN level rescue	Might be **incomplete in peripheral tissues**.	Might be incomplete if immunogenicity is developed after multiple doses.	

Table 2. Comparative table between the three types of therapy discussed in this work.

4.4. Future of SMA therapy

Considering the fact that Nusinersen has already been approved by the FDA, it becomes impossible to think about the future of SMA therapy without talking about synergy. As it would not be moral to deny patients an existing treatment, new drugs will have to be able to work alongside with Nusinersen, complement its effects, and combinatorial models will have to be used for clinical trials [42]. Not only that, but the possibility that rescuing the phenotype only in αMNs might not be sufficient to fully cure the muscular atrophy, suggests there is still a lot to learn about SMN's role in the peripheral tissues.

Furthermore, it is still unclear what other symptoms patients currently being treated with Nusinersen might develop as they grow up, and whether the lack of SMN during development will have lasting effects, even after the administration of the drug. Other patients, such as those with milder forms of the disease that do not get diagnosed until later in life, might also not respond as well to Nusinersen as type I SMA patients have. As these new symptoms are being reported, complementary treatments and further support of care in hospitals for the new clinical challenges they will bring along, will be needed [42,44]. Similarly, establishing a therapeutic time window would allow to minimize these developmental issues. Through post-natal screening, it would be possible to initiate the treatment during the pre-symptomatic stage, thus minimizing the amount of neurodegeneration that takes place. While this window is better known for type I SMA – most of the neurodegeneration takes place during the first 6 months of life – such is not the case for other SMA phenotypes [21].

HYPOTHESIS AND OBJETIVES

Therapies aimed to increase the levels of defective SMN protein, such as the antisense oligonucleotide (ASO) Nusinersen (Spinraza™), have considerably changed the landscape of SMA clinical management. Assays in mouse models of severe SMA have shown that this ASO significantly extends lifespan and improves motor behavior. These findings have encouraged a rapid transition of pre-clinical to clinical trials, in which administration of this agent has resulted in remarkable improvements in SMA type I patients. Despite the promising results with nusinersen, the cellular and molecular mechanisms underlying its pharmacological action are scarcely known. This point is important in order to trace complementary therapies targeting peripheral tissues, particularly skeletal myofibers, which persist disturbed despite Nusinersen treatment. In this vein, there is growing evidence that, besides MNs, numerous peripheral organs are severely affected in SMA pathology. Consequently, increasing SMN levels exclusively in MNs, as achieved with the currently routes of this drug administration, appears not to be enough for the treatment to be effective.

In this context, our work is aimed to examine the impact of the ICV administration of Nusinersen at neonatal period on pathological changes provoked by the SMN deficiency in αMNs, particularly in nuclear pre-mRNA processing machinery and mature mRNA export to cytoplasm, as well as motor performances, using the SMNΔ7 mouse model of SMA.

The main objectives are:

1. To test to which extent motor function can be improved or reverted with ICV administration of Nusinersen in neonatal mice.
2. To identify the cellular bases of Nusinersen effects at the motor unit level. Particularly:
    a. The degree of recovery of αMNs
    b. The expression of two key genes for αMNs homeostasis such as *Chodl* and *ChAT*
    c. The behavior of CBs in αMNs, which are involved in snRNP biogenesis
    d. The subcellular distribution of poly(A) RNAs in the nucleus and cytoplasm of αMNs, with a special emphasis on the recovery of mRNA export and consequent decrease of PARGs.
    e. The organization of protein synthesis machinery, particularly of Nissl bodies.
    f. The size and organization of skeletal muscle fibers, including the oxidative pattern estimated with the SDH assay.

We consider that the new concepts emerging from this work will facilitate a better understanding of the complexity of cellular mechanisms of the disease, and also increase our knowledge on the benefits and caveats of the current therapies with the splicing modulator Nusinersen for SMA.

MATERIALS AND METHODS

1. Animal procedures

1.1. The SMNΔ7 mouse model

The model used for the experiments is the SMNΔ7 transgenic mice, an SMA type I mice model (Jackson Laboratory stock number 005025). In this model, the mouse *Smn* gene was disrupted and, additionally, two copies of the human transgene *SMN2*, along with the cDNA coding for the truncated protein SMNΔ7 ($Smn^{-/-}$; $SMN2^{+/+}$; $SMN\Delta7^{+/+}$) were introduced into the mouse genome [47]. This mouse, created by the Brughes Lab in 2005, show an homozygous recessive phenotype, in which a loss of muscle mass can be seen from birth, and have a two-week life expectancy [47].

To obtain the SMNΔ7 animals, heterozygous knockouts ($Smn^{+/-}$; $SMN2^{+/+}$; $SMN\Delta7^{+/+}$) were crossed. As controls, $Smn^{+/+}$; $SMN2^{+/+}$; $SMN\Delta7^{+/+}$ (WT) mice were used. On P0, a small sample from the tail was clipped to extract the gDNA and the mice were genotyped by PCR.

1.2. PCR genotyping

To confirm each mouse's genotype by PCR, a tip of the mouse tail is cut and gDNA extracted using the Phire Tissue Direct PCR Master Mix kit (Thermo). PCR (polymerase chain reaction) allows the amplification of specific genes, which can then be run through horizontal electrophoresis to compare the size of the amplified DNA with a marker of known standards. To detect the alleles *Smn*+ and *Smn*- we designed PCR primers so the two products have different lengths and are easy to differentiate with PCR (**Figure 11**). Their specific sequence primers were: *Smn*+ and *Smn*- forward 5´-CTCCGGGATATTGGGA TTG-3´; *Smn*+ reverse 5´-TTTCTTCTGGCTGTGCCTTT-3´ and *Smn*- reverse 5´-GG TAACGCCAGGGTTTTCC-3´. Since *Smn*+ and *Smn*- allele amplicons show different sizes (800 bp for *Smn*+ and 500 for *Smn*-), it is possible to directly determine the genotype of the mouse them in the agarose gel.

For the whole genotyping procedure, we used the Thermo Scientific, Phire Tissue Direct PCR Master Mix kit. The gDNA is extracted by incubating the tails tips with the extraction buffer and centrifugation, according to the manufacturer's instructions. The supernatant is collected, and the primers are added to it, as well as the PCR Master Mix. For amplification we used a termocycler during 30 amplification cycles, and then the samples are analyzed in an agarose gel (1%) with UV transillumination.

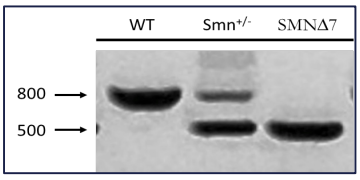

Figure 11. Representative example of a SMNΔ7 genotyping PCR. Bands for the *Smn*+ allele, appear at 800bp and for *Smn*- allele at 500 bp.

1.3. Nusinersen intracerebroventricular administration

Intrathecal delivery methods enable the administration of soluble therapeutics directly into the central nervous system (CNS), in order to bypass the blood-brain barrier (BBB), and are commonly used to treat a variety of diseases in pediatric and adult patients. As an intrathecal delivery method, the intracerebroventricular (ICV) route of administration introduces the therapeutic agent into the cerebral ventricles. In our model, we delivered a single dose of 6,5 mg/kg of the ASO Nusinersen to both, WT and SMNΔ7 mice at P0-1, via 4µl ICV injection of Spinraza™ (Biogen). As control group, we administered an equal volume (4µl) of 0,9% saline solution. All mice were monitored daily and sacrificed at P12.

To do the ICV delivery procedure, mice are cryo-anesthetized for a couple of minutes on an ice surface with tissues to avoid direct contact of the skin and the ice. Holding the mouse by the skin of its neck against a light source, we located the sagittal suture in the skull. The needle should be inserted approximately 0,25 mm lateral to the sagittal suture, and 0,5 – 0,75 mm rostral to the neonatal coronary suture (**Figure 12**). Using a 1ml Hamilton syringe loaded with 4µl of Nusinersen (5mg/12ml) we introduce the needle to only penetrate the skull 2 mm. Then, slowly inject the solution and monitor for ruptured vessels or facial swelling. Wait 15 seconds before removing the needle, and let the mice recover for 5-10 minutes in a warmed container or until they are responsive [48].

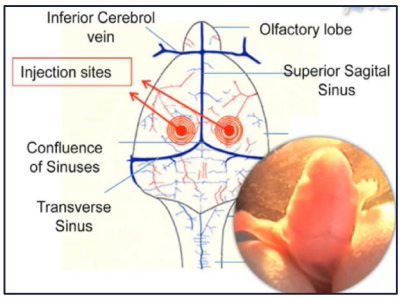

Figure 12. View of the head of a neonatal mouse against a light source. The transverse sinus can be seen through the skin, helping determine where the injection will be made. Taken from Glascock et al 2011 [48].

1.4. Motor righting reflex test

The motor righting reflex test was first described by Altman and Sudarsan in 1975 [49], and ever since has been used as a measure of rats and mice motor coordination, as there are multiple movements involved in turning the body 180º [49].

The test consists in placing the mouse on its back and measuring the time that it takes for the mouse to right itself on the surface. As this is a reflex and requires no learning, it's ideal for neonatal testing. In this work, the test was conducted according to the protocol of Feather-Schussler and Ferguson [50]. It consists of holding the mouse on its back against a surface for five seconds, and then releasing it. Then, the time is measured until it returns to prone position, up to 30 sec for each test. The motor righting reflex test was performed thrice per stage, at P0, P3, P6, P9 and P12 in control WT (0,9% NaCl), vehicle-treated SMNΔ7 mice (0,9% NaCl) or Nusinersen-treated SMNΔ7 mice (6,5 mg/kg).

1.5. Tissue extraction

To extract the spinal cord, a very soft tissue, the entire thoracic cage is extracted. The mice are sacrificed and then the torso is cut off under the forelimbs and above the hindlimbs. The skin is removed, and then the ribcage is dissected and fixed by immersion in 3,7% freshly prepared paraformaldehyde (PFA) (**Figure 13A-C**). After a few hours, when the tissue has already hardened slightly, the bone is cut to reveal the spinal cord, which is then extracted with forceps) (**Figure 13D-E**). The lumbar section is then located and cut from it.

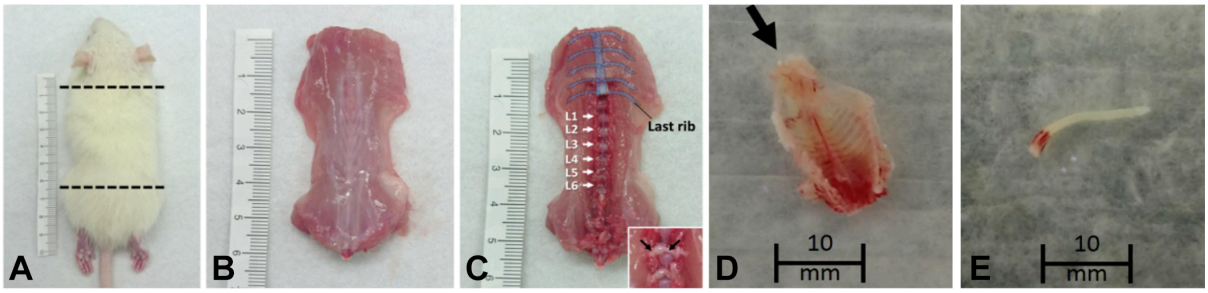

Figure 13. A-C. Extraction of the toracic cage and spine of a mouse. Images taken from Eldeiry, 2017 [72]. **D-E**. Extraction of the spinal cord from a ribcage. Images taken from Lin, 2018. [73]

As for the muscle samples, from the hindlimbs, the *tibialis anterior* (TA) was obtained (**Figure 14**). The skin is removed from a sacrificed animal, and the limb is secured with the help of pins. The first tendon in the ankle is stretched with forceps and cut with a blade, pulling the muscle away from the bone until the knee is reached. Once the muscle is completely separated, it is pinned to cork and immersing it in ice-cold relaxing buffer (100 mM NaCl, 2 mM KCl, 2 mM MgCl2, 6 mM K3PO4, 1 mM EGTA, and 0.1% glucose; pH 7.0), then kept at 4ºC until fixed in 3.7% PFA. The fragments are cryoprotected in 15% and 30% sucrose in PBS (phosphate saline buffer: 137 mM NaCl, 2.7 mM KCl, 8 mM Na2HPO4, and 2 mM KH2PO4; pH 7.4) until they sink to the bottom of the jar. Then, they are embedded in Tissue-Tek OCT Compound (Sakura FineTek USA) and frozen on a chilled metal block in dry ice. Afterwards, cryosections are obtained (8 µm-thick) and mounted on SuperFrost slides that can be stored at -80ºC until use.

Figure 14. Extraction of TA muscle from a mouse's hindlimb. Image from Wang, 2017. [74]

2. Cell Biology procedures

2.1. Succinate dehydrogenase (SDH) assay

The SDH is an enzyme that participates in the citric acid cycle, and in the electron transmission chain, both processes taking place in the mitochondria. For this reason, it is used as a marker for mitochondria and high levels of SDH in muscle indicate the oxidative activity of the fibers. When the SDH in the tissue comes in contact with succinic acid from the buffer, an electron transfer occurs and causes a color change that can be measured. As explained above, the content of mitochondria and the oxidative activity of each fiber determines its type. Type I myofibers have the highest SDH response, while type IIb have the least, with type IIa in between these two. This test was performed in order to understand the effect of the Nusinersen on the muscle fiber phenotype.

To do so, cryosections of the non-fixed TA muscle (8 μm) were incubated in a SDH reaction mixture (1.5 mM nitroblue tetrazolium, 5 mM EDTA, 48 mM succinic acid, 0.75 mM sodium azide, 30 mM methylphenylmethyl sulfate, and phosphate buffered pH 7), whereas the controls were incubated in succinic acid-free medium. Afterwards, samples were air-dried and mounted. They were observed under a fluorescence microscope (Zeiss, Axioscop Plus) under an oil objective of either 40x or 63x. Once images were captured, a morphometric analysis was performed of at least 100 myofibers per animal (n=3 in each group). Fiber diameter was measured on randomly collected images (40x) using the ImageJ software (National Institutes of Health).

2.2. Immunofluorescence and confocal microscopy

Four mice per group were fixed by perfusion with 3.7% freshly-prepared PFA in PBS under deep anesthesia with pentobarbital (50 mg/kg). Once fully asleep, the mice were pinned to a board and an incision on the chest area was made to access the heart. A syringe with the PFA was inserted on the left ventricle, and the right atrium is perforated so that the blood may exit. After all the PFA has entered the body and the fluid leaving through the atrium incision is no longer blood, the perfusion is finished. The animals were then cut off under the forelimbs and just above the hindlimbs, leaving only the trunk. From the trunk, the skin is removed to be able to pinch the column with our fingers, exposing the spinal cord as a small white dot. Once located, saline solution is introduced with a syringe to push the spinal cord through the opposite end into a Petri dish. The tissue is post-fixed for 6 hours and washed in PBS.

After post-fixation, the samples were cut into 160 μm-thick transverse sections with a vibratome, and dissected into small fragments from the anterior horn. These were then transferred to a drop of PBS on a positively charged slide (Superfrost Plus, Thermo Scientific, Germany). After that, a slide cover is placed on top and the sample is tapped gently in a perpendicular angle, with a histologic needle. After a few seconds, the neurons will have dissociated. The slides are placed face down on metal plaques, inside a container with dry ice. To prepare them further for immunofluorescence, the slide cover is removed, and samples are treated with glycine to eliminate the aldehyde residues left by fixation, and then permeabilized with PBS-Triton-X-100 0,5% for 45 minutes at room temperature, and washed with PBS-Tween-20 0,05%.

After that the area around the sample is delimited with a diamond pen, before adding the primary antibody (7 µl), diluted in PBS with 1% BSA. The samples are kept in a dark and humid chamber at room temperature for three hours, or overnight at 4ºC [51,52].

The primary antibodies were: mouse monoclonal anti-SMN (diluted 1:100, catalog no. 610646, BD Transduction Laboratories, USA); mouse monoclonal anti-TMG-cap (NA02A, Oncogene, USA); mouse monoclonal anti-fibrillarin (diluted 1:100, catalog no. ab4566, Abcam, USA); rabbit polyclonal anti-coilin (1:500, 204.10, Prof. A. Lamond, Dundee, UK); and goat polyclonal anti-choline acetyltransferase (ChAT) (1:200, AB144P, Millipore, MA, USA). As for the secondary antibodies, they were conjugated with FITC, Texas Red or Cy3, or Cy5 (diluted 1:75, Jackson, USA). Some samples were counterstained with propidium iodide (PI) or Phalloidin-FITC, and samples were mounted with ProLong Anti-Fading Medium (Invitrogen).

Using a laser scanning confocal microscope (LSM510, Zeiss, Germany – 63x oil 1.4 NA objective), the samples were excited sequentially at 488 nm and 543 nm to obtain images, thus avoiding signal overlap. The intensity of the signal was generated using confocal images of double immunolabeled samples and processing the images with Adobe Photoshop CC6 software.

2.3. In situ hybridization of poly(A)RNAs

Fluorescence in situ hybridization (FISH) was performed on αMN dissociates to detect the spatial distribution of polyA RNA, using an oligonucleotide probe conjugated with biotin. The preparations are permeabilized with TBS-E-SDS for 15 min at 37ºC so that the probe could reach the RNA. Then, they are washed thrice in 6x SSPE-0,1% Tween 20 for 15 min, and incubated with the tRNA probe for 3 hours at 42ºC in a humidified chamber. After hybridization, the samples are washed in 6xSSC, and then in 4xSSC-0,1% Tween 20 (15 min each, room temperature). All samples were mounted with Vectashield (Vector, USA) and the signal was detected with FITC-avidin.

3. Molecular Biology procedures

3.1. qRT-PCR for relative gene expression analysis

Quantitative reverse transcription polymerase chain reaction, or qRT-PCR, combines the PCR amplification of a specific gene with the ability to measure how long it takes for that amplification to reach a peak signal. To do this, the nucleotides that will create the new DNA strands carry with them a fluorochrome that becomes visible when it joins the complementary chain, allowing a real time observation of the chain reaction speed, and the concentration of new DNA. Because it is performed starting from a mRNA sample, it is then converted in DNA (complementary DNA, cDNA) via reverse transcription with a High Capacity cDNA Reverse Transcription Kit (Life Technologies).

mRNA was extracted from the spinal cord of four mice per group, isolated with TRIzol (Invitrogen, Carlsbad) following the manufacturer's instructions, and purified with the RNeasy kit (Qiagen, Hilden,

Germany). The expression of *Gapdh, ChAT* and *Chodl* was determined using gene-specific SYBR Green-based primers (Takara). The fluorescence is measured during the 40 cycles of PCR and the threshold cycle (Ct) is established on the cycle that the fluorescence is first captured, once the collective signal from all the DNA being amplified is enough to trigger the machine. The results were normalized to GAPDH, and the comparison between relative gene expression of *ChAT* and *Chodl* was calculated following the 2-(ΔΔCt) equation [53]. The primers for pre-mRNA of *ChAT* were 5´-CTTGGGGCCAGTCTGATAGC-3′ and 5′-GGA CACATGGCTAGAAGGGG-3′, for the pre-mRNA of *Chodl* 5′-GCTGTTGTCTCCCGCATCTT-3′ and 5′-AAGTGGAAGCGTTTGGGATT-3′, and for the pre-mRNA of *Gapdh* 5'- AGGTCGGTG TGAACGGATTTG-3' and 5'- TGTAGACCATGTAGTTGAGGTCA-3'.

3.2. SDS-PAGE and immunoblotting

Samples of the spinal cords and muscle were obtained from not perfused animals (n=3 in WT and SMNΔ7 groups; n=4 in Nusinersen-treated SMNΔ7 group). They were lysed in a lysing buffer at 4ºC (50 mM Tris (pH 8), 150 mM NaCl, 2% Nonidet NP-40, 1 mM MgCl2, 1 mM dithiothreitol, and 10% glycerol and supplemented with EDTA-free complete protease inhibitor cocktail and PhosphoSTOP (Roche)), then sonicated to break up the tissue completely with short pulses of five seconds, then placed in ice. Then they were cleared by centrifugation at 14000 rpm for 10 min at 4ºC, then diluted in an equivalent volume of 2x (Laemmli loading buffer).

To separate the proteins, commercial gels (4-20% NuPage TG SDS-PAGE gels, Invitrogen) were used. Afterwards, the proteins get transferred to a nitrocellulose membrane using standard procedures, which is blocked with milk protein. Mouse monoclonal anti-SMN (1:5000) and rabbit polyclonal anti-lamin A/C (1:1000) are used, and after adding the secondary anti-mouse and anti-rabbit antibodies, the protein bands are visualized with an Odyssey™ Infrared-Imaging System (Li-Cor Biosciences). For quantitative analysis of the blots, ImageJ software was used (U.S. National Institutes of Health, Bethesda, Maryland, USA, http://imagej.nih.gov.ij).

4. Statistical analysis

The data in this work has been expressed as mean ± SD and has been analyzed using GraphPad Prism 7 software and PASW Statistics 22 (SPSS, Inc.) packages. Four mice per group were examined, when quantification analysis was performed to evaluate the mean number of CBs per αMN and the proportion of PARGs-containing αMNs in at least 100 αMNs per group. This was done by examining the images obtained from neuronal dissociates after observing the nuclei under a 40x objective throughout various focal planes. The statistical analysis was assessed by one-way ANOVA or mixed-design two-way ANOVA (Split-Plot ANOVA), followed by the Bonferroni post hoc test (SPSS) or Student's t test (GraphPad) as indicated in the figure legend. In all cases, differences were considered to be statistically significant if $p < 0.05$.

RESULTS

The severe forms of SMA, type 0 and I, are associated with early mortality in most cases and severe disability in survivors. As mentioned, SMA is characterized by progressive muscle weakness caused by the loss of spinal cord αMNs. Fundamental activities using muscles, such as walking, sitting up, controlling head movement, breathing, and swallowing is affected in SMA. Movement progressively becomes slower and its ability to the voluntary control may be lost completely in the later stages of the disease. Currently, there is no cure for SMA, but there are encouraging treatments as novel genetic therapies based on the use of the antisense oligonucleotides (ASOs).

The ASO Nusinersen (now available as Spinraza™ from BIOGEN), promotes production of full-length SMN protein targeting the *SMN2* gene, and was recently approved by the European Medicines Agency and the US Food and Drug Administration. Clinical studies in type I SMA patients, demonstrate that Nusinersen is safe and well tolerated and no drug-related adverse events are observed, doubling SMN levels after a single dose, prolonging survival of patients and allowing motor milestone acquisition [6]. Patients with type II SMA also show progress on different motor scales after Nusinersen treatment [54]. Nusinersen thus represents the first efficacious marked approved drug in type I and type II SMA [55].

In 2018, our laboratory signed an MTA contract with the pharmaceutical company BIOGEN to analyze if the restoration of SMN expression with the administration of Nusinersen reverts the severe dysfunction of nuclear RNA metabolism previously reported by our group in αMNs of the SMNΔ7 mice [56,57]. For that purpose, an effective Nusinersen treatment protocol, based on the intracerebroventricular (ICV) injection of ASOs in neonatal (P0-1) SMNΔ7 mice, was adopted [58]. The results herein presented show the neuroprotective effects of Nusinersen based on the restoration of neuronal RNA homeostasis as well as the improvement on motor function [1].

1. Treatment with ASO-nusinersen robustly recovers the growth curve, enhances motor function, and dramatically reduces αMN loss.

Previous results from our laboratory had shown that, in the mouse model of type I SMA, the SMNΔ7 mouse, SMN deficiency produces, as one of the earliest signs of αMN degeneration, the functional **depletion of CBs and the loss of CB-nucleolus interactions**. This neuronal response induces a progressive nucleolar dysfunction in ribosome biogenesis with reorganization and loss of nucleolar transcription units, segregation of dense fibrillar and granular components, retention of SUMO-conjugated proteins in intranucleolar bodies and a reactive, compensatory, up-regulation of both mature 18S rRNA and genes encoding key nucleolar proteins, such as the upstream binding factor (UBF), fibrillarin, nucleolin and nucleophosmin [56]. These CB and nucleolar alterations might participate in the dysfunction of rRNA synthesis/processing reported in SMA by several groups, including ours. Consequently, we support that SMA must be included in the emerging group of pathologies known as **"RNAopathies"** [39].

Later, our group showed that αMN-SMNΔ7, exhibit the abnormal nuclear accumulation of polyadenylated RNAs in specific granules, known as **PARGs**. These were also enriched in the splicing regulator Sam68. Despite the absence the other RNA-binding proteins in these PARGs, the abnormal nuclear accumulation of polyadenylated mRNAs suggests that they cannot be exported to the cytoplasm for translation. Furthermore, these effects were accompanied by changes in the alternative splicing of the Sam68-dependent *Bcl-x* and *Nrnx1* genes, as well as changes in the relative accumulation of the intron-containing *Chat, Chodl, Myh9* and *Myh14* mRNAs, which are all important for MN functions [57].

Now, in the work herein presented, our first aim was to analyze the global effects of the treatment with the ASO-Nusinersen in neonatal SMNΔ7 mice (P0-1). Although low levels of SMN are systemic, the primary affected cell population is αMNs. Since ASOs do not cross the blood–brain barrier (BBB) when administered systemically [59], to reach the αMNs we decided to administer Nusinersen via ICV (**Figure 15A**), according to the protocol described by Glascock et al 2011 [48]. The experimental groups were: (i) WT treated with 4µl of Nusinersen (dose 6,5mg/Kg), (ii) WT treated with 4µl of 0.9% saline solution (hereafter, WT), (iii) SMNΔ7 treated with Nusinersen (dose 6,5mg/Kg), and (iv) SMNΔ7 treated with 4µl of 0.9% saline solution (hereafter, SMNΔ7). All mice recovered shortly after injection without any detrimental side effects.

First, we wanted to evaluate the efficiency of the treatment with Nusinersen on the restoration of SMN protein levels in both the CNS (SMN levels should be back to normal if ICV delivery was performed successfully) and in a non-CNS tissue as the skeletal muscle (SMN levels should be low). To test this, western blot analyses were performed in tissue lysates collected at P12 from the four study groups (**Figure 15B**). We found that SMN levels in Nusinersen-treated SMNΔ7 spinal cords samples were 2.5 times higher than in the vehicle-treated SMNΔ7 samples. When compared to the WT groups, the SMN level reached approximately 70% of their level (**Figure 15B**, left panel). Furthermore, skeletal muscle samples from Nusinersen-treated SMNΔ7 mice confirmed that Nusinersen does not reach organs outside the CNS, since SMN protein levels were not increased relative to untreated SMNΔ7 mice (**Figure 15B**, right panel).

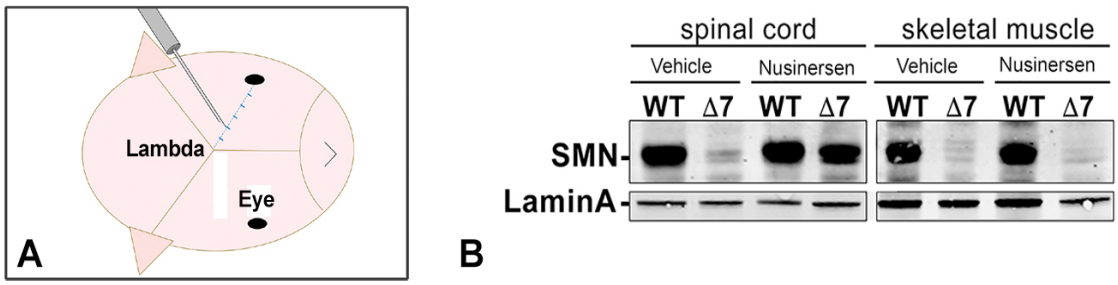

Figure 15. (A) Illustration of the intrathecal injection point of the ASO-nusinersen (Spinraza™). **(B)** Western blot analysis of SMN protein levels in whole spinal cord and skeletal muscle lysates at P12. In the SMNΔ7 mouse SMN levels are low in both spinal cord and muscle, and it recovers when Nusinersen is injected, but only in the spinal cord, not in muscle. The SMN bands were normalized to laminA, a protein present in the nuclear lamina, associated to the nuclear envelope. The images were analyzed using ImageJ.

Once verified that Nusinersen was efficiently being delivery to the CNS through the ICV injection, and that SMN protein levels were restored near to WT levels in the Nusinersen-treated SMNΔ7 spinal cord samples, we decided to study the global impact of αMN-specific SMN restoration in the whole body growth, net weight gain and motor function of SMNΔ7 mice treated with one single dose of ASOs at P0-1. The visual observation of SMNΔ7 mice showed that they are already born lacking mobility and muscle mass. As they grow, they seem to struggle to grow in length and gain weight at the same rate as WT littermates (**Figure 16A**). At the clinical phase (P6 to P12), symptoms appear more evident and progress until death occurs between P12 and P14. However, when we compared the Nusinersen-SMNΔ7 mice to their WT littermates were almost indistinguishable (**Figure 16B**), and although they had ambulation capacity a moderate hindlimb paresis was noticeable in these animals when compared to WT mice.

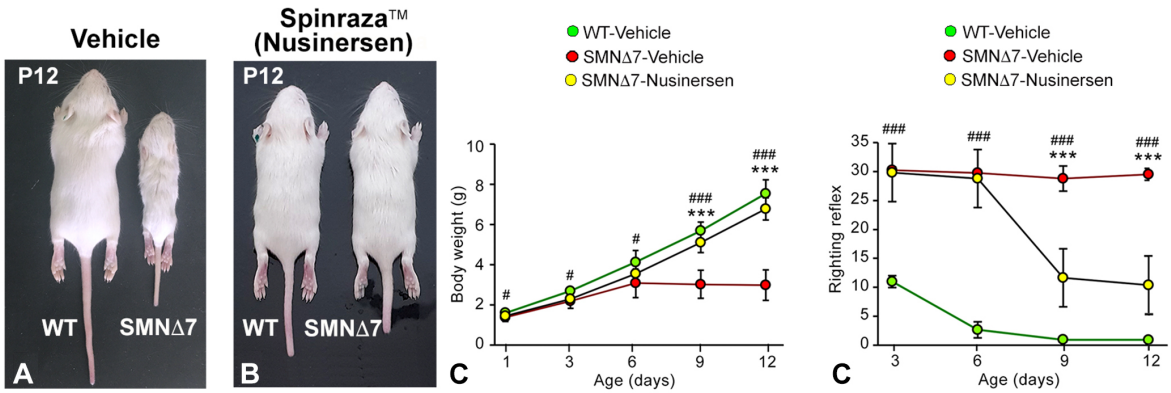

Figure 16. (A) Comparison between a WT and a SMNΔ7 mouse at P12. **(B)** Comparison between a WT and a Nusinersen-treated SMNΔ7 mouse at P12. **(C)** Graph comparison of body weight (mean ± SD) between WT, SMNΔ7 and nusinersen-treated SMNΔ7 mice from P0 to P12 (n = 8 mice per group). The Nusinersen-treated SMNΔ7 mice (yellow) reach weights comparable to the WT group (green), unlike the untreated SMNΔ7 group (red). #$p < 0.01$, ###$p < 0.0001$: WT vs. SMNΔ7; ***$p < 0.0001$: vehicle-treated SMNΔ7 vs. nusinersen-treated SMNΔ7. **(D)** Graph showing the time needed to acquire the righting motor reflex and the time needed to complete the test (mean ± SD). The Nusinersen-treated SMNΔ7 mice (yellow) acquire the reflex a little later and take longer to complete the test than the WT group (green), but the response is much improved from the untreated SMNΔ7 mice (red), who never acquire the reflex to begin with. (n = 8 mice per group). ###$p < 0.0001$: WT vs. SMNΔ7; ***$p < 0.0001$: vehicle-treated SMNΔ7 vs. Nusinersen-treated SMNΔ7. In C,D, data were analyzed by a one-way ANOVA, followed by the Bonferroni post hoc test using SPSS.

Next, to compare the body growth rate, vehicle-treated WT and SMNΔ7 Fig. 2RB 7 mice, as well as Nusinersen-treated SMNΔ7, were weighted at P0, P3, P6, P9 and P12. While the Nusinersen-treated WT group (data not included in the graph) did not show any significant body weight differences from the vehicle-treated WT mice, it was clear that the treatment on SMNΔ7 mice had a positive impact. Their growth in weight was comparable to that of the WT group after P6, and about double the growth of vehicle-treated SMNΔ7 mice at P12 (**Figure 16C**). Furthermore, we also analyzed motor functions of the Nusinersen-SMNΔ7 mice, using the righting reflex test. In this test, the mouse is placed on its back and the time it needs to right itself is measured up to 30 seconds. This evaluates the overall muscle strength and motor coordination of the mice. In the case of untreated SMNΔ7 mice, they never acquire the righting

reflex during the period studied (P0-P12), while both Nusinersen-treated SMNΔ7 and WT mice are capable of righting themselves from P3 onward. However, Nusinersen-treated SMNΔ7 mice required more time to do so (**Figure 16D**). It is noteworthy, that although SMA severely impairs mobility due to muscular atrophy, which was observed in the vehicle-SMNΔ7 group, Nusinersen-treated SMNΔ7 mice only exhibit moderate hindlimb atrophy, and they are able to walk on their own.

Western blot analysis of the *tibialis anterior* (TA) muscle clearly indicated that Nusinersen does not cross the BBB in neonatal mice, leaving the peripheral organs unable to produce full length SMN protein. Therefore, seems sensible to deduce that the clinical effects of the ASO treatment are primarily due to the increased expression of SMN in the spinal cord. To examine SMN expression and distribution specifically in the αMNs, we performed SMN immunolabeling experiments using transversal cryosections from whole spinal cords at the L5 level. Thus, the SMN staining pattern in Nusinersen-treated SMNΔ7 αMNs was similar to the one in WT neurons, that included a diffuse signal in the cytoplasm, and accumulation of SMN signal in nuclear CBs (**Figure 17A and C**). On the contrary, vehicle-treated SMNΔ7 αMNs exhibited a notably weak cytoplasmic signal of SMN, and CBs were rarely observed (**Figure 17B**).

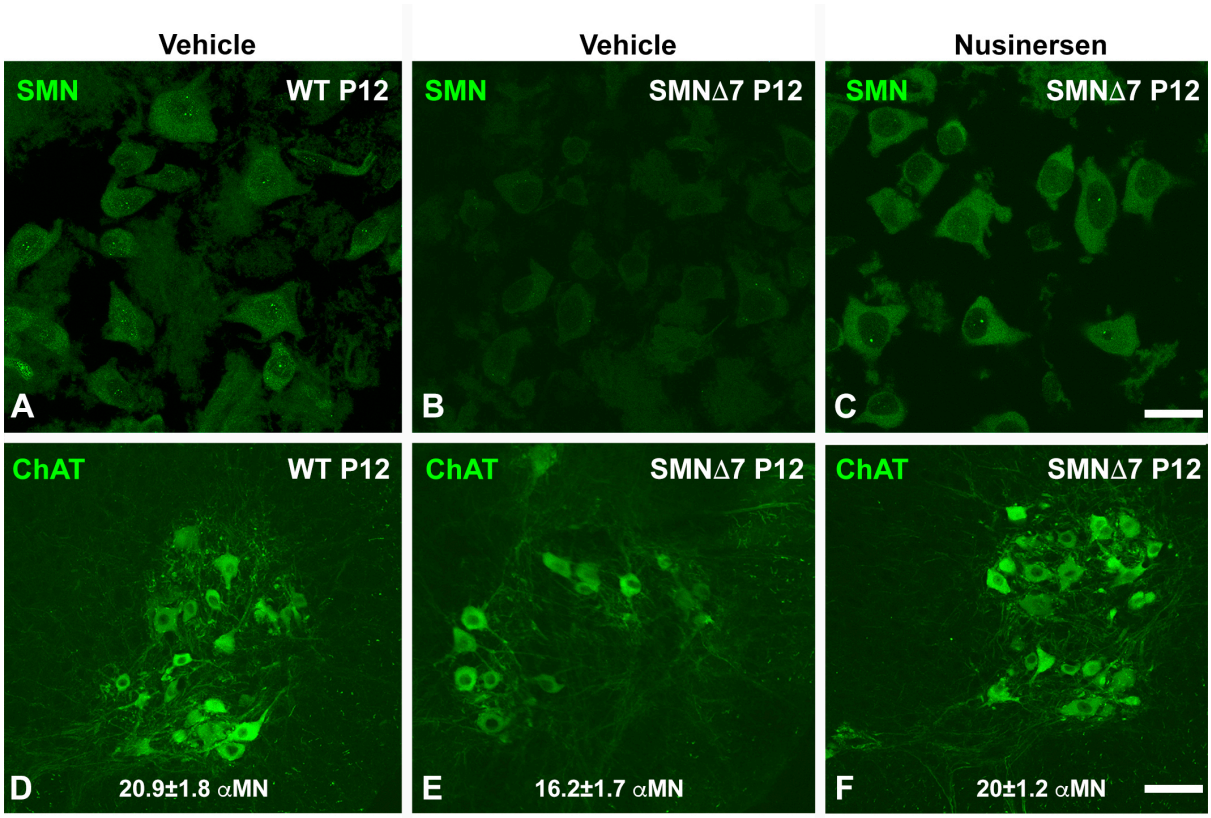

Figure 17. (A–C) Immunodetection of SMN, where the treatment with nusinersen rescues the typical SMN staining pattern (A) in nusinersen-treated SMNΔ7 cells (C) – diffuse cytoplasmatic signal and concentrated in CBs, while the untreated SMNΔ7 neurons (B) show a much weaker signal in the cytoplasm and CB depletion. **(D–F)** Immunodetection of ChAT in the anterior horn of spinal cord allows to count the number of αMNs and compare the average between groups. The Nusinersen-treated SMNΔ7 cells (F) recover in number to be comparable with the WT animals (D), while the untreated animal has less αMNs (E). Scale bars: 10 μm (A–C), 30 μm (D–F).

In terms of αMN survival, immunostaining for ChAT, a marker of αMNs, was performed, followed by quantitative analysis of the average percentage of ChAT-positive MNs at each anterior horn on 8-μm thick cryosections (**Figure 17D-F**). In Nusinersen-treated anterior horns, the αMN population is preserved when compared to WT, with no significant differences in the mean number of αMNs per section, while in vehicle-treated SMNΔ7 mice had a clear depletion of αMNs per anterior horn, as seen in **Figure 17D-F.**

Once observed that Nusinersen treatment preserves αMNs and presumably the formation and maintenance of the NMJ, we investigated whether it can also prevent the neurogenic myopathy that the SMNΔ7 mice develop. First, to determine the existence of muscular atrophy, we analyzed the myofiber size distribution in cross-cryosections of the TA muscles stained with phalloidin-FITC, a marker of thin actin filaments (**Figure 18A-C**). Despite the reduced level of SMN protein in SMN Δ 7 mice muscles (**Figure 15B**, right panel), non-significant differences in myofiber diameter were found between saline-WT mice and Nusinersen-treated SMNΔ7 mice at the symptomatic P12 stage (**Figure 18G**). It is noteworthy the significant reduction of the myofiber diameter detected in vehicle-SMNΔ7 mice compared with WT and Nusinersen-SMNΔ7 mice (**Figure 18G**).

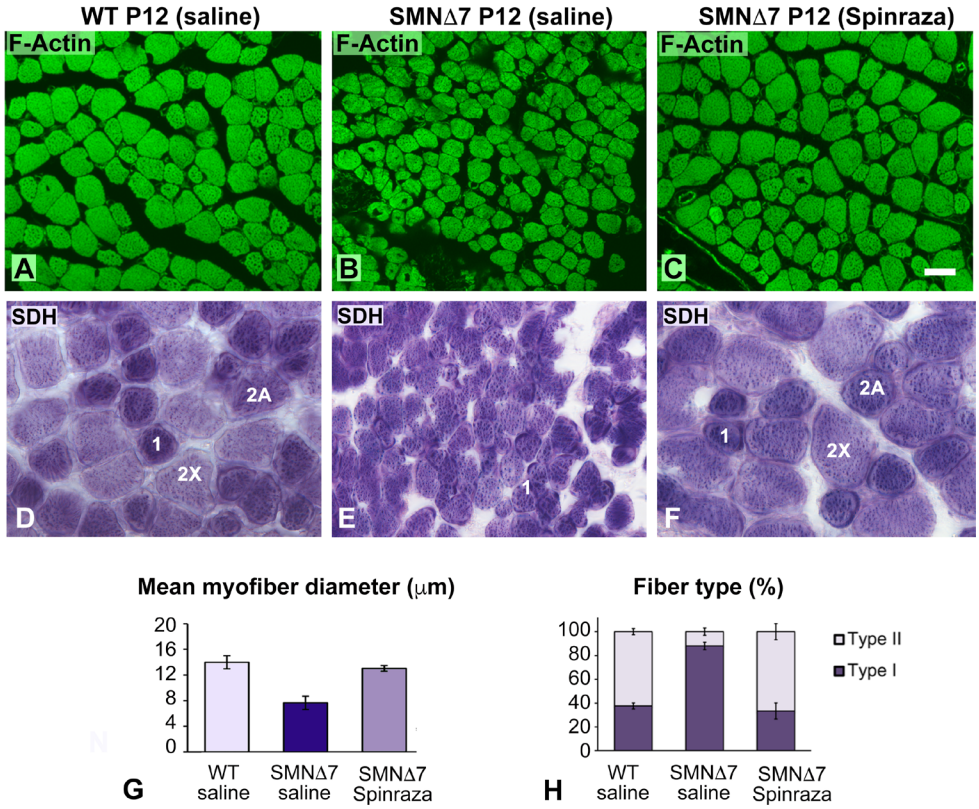

Figure 18. (A–C) Phalloidin-FITC staining of transverse cryosections of TA muscle at P12, showing distribution of myofiber in WT muscle (A), and how the Nusinersen-treated mice recovered the myofiber normal diameter (C) vs the untreated animals who showed atrophied fibers with smaller diameters (B). **(D–F)** SDH histochemical staining of WT (D), SMNΔ7 (E) and nusinersen-treated SMNΔ7 TA muscle (F) at P12. The different myofiber types are labeled in the image (1, 2A, 2X). While in untreated SMNΔ7 mice the main phenotype is the smaller type 1 myofibers, the Nusinersen-treated SMNΔ7 mice recover the same phenotype as the WT animals. **(G)** Quantitative analysis of the mean myofiber diameter at P12 (mean ± SD). **(H)** Quantitative analysis myofiber type on transverse TA muscle based on SDH staining. Scale bars: 15 μm (A-F).

To further understand the myofiber response to Nusinersen treatment, we performed the succinic dehydrogenase (SDH) histochemical assay, as a marker of the mitochondrial oxidative activity. SDH histochemistry on cross-cryosections of the TA muscle revealed that both WT and Nusinersen-treated SMNΔ7 myofibers exhibited a staining checkboard pattern of a mixed muscle with a similar myofiber size distribution (**Figure 18 D and F**). Moreover, there was a comparable proportion of myofibers whose SDH oxidative activity corresponded to either type 1 or type 2A and 2X (**Figure 18H**). In contrast, vehicle-treated SMNΔ7 myofibers were clearly atrophic with reduced diameter, as demonstrated in our previous analysis (**Figure 18G**), and an oxidative intensity of stain predominantly corresponding to type 1 (**Figure 18E, H**).

2. Nusinersen treatment prevents disruption and loss of canonical CBs in αMN of the SMA model.

Once we have confirmed that Nusinersen treatment normalizes SMN protein levels in the spinal cord and preserves αMN population, we next wanted to investigate the status in terms of formation and functionality of canonical CBs in the Nusinersen-treated SMNΔ7 αMNs. Canonically, CBs are spherical structures of around 0,5 μm of diameter, whose main component is coilin. Since these nuclear organelles are involved in pre-mRNA processing, the number and size of CBs depend on transcription rate of the cell, changing to accommodate the requirements for pre-mRNA splicing. SMN plays an important role in formation of CBs, and previous studies have shown that upon SMN protein depletion, canonical CBs disappear, followed by relocalization of coilin as perinucleolar caps and/or within the nucleolus [37,60]. Thus, **CB disruption can be considered an early nuclear sign of αMN degeneration in SMA**.

First, we performed double immunolabeling experiments to visualize coilin, the structural protein and molecular marker of CBs, and SMN. The SMN distribution, as mentioned above, was diffuse in the cytoplasm and concentrated in nuclear bodies. These were identified as canonical CBs because they concentrated both SMN and coilin. Moreover, CBs showed a preferential association with the nucleolus in both WT and Nusinersen-treated SMNΔ7 αMNs (**Figure 19A and C**). This was, however, not the case in the vehicle-SMNΔ7 αMNs, where coilin-positive aggregates were depleted of SMN an coilin relocalized forming perinucleolar caps where SMN was scarcely detected (**Figure 19B**). Next, to determine the precise effect of Nusinersen treatment on CB formation, a quantitative analysis of the mean number of CB per nucleus was performed. To do this, neuronal dissociates were coimmunostained for coilin and SMN. No significative differences were found between WT and Nusinersen-treated SMNΔ7 αMNs at P12, however, in vehicle-treated SMNΔ7 αMNs at P12, during the clinical phase, the mean number of CB per nucleus was drastically reduced, as indicated in **Figure 19A-C**.

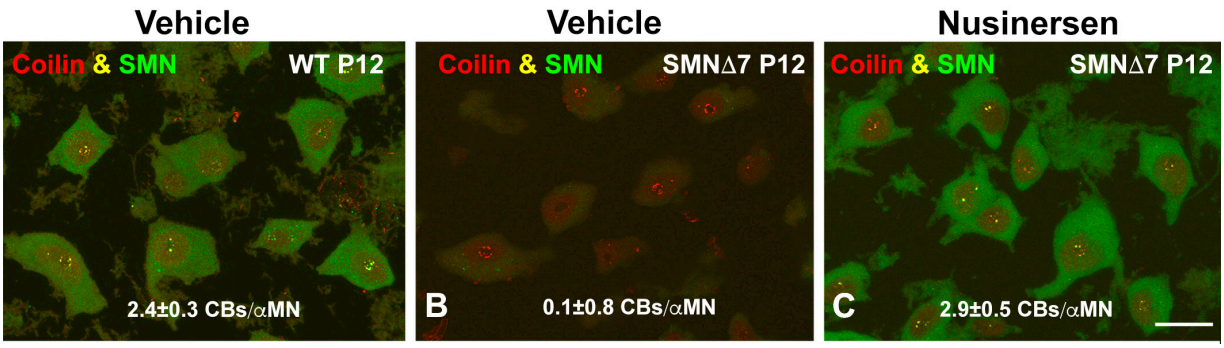

Figure 19. (A–C) Confocal images of dissociated αMNs from WT (A), SMNΔ7 (B) and nusinersen- treated SMNΔ7 mice (C) double immunolabeled for coilin (red) and SMN (green). In both WT and Nusinersen-treated SMNΔ7 αMNs there are canonical CBs, in which coilin and SMN colocalize. However, in untreated SMNΔ7 αMNs the coilin forms perinucleolar caps, and the SMN signal is very weak in comparison to the other two. Scale bars: 20 μm (A–C).

To confirm that Nusinersen induces the concentration of SMN in CBs, we performed a detailed co-localization analysis from the confocal fluorescent signals from both SMN (green) and coilin (red). Thus, as shown in **Figure 20A, C**, the profile of fluorescence intensity signals across a line that passed through two CBs from a WT or a Nusinersen-treated SMNΔ7 αMN confirmed the co-localization of coilin and SMN in canonical CBs. In contrast, in vehicle-treated SMNΔ7 αMNs, the linear profile shows the absence of fluorescence SMN signal from perinucleolar coilin-positive caps (**Figure 20B**).

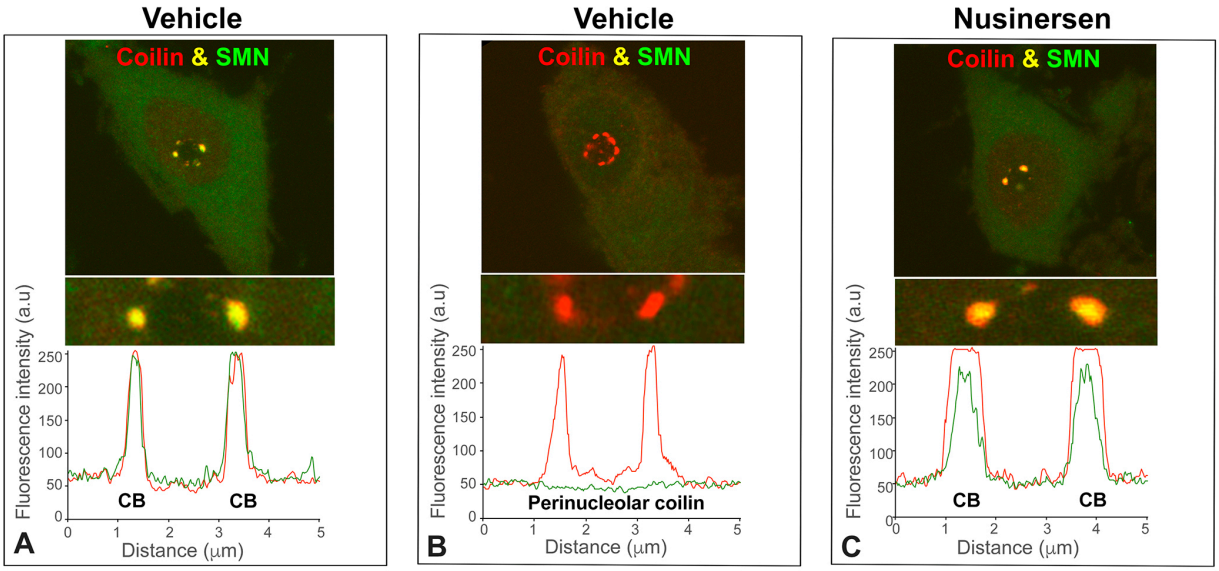

Figure 20. Confocal images of dissociated αMNs from WT **(A)**, SMNΔ7 **(B)** and Nusinersen-treated SMNΔ7 mice **(C)** double immunolabeled for coilin (red) and SMN (green). Upon performing a colocalization analysis, the profile of fluorescence signal across two CBs shows whether colocalization is precise in canonical CBs. In WT and Nusinersen-treated SMNΔ7 αMNs, the profiles show the fluorescence has an intensity peak in both signals in the same location (A, C). However, in untreated SMNΔ7 mice there is no SMN signal (B). The intensity of the signal was analyzed with ImageJ software.

To determine whether the CBs formed in Nusinersen-treated SMNΔ7 αMNs were functional in spliceosomal snRNP maturation or snoRNPs biogenesis, double immunolabeling for coilin with TMG-cap or fibrillarin was performed. TMG-cap is a marker for the 5' end of snRNAs and is used as a spliceosomal snRNPs marker. Fibrillarin is a protein component of nucleolar snoRNPs that is concentrated in the fibrillar centers of the nucleolus and canonical CBs. Both signals, each corresponding to molecular markers of snRNP and snoRNPs, respectively, colocalized with coilin in the CBs of WT and Nusinersen-treated SMNΔ7 αMNs (**Figure 21A-F**). However, this was not the case for perinucleolar caps of vehicle-treated SMNΔ7 αMNs, indicating these coilin-positive structures cannot participate in the biogenesis of both, snRNPs nor snoRNPs. These observations were also confirmed by the profiling of the confocal fluorescence signals across a line (red for coilin and green for TMG-cap or Fibrillarin) shown in the **Figure 21**. As a final note, Gems, coilin-negative and SMN-positive nuclear bodies, were absent in all experimental groups studied.

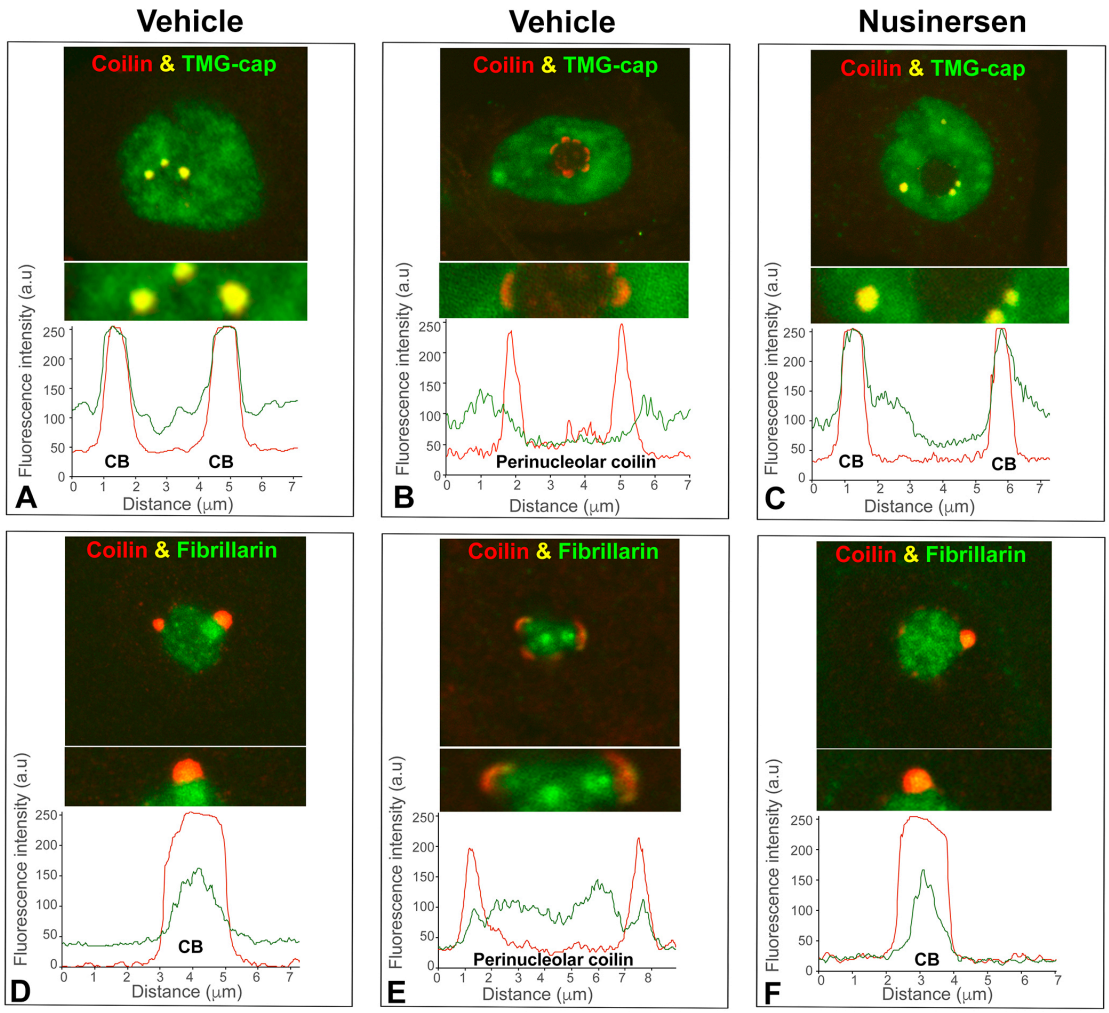

Figure 21. (A–F) Confocal images of dissociated αMNs from WT **(A, D)**, SMNΔ7 **(B, E)** and Nusinersen-treated SMNΔ7 mice **(C,F)** double immunolabeled for coilin (red, A–F), TMG-cap (green, A–C), and fibrillarin (green, D–F). The profile of fluorescence signal across areas concentrating coilin shows whether colocalization exists with a marker of snoRNP (fibrillarin) or a marker of snRNP (TMG-cap) maturation processes. The intensity of the signal was analyzed with LSM510 software.

3. Nusinersen rescues the transcription rate of Chodl and ChAT pre-mRNAs.

Due to the essential function of SMN in pre-mRNA splicing, various essential genes for αMN homeostasis may be affected in SMA mice models. The genes we chose to study the effects of Nusinersen on transcription rate were *Chodl* (chondrolectin) and *ChAT* (choline acetyl transferase), two important genes for αMN homeostasis that have been found to be highly expressed in αMNs, and whose expression becomes dysregulated in SMA. While, chondrolectin is involved in motor axon growth [61,62], choline acetyl transferase is the key enzyme in the synthesis of the main αMN neurotransmitter acetylcholine. For this reason choline acetyl transferase is commonly used as a marker of αMNs [63].

To determine whether treatment with Nusinersen was able to rescue the transcription rate of these two genes, an analysis by qRT-PCR in spinal cord RNA extracts (P12) was performed. In SMNΔ7 samples, pre-mRNA levels for both genes were significantly lower than in WT samples. Remarkably, the pre-mRNA levels in Nusinersen-treated SMNΔ7 mice were comparable to that of WT (**Figure 22**).

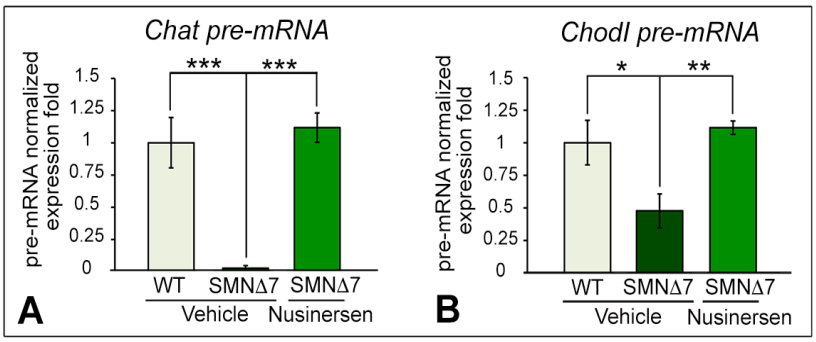

Figure 22. (A, B) RT-PCR analysis of the expression of ChAT (A) and Chodl (B) pre-mRNAs in whole spinal cord RNA extracts from WT, SMNΔ7 and nusinersen-treated SMNΔ7 mice at P12. Both genes were normalized to the expression of GAPDH, and the results show that mRNA expression in Nusinersen-treated SMNΔ7 mice is comparable to that of WT, while being demonstrably lower in untreated SMNΔ7 animals. Bars represent the mean ± SD, *$p < 0.05$ and ***$p < 0.0005$ ($n = 4$ mice per group, Student's t test analysis was performed using GraphPad).

4. Nusinersen treatment normalizes the distribution of the protein synthesis machinery and polyadenylated mRNAs in SMNΔ7.

During the process of transcription, mRNA undergoes polyadenylation as one of the necessary modification steps before nuclear export. However, when a disturbance of the nuclear pre-mRNA processing occurs, those mRNAs are kept in the nucleus, where they accumulate [57]. In the case of SMA, as previously reported by our laboratory and others, there is a marked perturbation of pre-mRNA splicing resulting in a defective mRNA maturation and the nuclear retention of incorrectly processed mRNAs in nuclear structures called "poly(A) RNA granules" (PARGs)[56,57,64].

In this work, we have previously shown that treatment with Nusinersen restores SMN protein levels in αMNs (**Figure 15B**, left panel). Since one of the major roles of SMN is the assembly of spliceosomal snRNPs, which is essential for the correct pre-mRNA splicing and mRNA export, we wanted to investigate

whether Nusinersen treatment rescues the dysfunction in mRNA processing observed in SMNΔ7 αMNs. For this purpose, we examined the distribution of poly(A) RNAs with *in situ* hybridization with a poly-dT probe. In the nucleus of WT αMNs, poly(A) RNAs appeared diffusely distributed, excluding the nucleolus, and accumulated in the nuclear speckles of splicing factors. In addition, poly(A) RNAs was diffusely distributed throughout the cytoplasm (**Figure 23A and D**). This distribution was mirrored by the Nusinersen-treated SMNΔ7 αMNs (**Figure 23C and F**). In the case of vehicle-treated SMNΔ7 αMNs, the cytoplasmic signal of polyadenylated mRNAs was notably reduced as compared to WT αMN. Interestingly, an important fraction of nuclear poly(A) RNAs were aggregated in PARGs (**Figure 23B and E**). In contrast, the presence of PARGs was significantly reduced in Nusinersen-treated αMNs (**Figure 23G**). The few remaining PARGs probably corresponded to granules formed previous to the Nusinersen administration, either during the fetal stage or the perinatal period.

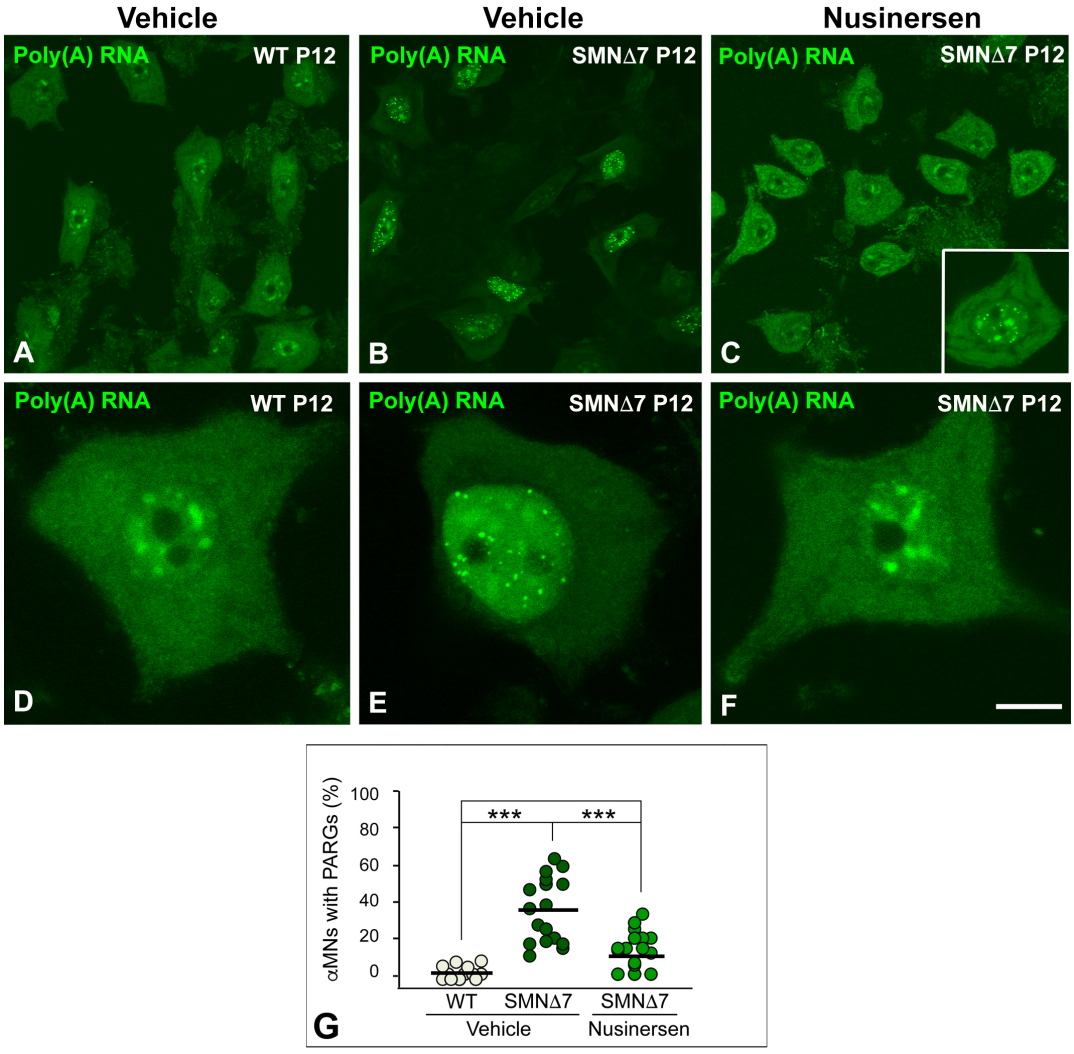

Figure 23. (A–F) FISH for poly(A) RNAs in WT (A, D), SMNΔ7 (B, E) and Nusinersen-treated SMNΔ7 (C, F) αMNs at P12. The pattern of poly(A) RNA hybridization signal was comparable between WT and Nusinersen-treated SMNΔ7 αMNs. Untreated SMNΔ7 αMNs had numerous PARGs and a notable reduction of FISH signal in the cytoplasm. PARGs were also found in Nusinersen-treated SMNΔ7 αMNs. (C, inset). Scale bars: 25 μm (A–C) and 5 μm (D–F). **(G)** Graph comparing the mean percentages of αMNs with PARGs between the three different groups. Student's t test analysis was performed using GraphPad (***p<0.0005).

The "sequestration" of polyadenylated mRNAs in PARGs may be a neuroprotective mechanism to prevent nuclear export and cytoplasmic translation of aberrant or unprocessed mRNA transcripts, which presumably are targeted for RNA decay.

Finally, we decided to investigate whether Nusinersen-induced SMN upregulation and improved RNA homeostasis was also enough to restore protein synthesis machinery. For this purpose, we used the cytochemical staining for RNA-rich structures with propidium iodide (PI). As shown in **Figure 24A**, WT αMNs showed prominent areas of the cytoplasm enriched in rough endoplasmic reticulum and free polyribosomes, classically known as "Nissl bodies". A similar distribution pattern of Nissl bodies was seen in Nusinersen-treated SMNΔ7 αMNs (**Figure 24C**). However, in vehicle-treated SMNΔ7 αMNs a severe disruption of the Nissl bodies (central chromatolysis) was observed and almost all the αMNs exhibited eccentric nuclei (**Figure 24B**).

.

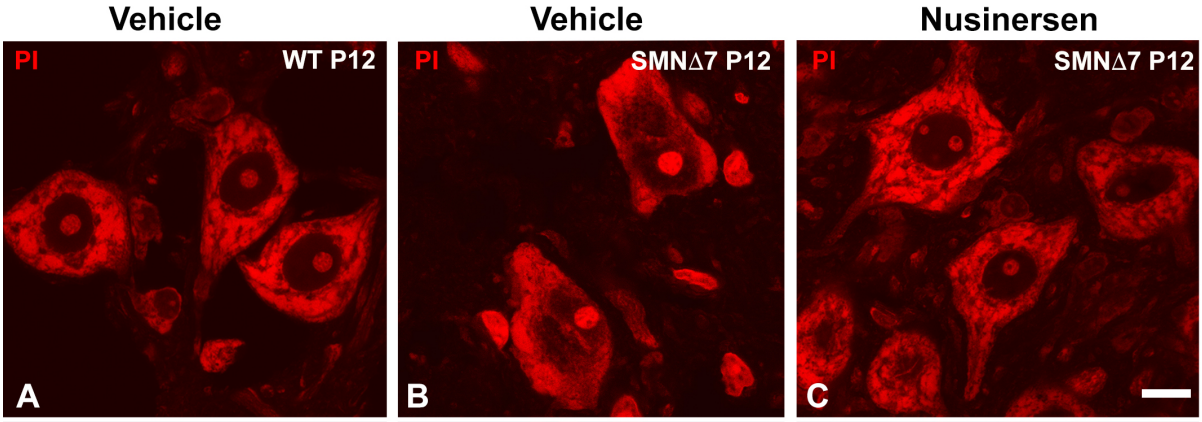

Figure 24. (A–C) Propidium iodide (PI) staining on dissociated spinal cord αMNs from WT (A), SMNΔ7 (B) and Nusinersen-treated SMNΔ7 mice (C) at P12. PI stains RNA-rich structures, showcasing the nucleolus and the protein synthesis machinery (Nissl substance). In the case of SMNΔ7 αMNs, there was a notable rescue of the Nissl bodies while, in untreated SMNΔ7 αMNs, the central chromatolysis is prominent. Scale bars: 15 μm.

DISCUSSION

As has been stated throughout this work and previous studies, αMNs are the main cellular target of SMA, although recent scientific evidence indicate the primary importance of other non-neural peripheral tissues and organs [2,3]. In type I SMA patients and mouse models of the disease, the progressive degeneration of αMNs leads to muscle denervation and muscle atrophy, eventually culminating in death by respiratory failure [10]. This degeneration is partially caused by the abnormal structural reorganization and dysfunction of nuclear compartments involved in RNA processing, as evidenced by the presence of PARGs and the depletion of CBs [57].

Previous studies from our laboratory in the SMNΔ7 mouse model of type I SMA have shown that PARGs are formed by incorrectly processed mRNAs, which retain introns and accumulate in nuclear granules, preventing the nuclear export of aberrant transcripts for translation [65]. In this context, the formation of PARGs acts as a neuroprotective mechanism, preventing the nuclear export of these aberrant transcripts to avoid spending extra energy in translating them and then clearing the resulting aberrant proteins [57,66]. However, by the same token, this leads to lower amounts of mature mRNAs for translation, resulting in a dramatic disassembly of protein synthesis machinery in the cytoplasm. The consequence is a reduced production of essential proteins for αMNs homeostasis which eventually leads to neuronal death [56,57,65].

The aim of this work is to assess the effects of Nusinersen in the SMNΔ7 mouse model of type I SMA. Previous studies have demonstrated that the administration of Nusinersen is linked to a longer lifespan and prevention of αMNs degeneration and myopathy [58,67]. This has been corroborated by our results, where Nusinersen selectively restored SMN levels in the spinal cord and contributed to normalizing the growth curve and improving motor function at the late symptomatic stage in this mouse model (P12). Furthermore, we have also confirmed that Nusinersen preserves αMN population, and the nuclear organization of mRNA processing compartments, as well as the cellular protein synthesis machinery.

One point where some studies seem to disagree, is whether SMN recovery in peripheral tissues can compensate for low levels of SMN in the spinal cord. Studies with the ASO10-27 seem to indicate that is the case [68], however, although a small amount of Nusinersen may be cleared with cerebrospinal fluid into the blood, our team and others indicate otherwise [69]. Our results support that the recovery of SMN levels in spinal cord is essential for αMN and skeletal myofiber homeostasis. In fact, the myofiber size distribution and the oxidative pattern of myofibers, estimated with the SDH assay, are rescued in our model only through spinal cord recovery, without normalizing the levels of SMN in muscle. These differences may be caused by the use of different mouse models, and treatment protocols for the ASO.

As for the molecular mechanism behind Nusinersen, by binding to the ISS-N1 in SMN2 pre-mRNA it is essential in SMN2 splicing regulation, favoring the inclusion of exon 7 into the full-length transcript [58,67,70]. In the treated SMNΔ7 group we found a recover of both number and molecular composition of CBs. CBs are transcription-dependent nuclear organelles, round shaped and approximately 0,5 μm of diameter, in which snRNP biogenesis is substantially more efficiently than in nucleoplasm [23]. In SMA, since

they lack enough SMN, CBs become disrupted, resulting in a severe inhibition of spliceosomal snRNP biogenesis and reduced availability of mature snRNP for the spliceosome assembly [22]. Depletion of CBs leads to a decrease in proper pre-mRNA splicing of several mRNAs essential for αMNs physiology, a lack of those in the cell and eventual αMN degeneration. For this reason, the depletion of CBs and the relocalization of coilin, the main molecular marker of CBs, as perinucleolar caps, are considered ~~an~~ early signs of neuronal dysfunction [37,56,60].

As evidence of this Nusinersen-induced recovery of transcription, our results show that *Chodl* and *ChAT* mRNAs – both essential for αMN survival [61,62]– are expressed at normal levels in Nusinersen-treated SMNΔ7 mice. This is consistent with the increase in canonical CBs, and the recovery of the protein synthesis machinery [18]. Moreover, we show that Nusinersen rescues the normal compartmentalization of polyadenylated mRNAs. It is well established that all mRNAs, except for histone mRNAs, are polyadenylated in the nucleus as part of a nuclear export signal, which is also needed for translation [71]. In SMA and other diseases, these polyadenylated mRNAs have been shown to form granules in the nucleoplasm (PARGs) [57]. Our results suggest that PARGs contain unspliced or aberrant transcripts that become sequestered in the nucleus. In this context, the formation of PARGs has been associated with a splicing perturbation partially caused by a defective snRNP biogenesis in CBs. Indeed, in Nusinersen-treated SMNΔ7 mice, in which CB number is normalized in αMNs, the incidence of PARGs is very reduced when compared to untreated SMNΔ7 neurons depleted of CBs. We believe that the reason why PARGs do not completely disappear, is because low levels of SMN start to affect the neurons *in utero* and some PARGs can persist from the fetal or neonatal period, prior to Nusisnersen administration. Therefore, the reduced number of PARGs found in Nusinersen-treated animals is consistent with the rescue of CB number, as well as the recovery of mRNA processing machinery and export.

In conclusion, in this work we demonstrate that there is a Nusinersen-dependent rescue of (i) molecular assembly of canonical CBs, (ii) expression of *Chodl* and *ChAT* primary transcripts, (iii) nuclear and cytoplasmic distribution of polyadenylated mRNAs and (iv) the organization of the protein synthesis machinery in αMNs of the SMNΔ7 mouse. This recovery seems essential for neuronal homeostasis and survival. Moreover, the αMN survival has been shown to partially recover the myopathy present in this disease. The reason for the incomplete recovery of the peripheral tissues, particularly of the muscle, may be the ICV administration of the ASO, which prevents Nusinersen from reaching the tissues outside of the CNS.

In light of these findings, further studies may focus on Nusinersen's effect on skeletal myofiber pathology. SMNΔ7 myofibers show disruption of the sarcomeres and actin dynamics. To this effect, studying the simultaneous administration of Nusinersen subcutaneously and intracerebroventricularly will be necessary.

BIBLIOGRAPHY

1. Berciano, M. T. *et al.* Nusinersen ameliorates motor function and prevents motoneuron Cajal body disassembly and abnormal poly(A) RNA distribution in a SMA mouse model. *Sci. Rep.* **10**, 10738 (2020).
2. Singh, R. N., Howell, M. D., Ottesen, E. W. & Singh, N. N. Diverse role of survival motor neuron protein. *Biochimica et Biophysica Acta - Gene Regulatory Mechanisms* **1860**, 299–315 (2017).
3. Chaytow, H., Huang, Y.-T., Gillingwater, T. H. & Faller, K. M. E. The role of survival motor neuron protein (SMN) in protein homeostasis. *Cell. Mol. Life Sci.* **75**, 3877–3894 (2018).
4. Burghes, A. H. M. & Beattie, C. E. Spinal muscular atrophy: Why do low levels of survival motor neuron protein make motor neurons sick? *Nat. Rev. Neurosci.* **10**, 597–609 (2009).
5. Martínez Hernández, R. Tesis Doctoral: Desarrollo neuromuscular en la atrofia muscular espinal. (Universidad de Barcelona, 2012).
6. Berciano, M. T. *et al.* Mislocalization of SMN from the I-band and M-band in human skeletal myofibers in spinal muscular atrophy associates with primary structural alterations of the sarcomere. *Cell Tissue Res.* 1–18 (2020).
7. Wang, C. H. *et al.* Consensus Statement for Standard of Care in Spinal Muscular Atrophy Current Problems in the Medical Care of Patients With Spinal Muscular Atrophy Spinal muscular atrophy is a recessively inherited neuro-muscular disease characterized by degeneration of spinal. *J. Child Neurol.* **22**, 1027–1049 (2007).
8. Tizzano, E. F. *Prevención de la discapacidad. Atrofia Muscular Espinal: Contribuciones para el conocimiento, prevención y tratamiento de la enfermedad y para la organización de familias. Ministerio de Trabajo y Asuntos Sociales* (2007).
9. Tisdale, S. & Pellizzoni, L. Disease mechanisms and therapeutic approaches in spinal muscular atrophy. *J. Neurosci.* **35**, 8691–8700 (2015).
10. Lefebvre, S. *et al.* Identification and characterization of a spinal muscular atrophy-determining gene. *Cell* **80**, 155–165 (1995).
11. Lefebvre, S. *et al.* Correlation between severity and SMN protein level in spinal muscular atrophy. *Nat. Genet.* **16**, 265–269 (1997).
12. Grotto, S. *et al.* Type 0 Spinal Muscular Atrophy: Further Delineation of Prenatal and Postnatal Features in 16 Patients. *J. Neuromuscul. Dis.* **3**, 487–495 (2016).
13. Brzustowicz, L. M. *et al.* Genetic mapping of chronic childhood-onset spinal muscular atrophy to chromosome 5q1 1.2-13.3. *Nature* **344**, 540–541 (1990).
14. Melki, J. *et al.* Mapping of acute (type I) spinal muscular atrophy to chromosome 5q12-q14. *Lancet* **336**, 271–273 (1990).
15. Rochette, C. F., Gilbert, N. & Simard, L. R. SMN gene duplication and the emergence of the SMN2 gene occurred in distinct hominids: SMN2 is unique to Homo sapiens. *Hum. Genet.* **108**, 255–266 (2001).

16. Singh, R. N. & Singh, N. N. Mechanism of Splicing Regulation of Spinal Muscular Atrophy Genes. *Adv Neurobiol.* **20**, 31–61 (2018).
17. Singh, N. N., Howell, M. D., Androphy, E. J. & Singh, R. N. How the discovery of ISS-N1 led to the first medical therapy for spinal muscular atrophy. *Gene Therapy* **24**, 520–526 (2017).
18. Lafarga, M., Tapia, O., Romero, A. M. & Berciano, M. T. Cajal bodies in neurons. *RNA Biol.* **14**, 712–725 (2017).
19. Li, D. K., Tisdale, S., Lotti, F. & Pellizzoni, L. SMN control of RNP assembly: From post-transcriptional gene regulation to motor neuron disease. *Seminars in Cell and Developmental Biology* **32**, 22–29 (2014).
20. Gray, K. M. *et al.* Self-oligomerization regulates stability of survival motor neuron protein isoforms by sequestering an SCF Slmb degron . *Mol. Biol. Cell* **29**, 96–110 (2018).
21. Barquín, A. Tesis Doctoral: Disfunción del Metabolismo del RNA en las motoneuronas de la Atrofia Muscular Espinal. (Universidad de Cantabria, 2018).
22. Matera, A. G. & Wang, Z. A day in the life of the spliceosome. *Nature Reviews Molecular Cell Biology* **15**, 108–121 (2014).
23. Machyna, M., Heyn, P. & Neugebauer, K. M. Cajal bodies: Where form meets function. *Wiley Interdisciplinary Reviews: RNA* **4**, 17–34 (2013).
24. Rossoll, W. *et al.* Smn, the spinal muscular atrophy-determining gene product, modulates axon growth and localization of-actin mRNA in growth cones of motoneurons. *J. Cell Biol.* **163**, 801–812 (2003).
25. Jablonka, S. *et al.* Co-regulation of survival of motor neuron (SMN) protein and its interactor SIP1 during development and in spinal muscular atrophy. *Hum. Mol. Genet.* **10**, 497–505 (2001).
26. Giavazzi, A., Setola, V., Simonati, A. & Battaglia, G. Neuronal-Specific Roles of the Survival Motor Neuron Protein. *J. Neuropathol. Exp. Neurol.* **65**, 267–277 (2006).
27. Rossoll, W. *et al.* Specific interaction of Smn, the spinal muscular atrophy determining gene product, with hnRNP-R and gry-rbp/hnRNP-Q: A role for Smn in RNA processing in motor axons? *Hum. Mol. Genet.* **11**, 93–105 (2002).
28. Fallini, C., Donlin-Asp, P. G., Rouanet, J. P., Bassell, G. J. & Rossoll, W. Deficiency of the survival of motor neuron protein impairs mrna localization and local translation in the growth cone of motor neurons. *J. Neurosci.* **36**, 3811–3820 (2016).
29. Sanchez, G. *et al.* A novel function for the survival motoneuron protein as a translational regulator. *Hum. Mol. Genet.* **22**, 668–684 (2013).
30. Catapano, F. *et al.* Altered Levels of MicroRNA-9, -206, and -132 in Spinal Muscular Atrophy and Their Response to Antisense Oligonucleotide Therapy. (2016).
31. Kye, M. J. eon. *et al.* SMN regulates axonal local translation via miR-183/mTOR pathway. *Hum. Mol. Genet.* **23**, 6318–6331 (2014).
32. Ning, K. *et al.* PTEN depletion rescues axonal growth defect and improves survival in SMN-

deficient motor neurons. *Hum. Mol. Genet.* **19**, 3159–3168 (2010).

33. Narcís Majos, J. O. Tesis Doctoral: Disfunción de la biogénesis de pre-mRNAs y pre-rRNAs en motoneuronas en el modelo murino SMNΔ7 de atrofia muscular espinal. (Universidad de Cantabria, 2019).
34. Stifani, N. Motor neurons and the generation of spinal motor neuron diversity. *Frontiers in Cellular Neuroscience* **8**, 293 (2014).
35. Ross, M. H. & Pawlina, W. Capítulo 11. Tejido muscular. in *Histología Texto y Atlas. Correlación con biología celular y molecular.* 339–384 (Wolters Kluwer, 2015).
36. Manuel, M. & Zytnicki, D. Alpha, beta and gamma motoneurons: Functional diversity in the motor systems final pathway. *J. Integr. Neurosci.* **10**, 243–276 (2011).
37. Tapia, O. *et al.* Reorganization of Cajal bodies and nucleolar targeting of coilin in motor neurons of type i spinal muscular atrophy. *Histochem. Cell Biol.* **137**, 657–667 (2012).
38. Tisdale, S. & Pellizzoni, L. RNA-Processing Dysfunction in Spinal Muscular Atrophy. in *Spinal Muscular Atrophy: Disease Mechanisms and Therapy* 113–131 (Elsevier Inc., 2017).
39. Ibrahim, F., Nakaya, T. & Mourelatos, Z. RNA dysregulation in diseases of motor neurons. *Annual Review of Pathology: Mechanisms of Disease* **7**, 323–352 (2012).
40. Boyer, J. G., Bowerman, M. & Kothary, R. The many faces of SMN: deciphering the function critical to spinal muscular atrophy pathogenesis. *Future Neurol.* **5**, 873–890 (2010).
41. Bowerman, M. *et al.* Therapeutic strategies for spinal muscular atrophy: SMN and beyond. *DMM Disease Models and Mechanisms* **10**, 943–954 (2017).
42. Talbot, K. & Tizzano, E. F. The clinical landscape for SMA in a new therapeutic era. *Gene Therapy* **24**, 529–533 (2017).
43. Rao, V. K., Kapp, D. & Schroth, M. *Journal of Managed Care & Specialty Pharmacy Gene Therapy for Spinal Muscular Atrophy: An Emerging Treatment Option for a Devastating Disease. Journal of Managed Care & Specialty Pharmacy ® Previously published as JMCP, the Journal of Managed Care Pharmacy ® A Peer-Reviewed Journal of the Academy of Managed Care Pharmacy* ■ **24**, (2018).
44. Shorrock, H. K., Gillingwater, T. H. & Groen, E. J. N. Overview of Current Drugs and Molecules in Development for Spinal Muscular Atrophy Therapy. *Drugs* **78**, 293–305 (2018).
45. Duque, S. I. *et al.* A large animal model of spinal muscular atrophy and correction of phenotype. *Ann. Neurol.* **77**, 399–414 (2015).
46. Finkel, R. S. *et al.* Nusinersen versus Sham Control in Infantile-Onset Spinal Muscular Atrophy. *N. Engl. J. Med.* **377**, 1723–1732 (2017).
47. Le, T. T. *et al.* SMNΔ7, the major product of the centromeric survival motor neuron (SMN2) gene, extends survival in mice with spinal muscular atrophy and associates with full-length SMN. *Hum. Mol. Genet.* **14**, 845–857 (2005).
48. Glascock, J. J. *et al.* Delivery of therapeutic agents through intracerebroventricular (ICV) and intravenous (IV) injection in mice. *J. Vis. Exp.* 2968 (2011).

49. Altman, J. & Sudarshan, K. Postnatal development of locomotion in the laboratory rat. *Anim. Behav.* **23**, 896–920 (1975).
50. Feather-Schussler, D. N. & Ferguson, T. S. A battery of motor tests in a neonatal mouse model of cerebral palsy. *J. Vis. Exp.* **117**, 53569 (2016).
51. Pena, E., Berciano, M., Fernandez, R., Ojeda, J. & Lafarga, M. Neuronal body size correlates with the number of nucleoli and Cajal bodies, and with the organization of the splicing machinery in rat trigeminal ganglion neurons. *J. Comp. Neurol.* **430**, 250–263 (2001).
52. Baltanás, F. C. *et al.* Nucleolar disruption and cajal body disassembly are nuclear hallmarks of DNA damage-induced neurodegeneration in Purkinje cells. *Brain Pathol.* **21**, 374–388 (2011).
53. Livak, K. J. & Schmittgen, T. D. Analysis of Relative Gene Expression Data Using Real-Time Quantitative PCR and the 2−ΔΔCT Method. *Methods* **25**, 402–408 (2001).
54. Mercuri, E. *et al.* Nusinersen versus Sham Control in Later-Onset Spinal Muscular Atrophy. *N. Engl. J. Med.* **378**, 625–635 (2018).
55. Gidaro, T. & Servais, L. Nusinersen treatment of spinal muscular atrophy: current knowledge and existing gaps. *Developmental Medicine and Child Neurology* **61**, 19–24 (2019).
56. Tapia, O. *et al.* Cellular bases of the RNA metabolism dysfunction in motor neurons of a murine model of spinal muscular atrophy: Role of Cajal bodies and the nucleolus. *Neurobiol. Dis.* **108**, 83–99 (2017).
57. Narcís, J. O. *et al.* Accumulation of poly(A) RNA in nuclear granules enriched in Sam68 in motor neurons from the SMNΔ7 mouse model of SMA. *Sci. Rep.* **8**, (2018).
58. Passini, M. A. *et al.* Antisense Oligonucleotides Delivered to the Mouse CNS Ameliorate Symptoms of Severe Spinal Muscular Atrophy. *Sci Transl Med.* **3**, (2011).
59. Geary, R. S., Yu, R. Z. & Levin, A. A. Pharmacokinetics of phosphorothioate antisense oligodeoxynucleotides. *Curr. Opin. Investig. Drugs* **2**, 562–573 (2001).
60. Lafarga, M., Casafont, I., Bengoechea, R., Tapia, O. & Berciano, M. T. Cajal's contribution to the knowledge of the neuronal cell nucleus. *Chromosoma* **118**, 437–443 (2009).
61. Zhong, Z. *et al.* Chondrolectin mediates growth cone interactions of motor axons with an intermediate target. *J. Neurosci.* **32**, 4426–4439 (2012).
62. Sleigh, J. N. *et al.* Chondrolectin affects cell survival and neuronal outgrowth in in vitro and in vivo models of spinal muscular atrophy. *Hum. Mol. Genet.* **23**, 855–869 (2014).
63. Bäumer, D. *et al.* Alternative Splicing Events Are a Late Feature of Pathology in a Mouse Model of Spinal Muscular Atrophy. *PLoS Genet.* **5**, e1000773 (2009).
64. Bernabò, P. *et al.* In Vivo Translatome Profiling in Spinal Muscular Atrophy Reveals a Role for SMN Protein in Ribosome Biology. *Cell Rep.* **21**, 953–965 (2017).
65. Jangi, M. *et al.* SMN deficiency in severe models of spinal muscular atrophy causes widespread intron retention and DNA damage. *Proc. Natl. Acad. Sci. U. S. A.* **114**, E2347–E2356 (2017).
66. Shan, P. *et al.* SIRT1 Functions as a Negative Regulator of Eukaryotic Poly(A)RNA Transport. *Curr.*

Biol. **27**, 2271-2284.e5 (2017).

67. Hua, Y. *et al.* Antisense correction of SMN2 splicing in the CNS rescues necrosis in a type III SMA mouse model. *Genes Dev.* **24**, 1634–1644 (2010).
68. Hua, Y. *et al.* Motor neuron cell-nonautonomous rescue of spinal muscular atrophy phenotypes in mild and severe transgenic mouse models. *Genes Dev.* **29**, 288–297 (2015).
69. Porensky, P. N. *et al.* A single administration of morpholino antisense oligomer rescues spinal muscular atrophy in mouse. *Hum. Mol. Genet.* **21**, 1625–1638 (2012).
70. Hua, Y., Vickers, T. A., Okunola, H. L., Bennett, C. F. & Krainer, A. R. Antisense Masking of an hnRNP A1/A2 Intronic Splicing Silencer Corrects SMN2 Splicing in Transgenic Mice. *Am. J. Hum. Genet.* **82**, 834–848 (2008).
71. Kühn, U. & Wahle, E. Structure and function of poly(A) binding proteins. *Biochimica et Biophysica Acta - Gene Structure and Expression* **1678**, 67–84 (2004).
72. Eldeiry, M., Yamanaka, K., Reece, T. B. & Aftab, M. Spinal cord neurons isolation and culture from neonatal mice. *J. Vis. Exp.* **125**, e55856 (2017).
73. Lin, Y. T. & Chen, J. C. Dorsal root ganglia isolation and primary culture to study neurotransmitter release. *J. Vis. Exp.* **140**, e57569 (2018).
74. Wang, C., Yue, F. & Kuang, S. Muscle Histology Characterization Using H&E Staining and Muscle Fiber Type Classification Using Immunofluorescence Staining. *BIO-PROTOCOL* **7**, (2017).

ANNEX

SCIENTIFIC REPORTS
nature research

Check for updates

OPEN

Nusinersen ameliorates motor function and prevents motoneuron Cajal body disassembly and abnormal poly(A) RNA distribution in a SMA mouse model

María T. Berciano[1,4,5,8], Alba Puente-Bedia[2,8], Almudena Medina-Samamé[3], José C. Rodríguez-Rey[1,4], Jordi Calderó[6], Miguel Lafarga[3,4,5] & Olga Tapia[4,5,7]✉

Spinal muscular atrophy (SMA) is a devastating autosomal recessive neuromuscular disease characterized by degeneration of spinal cord alpha motor neurons (αMNs). SMA is caused by the homozygous deletion or mutation of the *survival motor neuron 1* (*SMN1*) gene, resulting in reduced expression of SMN protein, which leads to αMN degeneration and muscle atrophy. The majority of transcripts of a second gene (*SMN2*) generate an alternative spliced isoform that lacks exon 7 and produces a truncated nonfunctional form of SMN. A major function of SMN is the biogenesis of spliceosomal snRNPs, which are essential components of the pre-mRNA splicing machinery, the spliceosome. In recent years, new potential therapies have been developed to increase SMN levels, including treatment with antisense oligonucleotides (ASOs). The ASO-nusinersen (Spinraza) promotes the inclusion of exon 7 in *SMN2* transcripts and notably enhances the production of full-length SMN in mouse models of SMA. In this work, we used the intracerebroventricular injection of nusinersen in the SMNΔ7 mouse model of SMA to evaluate the effects of this ASO on the behavior of Cajal bodies (CBs), nuclear structures involved in spliceosomal snRNP biogenesis, and the cellular distribution of polyadenylated mRNAs in αMNs. The administration of nusinersen at postnatal day (P) 1 normalized SMN expression in the spinal cord but not in skeletal muscle, rescued the growth curve and improved motor behavior at P12 (late symptomatic stage). Importantly, this ASO recovered the number of canonical CBs in MNs, significantly reduced the abnormal accumulation of polyadenylated RNAs in nuclear granules, and normalized the expression of the pre-mRNAs encoding chondrolectin and choline acetyltransferase, two key factors for αMN homeostasis. We propose that the splicing modulatory function of nusinersen in SMA αMN is mediated by the rescue of CB biogenesis, resulting in enhanced polyadenylated pre-mRNA transcription and splicing and nuclear export of mature mRNAs for translation. Our results support that the selective restoration of SMN expression in the spinal cord has a beneficial impact not only on αMNs but also on skeletal myofibers. However, the rescue of SMN expression in muscle appears to be necessary for the complete recovery of motor function.

Spinal muscular atrophy (SMA) is an autosomal recessive neuromuscular disease that is considered the main genetic cause of infant mortality. SMA is caused by the homozygous loss or mutation of the *survival of motor*

[1]Department of Molecular Biology, University of Cantabria, Santander, Spain. [2]Department of Physiology and Pharmacology, University of Cantabria, Santander, Spain. [3]Department of Anatomy and Cell Biology, University of Cantabria, Santander, Spain. [4]"Instituto de Investigación Marqués de Valdecilla" (IDIVAL), Santander, Spain. [5]"Centro de Investigación Biomédica en Red Sobre Enfermedades Neurodegenerativas" (CIBERNED), Madrid, Spain. [6]Department of Experimental Medicine and "Institut de Recerca Biomèdica de Lleida" (IRBLleida), University of Lleida, Lleida, Spain. [7]"Universidad Europea del Atlántico", Santander, Spain. [8]These authors contributed equally: María T. Berciano and Alba Puente-Bedia ✉email: otapia@idival.org

neuron 1 (*SMN1*) gene, leading to reduced levels of full-length SMN protein. SMN depletion triggers the selective degeneration of lower alpha motor neurons (αMNs), resulting in preferential atrophy of the proximal skeletal muscles with weakness and muscle paralysis[1–3].

In addition to the *SMN1* gene, humans ubiquitously express one or several copies of a closely related paralog gene called *SMN2*. This gene encodes a full-length SMN protein but presents one consistent difference, that is, the transition C to T (C6T) in exon 7. This change deactivates a splicing enhancer and introduces a splicing silencer, resulting in the exclusion of exon 7 in most *SMN2* transcripts[4,5]. These transcripts are translated into a truncated SMN (SMNΔ7) protein that is rapidly ubiquitylated and degraded by the proteasome system[5–7]. Although the expression of the *SMN2* gene is residual under physiological conditions, the deletion or mutation of *SMN1* confers the number of copies of *SMN2* considerable importance in modifying the severity of SMA phenotypes. Thus, the most severe and frequent SMA is that of type I, which usually has two copies of the *SMN2* gene. Patients with type II or III SMA have a higher copy number of *SMN2*[8–11].

The functional full-length SMN protein homo-oligomerizes and forms a stable complex (SMN-complex) with Gemin2-8 and Unrip proteins[3,12]. The SMN complex acts as a molecular chaperone to assist the cytoplasmic stage of the assembly of spliceosomal U snRNPs, which are essential splicing factors of the spliceosome[13,14]. Linked to this function of the SMN complex, the Cajal body (CB) is particularly relevant, given its implication in the biogenesis of both spliceosomal U snRNPs and nucleolar snoRNPs[15–18]. In particular, the enrichment of the CB in spliceosomal U snRNPs is consistent with the growing evidence of a spatial association of this organelle with certain transcriptionally active genomic loci of snRNAs[17,19–21]. Moreover, the physical association of CBs with the dense fibrillar component of the nucleolus, the site of synthesis and early processing of pre-rRNAs provides a molecular link for a nucleolus-CB interaction[18,22–24].

In this context, recent studies from our laboratory have shown that reduced SMN levels in αMNs of a type I SMA patient and the SMNΔ7 mouse model induce nuclear features of αMN degeneration, including depletion of canonical CBs, nucleolar stress and altered mRNA processing[25,26]. The dysfunction of mRNA processing in this SMA mouse is also characterized by (i) the early and progressive accumulation of polyadenylated mRNAs in nuclear granules called PARGs ("poly(A) RNA granules"), (ii) the increase in intron-containing pre-mRNAs, and (iii) the disruption of the protein synthesis machinery[25–27]. In fact, the dysfunction of RNA metabolism has enabled us to redefine the SMA as a RNA pathology, although it could also be considered a spliceopathy[28].

To explore whether normalizing SMN expression in SMNΔ7 αMNs during the neonatal period, prior to αMN degeneration, prevents CB depletion and splicing alterations with nuclear retention of unspliced pre-mRNAs in PARGs, we treated SMNΔ7 mice with the antisense oligonucleotide (ASO) nusinersen (Spinraza). This 2′-*O*-methoxyethyl (MOE)-modified ASO was designed to increase full-length SMN protein levels by promoting the inclusion of exon 7 in *SMN2* mRNAs. Nusinersen binds to a target site within intron 7, ≅ 10 nucleotides downstream of the 5′-splice site, known as ISS-N1 (intronic splicing silencer N1)[29]. This interaction displaces the splicing suppressor proteins hnRNP A1/A2 and enables spliceosomal U1 snRNPs to bind to the 5′-splice site, thereby promoting the inclusion of exon 7 in *SMN2* transcripts[29–35]. Previous studies in mouse SMA models have demonstrated that nusinersen, when administered directly into the cerebrospinal fluid (CSF), prolongs animal survival and prevents αMN and skeletal muscle pathology[31,36,37].

Our results in SMNΔ7 αMNs show that the intracerebroventricular (ICV) injection of nusinersen at the neonatal period (postnatal day [P] 1) (i) improves motor function, (ii) rescues the CB number, (iii) increases the expression of pre-mRNAs encoding chondrolectin (*Chodl*) and choline acetyltransferase (*Chat*), two key factors for αMN homeostasis[38], and (iv) reduces the nuclear retention of polyadenylated mRNAs into PARGs at the symptomatic P12 stage. These effects are accompanied by the restoration of the protein synthesis machinery, supporting an effective recovery of mRNA processing and translation.

Results

Treatment with ASO-nusinersen (Spinraza) robustly rescues the growth curve, enhances motor function and dramatically reduces αMN loss. Based on previous studies from our laboratory, we have established two temporary windows that demarcate the clinical evolution of SMNΔ7 mice: (i) the pre-clinical phase (from P0 to P6) and (ii) the clinical phase (from P7 to P12), when the clinical symptoms appear and progress, commonly leading to the death of mice between P12 and P14.

The ICV administration of nusinersen (Fig. 1A) at P1 was well tolerated with no obvious signs of toxicity or drug-related death. First, we studied the clinical evolution of SMNΔ7 mice treated or not treated with nusinersen. We evaluated the growth curve of mice by performing daily measurement of the body weight from P1 to P12 (Fig. 1C). We noticed that nusinersen treatment had a highly significant impact on body weight gain with a growth curve comparable to that of vehicle-treated WT (hereafter referred to as WT) mice from P6 to P12 (Fig. 1B–D). In fact, nusinersen-treated SMNΔ7 mice weighed approximately twice as much as the vehicle-treated mice (hereafter referred to as SMNΔ7) at P12 (Fig. 1B–D). On the other hand, nonsignificant differences in body weight were found between WT animals treated with vehicle and nusinersen, indicating that the administration of this ASO does not modify body weight under physiological conditions ("body weight follow-up × genotype": $F_{(4,40)} = 84.23$, $p < 0.0001$; "body weight follow-up × nusinersen treatment": $F_{(4,40)} = 57.64$, $p < 0.0001$).

Next, we investigated whether nusinersen treatment improves motor functions in SMNΔ7 mice by using the righting reflex test. This test evaluates the overall muscle strength and motor coordination, which are severely affected in SMA mice due to weakness of the limb and trunk muscles. The test assesses the time taken for the mouse placed on its back to right itself through 180° to a maximum of 30 s[39]. Whereas the SMNΔ7 mice did not acquire the righting reflex during the neonatal period studied (P1-P12) (Fig. 1E), both WT mice and nusinersen-treated SMNΔ7 mice acquired this motor reflex as early as P3, although the latter showed a temporary delay in the completion of the test (Fig. 1E) ("righting reflex follow-up × genotype": $F_{(3,39)} = 14.85$, $p < 0.0001$; "righting

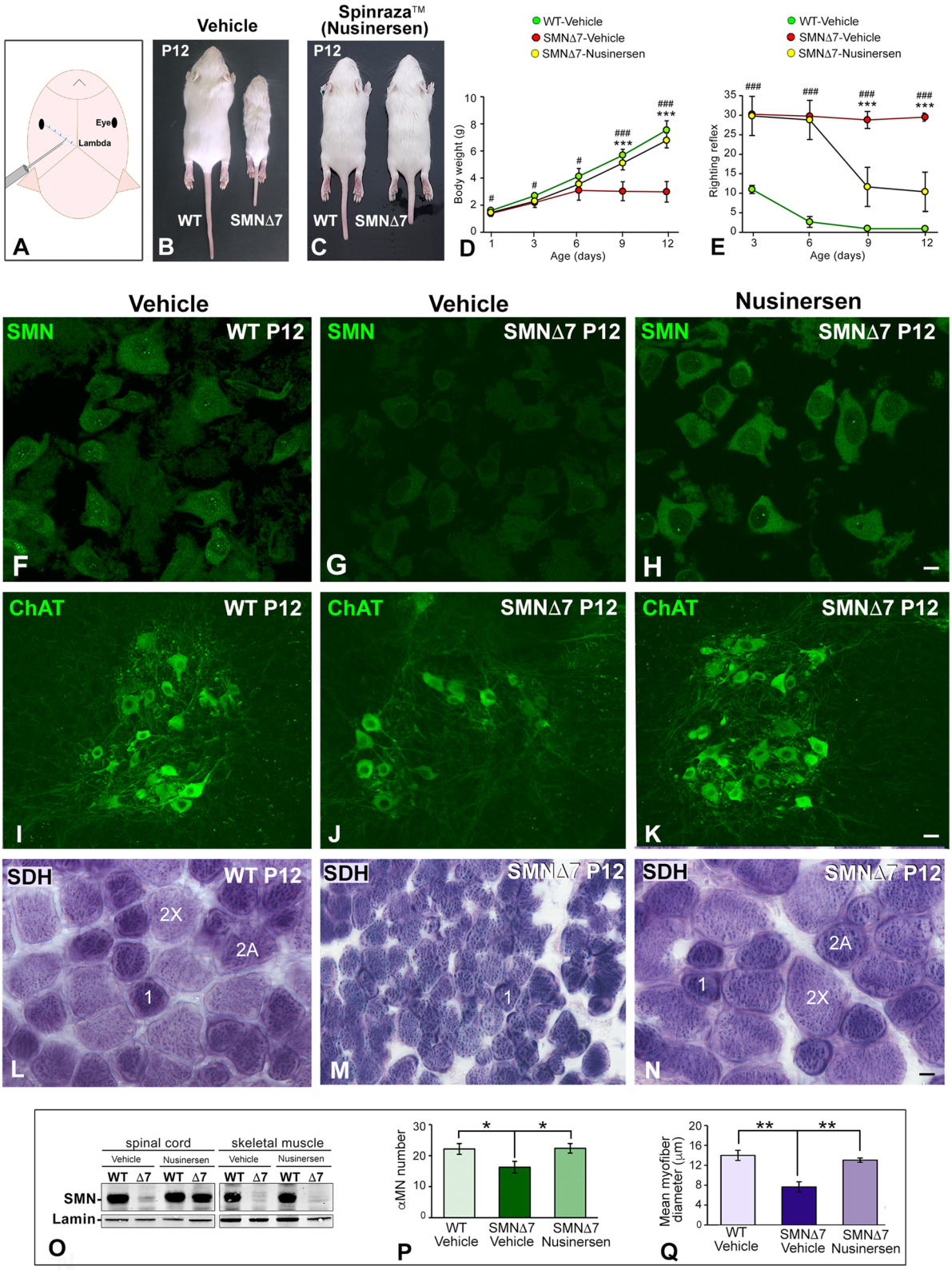

Figure 1. (**A**) Scheme illustrating the intrathecal injection point of the ASO-nusinersen (Spinraza). (**B**,**C**) Images showing differences in body size between WT and SMNΔ7 mice (**B**) and WT and nusinersen-treated SMNΔ7 mice (**C**) at P12. (**D**) Comparative analysis of body weight (mean ± SD) among WT, SMNΔ7 and nusinersen-treated SMNΔ7 mice from P0 to P12 (n = 8 mice per group). $^{\#}p < 0.01$, $^{\#\#\#}p < 0.0001$: WT vs. SMNΔ7; ***p < 0.0001: vehicle-treated SMNΔ7 vs. nusinersen-treated SMNΔ7. (**E**) Response to righting motor reflex acquisition (mean ± SD) at the indicated postnatal periods. Note how nusinersen treatment ameliorates the motor response in SMNΔ7 mice when compared to untreated SMNΔ7 mice (n = 8 mice per group). $^{\#\#\#}p < 0.0001$: WT vs. SMNΔ7; ***p < 0.0001: vehicle-treated SMNΔ7 vs. nusinersen-treated SMNΔ7.

In **C**,**D**, data were analyzed by a one-way ANOVA, followed by the Bonferroni post hoc test using SPSS. (**F**–**H**) Immunodetection of SMN reveals that nusinersen treatment rescues the typical SMN staining pattern in WT αMNs, which appears diffuse in the cytoplasm and concentrated in CBs (**F**,**H**). In contrast, αMNs from the untreated SMNΔ7 mouse exhibit a very weak cytoplasmic SMN signal and CB depletion (**G**). (**I**–**K**) Immunodetection of ChAT in the anterior horn of spinal cord showing how nusinersen treatment increases αMN number in the SMNΔ7 mouse compared with the untreated SMNΔ7 animals. (**L**–**N**) SDH histochemical staining of transverse cryosections of the TA muscle from WT, SMNΔ7 and nusinersen-treated SMNΔ7 mice at P12. In SMNΔ7 mice, this treatment rescues the myofiber phenotype found in WT muscle with a similar distribution of type 1, 2A and 2X myofibers (**L**,**N**). Note that the nusinersen-untreated SMNΔ7 muscle is preferentially composed of smaller type 1 myofibers (**M**). (**O**) Western blot analysis of SMN protein levels in whole spinal cord and skeletal muscle lysates at P12. Note the reduction in SMN levels in the spinal cord and muscle of the SMNΔ7 mouse and the recovery of SMN expression in the spinal cord but not in the muscle upon nusinersen treatment. SMN bands were normalized to lamin, and the relative expression levels of SMN were calculated using ImageJ. Full-length blots are presented in Supplementary Information. (**P**) Quantitative analysis of the number of αMNs (mean ± SD) in transverse cryosections of the spinal cord immunostained for ChAT. αMN counts were performed on the hemispinal cords of WT, SMNΔ7 and nusinersen-treated SMNΔ7 mice at P12. $*p < 0.05$ when WT and SMNΔ7 or vehicle-treated SMNΔ7 vs. nusinersen-treated SMNΔ7 mice were compared (n = 4 per group, Student's *t* test analysis was performed using GraphPad). (**Q**) Quantitative analysis of the myofiber diameter (mean ± SD) on transverse cryosections of the TA muscle histochemically stained for SDH detection. Measurements were performed in WT, SMNΔ7 and nusinersen-treated SMNΔ7 mouse muscles at P12. $**p < 0.005$ when WT and SMNΔ7 or vehicle-treated SMNΔ7 vs. nusinersen-treated SMNΔ7 mice were compared (n = 4 per group, Student's *t* test analysis was performed using GraphPad). Scale bars: 10 μm (**F**–**H**), 30 μm (**I**–**K**) and 5 μm (**L**–**N**).

reflex follow-up × nusinersen treatment": $F_{(3,39)} = 72.77$, $p < 0.0001$). Moreover, whereas SMNΔ7 mice exhibited very severe muscular atrophy, which affects the ability of moving, nusinersen-treated SMNΔ7 mice exhibited moderate hindlimb atrophy and preserved ambulation capacity; however, moderate hindlimb paresis was noticeable in these animals compared to WT mice (see Supplementary Video S1).

To determine whether the clinical improvement of nusinersen-treated SMNΔ7 mice was produced by normalizing SMN levels in the spinal cord, we performed a western blot analysis in tissue lysates at P12. The results in SMNΔ7 mice showed that nusinersen treatment increased SMN expression by 2.5 times in the spinal cord compared with untreated animals. The increase reached approximately 70% of SMN levels from WT samples (Fig. 1O). Next, we investigated whether nusinersen treatment modified SMN protein levels in muscle, a peripheral tissue essentially involved in SMA pathogenesis[40,41]. Western blot analysis of the tibialis anterior (TA) muscle lysates revealed that the neonatal ICV delivery of nusinersen in SMNΔ7 mice did not increase SMN expression in muscle at P12 (Fig. 1O). This result suggests that the therapeutic agent did not cross the blood–brain barrier in neonatal mice, and consequently, the beneficial clinical effect of nusinersen treatment should be mainly due to increased SMN expression in the spinal cord. Consistent with this view, SMN immunolabeling of dissociated αMNs showed that the staining pattern in nusinersen-treated SMNΔ7 neurons was similar to that found in WT neurons. SMN was diffusely distributed in the cytoplasm with a moderate intensity of fluorescent signal. In the nucleus SMN was specifically concentrated in CBs (Fig. 1F,H). Interestingly, αMNs from SMNΔ7 mice exhibited a notably weak cytoplasmic signal of SMN, and CBs were rarely observed (Fig. 1G).

To further understand the effects of nusinersen treatment on the survival of SMNΔ7 αMNs, we performed a quantitative analysis on spinal cord cryosections (lumbosacral region) immunostained for ChAT, a marker of αMNs[40,42]. As expected, nusinersen treatment preserved the population of αMNs in the anterior horn (Fig. 1I,K). Thus, no significant differences in the mean number of αMNs per section were found between WT mice and nusinersen-treated SMNΔ7 animals (Fig. 1P). In contrast, differences were significant when these two groups were compared with SMNΔ7 mice, which had an overt depletion of αMNs (Fig. 1J–K,P).

Since nusinersen treatment prevents αMN death and presumably the formation and maintenance of the neuromuscular junction, we next investigated whether this ASO can prevent muscle atrophy induced by neurogenic myopathy in SMNΔ7 mice. We estimated the myofiber size distribution on cross-cryosections of the TA muscle using the histochemical enzymatic assay for succinate dehydrogenase (SDH), a marker of mitochondrial oxidative activity[40]. Interestingly, despite the reduced SMN expression in the muscle of nusinersen-treated SMNΔ7 mice, nonsignificant differences in myofiber diameter were found between WT mice and nusinersen-treated SMNΔ7 mice at P12 (Fig. 1Q). However, a significant reduction in the myofiber diameter was detected in SMNΔ7 mice compared with nusinersen-treated mice (Fig. 1Q). Moreover, SDH histochemistry revealed that both WT and nusinersen-treated SMNΔ7 myofibers exhibited a staining checkboard pattern of a mixed muscle with a similar proportion of myofibers whose SDH oxidative activity corresponded to type 1, 2A and 2X (Fig. 1L,N). In contrast, vehicle-treated SMNΔ7 myofibers were clearly atrophic with reduced diameter and an oxidative intensity of stain predominantly corresponding to aerobic type 1 myofibers (Fig. 1M,Q). It should be noted that the administration of nusinersen in WT mice did not change the SDH pattern detected in vehicle-treated WT mice (data not shown).

Nusinersen treatment prevents the disruption and loss of canonical Cajal bodies (CBs) in αMNs of the SMA mouse. The CB is a transcription-dependent nuclear organelle whose number and size accommodate the cellular demands of pre-mRNA splicing[16,18]. Consistent with this notion, our previous studies in αMNs from an SMA patient and the SMNΔ7 mouse have shown that the αMN degeneration caused by SMN

deficiency includes an early depletion of canonical CBs and relocalization of coilin as perinucleolar caps and/or within the nucleolus[18,25]. Based on this observation, we considered that the disruption of CBs is an early nuclear sign of αMN degeneration in SMA.

Having established that nusinersen treatment preserves the normal population of αMNs and increases SMN protein levels in the spinal cord, we next investigated whether this agent rescues the formation and assembly of canonical CBs in SMNΔ7 αMNs. Double immunolabeling for coilin and SMN revealed the typical cytoplasmic distribution of SMN and the regular presence of canonical CBs, which concentrate coilin and SMN[16,18], in both WT and nusinersen-treated SMNΔ7 αMNs (Fig. 2A,C,D,F). Moreover, these canonical CBs showed a preferential association with the nucleolus (Fig. 2D,F), as previously reported in other mammalian neurons[18,22]. In contrast, the reduced cytoplasmic SMN staining observed in SMNΔ7 αMNs was accompanied by depletion of canonical CBs and formation of coilin-positive perinucleolar caps, where SMN was not or only slightly detected (Fig. 2B,E). Plots of linear profiles of coilin and SMN fluorescence intensity signals confirmed the colocalization of both molecules in canonical CBs and the absence of SMN in the perinucleolar caps (see Supplementary Fig. S2, A–C).

The neuroprotective effect of nusinersen treatment on SMNΔ7 αMNs was validated by a quantitative analysis of the mean number of CBs per nucleus in neuronal dissociates coimmunostained for coilin and SMN. Nonsignificant differences in the mean number of canonical CBs were detected between WT and nusinersen-treated SMNΔ7 αMNs at P12 (n = 4; 2.44 ± 0.34 vs. 2.94 ± 0.54; $p = 0.18$) (Fig. 2A,C). However, in the neurodegenerative phase of SMNΔ7 αMNs (P12), CB number was dramatically reduced compared with WT αMNs (n = 4; 0.08 ± 0.28 in SMNΔ7, vs. 2.44 ± 0.34 in WT; $p = 0.00009$) (Fig. 2A,B).

To further characterize the molecular organization of CBs, we performed double immunolabeling for coilin in combination with either TMG-cap, a marker of spliceosomal snRNPs that recognizes the 5′ end of snRNAs[43], or fibrillarin, a nucleolar snoRNP shared with the CB[18,22]. As expected, both TMG-cap and fibrillarin signals colocalized with coilin in the CBs of WT αMNs and nusinersen-treated SMNΔ7 αMNs (Fig. 2G,I,J,L; Supplementary Fig. S2D, F, G and I), indicating that these nuclear bodies are canonical functional CBs that concentrate splicing factors and snoRNPs in addition to coilin and SMN[16,44]. In contrast, perinucleolar caps of SMNΔ7 αMNs lacked a TMG-cap signal and had weak staining for fibrillarin (Fig. 2H,K).

Finally, it is noteworthy that Gems, coilin-negative and SMN-positive nuclear bodies[45,46] are conspicuously absent in αMNs in all experimental groups studied.

Nusinersen treatment rescues the transcription rate of *Chodl* and *ChAT* pre-mRNAs. Previous studies have demonstrated widespread defects in transcription and pre-mRNA splicing of essential genes for αMN homeostasis in cellular and animal models of SMA[27,47–51]. Among these genes, *Chodl* (chondrolectin) and *ChAT* (choline acetyltransferase) are highly expressed in αMNs, playing crucial functions in motor axon growth and neurotransmission, respectively[38,52]. Moreover, Chodl and ChAT are major gene products with dysregulated expression in SMA mouse αMNs[27,38].

To determine whether nusinersen treatment is able to rescue the transcription rate of *Chodl* and *ChAT*, we analyzed the expression levels of both pre-mRNAs by qRT-PCR in spinal cord RNA extracts at P12. We found a significant reduction in *Chodl* and *ChAT* pre-mRNAs in SMNΔ7 samples compared with WT samples (Fig. 3A). Remarkably, nusinersen treatment in SMNΔ7 mice rescued the transcription rates of both genes, which reached pre-mRNA levels comparable to WT ones (Fig. 3A).

Nusinersen treatment normalizes the distribution of the protein synthesis machinery and polyadenylated mRNAs in SMNΔ7 mice. Our group and others have previously shown a severe perturbation of the protein synthesis machinery with a remarkable nuclear and cytoplasmic redistribution of polyadenylated RNAs and chromatolysis in αMNs of SMA mouse models[26,27,53]. On this basis, we investigated whether nusinersen treatment is able to prevent this severe perturbation of neuronal homeostasis in SMNΔ7 αMNs. Cytochemical staining of RNA-rich structures with propidium iodide revealed prominent Nissl bodies (cytoplasmic areas enriched in rough endoplasmic reticulum and free polyribosomes[54]) distributed throughout the cytoplasm in both WT and nusinersen-treated SMNΔ7 αMNs (Fig. 3C,E). In contrast, most αMNs from SMNΔ7 mice exhibited different degrees of disruption of Nissl bodies, particularly central chromatolysis (Fig. 3D).

Next, we analyzed whether nusinersen treatment preserves the normal distribution of poly(A) RNAs, which include all mRNAs with the exception of histone mRNAs, as an indicator of proper nuclear mRNA processing and export to the cytoplasm. In situ hybridization with the poly-dT probe revealed that poly(A) RNA appeared diffusely distributed throughout the nucleus (excluding the nucleolus), highly concentrated in nuclear speckles and accumulated in extensive cytoplasmic areas of WT αMNs (Fig. 3F,I). In contrast, SMNΔ7 αMNs displayed a prominent nuclear aggregation of poly(A) RNAs in PARGs (Fig. 3G,J), round sharply defined bodies previously reported in mouse SMA αMNs and other neurons under stress conditions[27,55,56]. In addition, we found a cytoplasmic reduction in the poly(A) RNA hybridization signal, suggesting a decreased availability of mRNA for translation (Fig. 3G,J). Interestingly, SMNΔ7 αMNs treated with nusinersen tended to normalize the nuclear and cytoplasmic distribution of polyadenylated mRNAs observed in WT αMNs (Fig. 3H,K). Furthermore, the proportion of αMNs carrying PARGs was significantly reduced in nusinersen-treated SMNΔ7 mice compared to SMNΔ7 animals (Fig. 3B). Since the formation of PARGs begins during the perinatal period[27], probably before drug administration, we assume that the reduced number of PARGs found in nusinersen-treated SMNΔ7 αMNs is a remnant of the fetal or perinatal stage. We suggest that the nuclear retention of poly(A) RNA into PARGs can be a neuroprotective mechanism to prevent the nuclear export and translation of unprocessed or aberrant polyadenylated mRNAs.

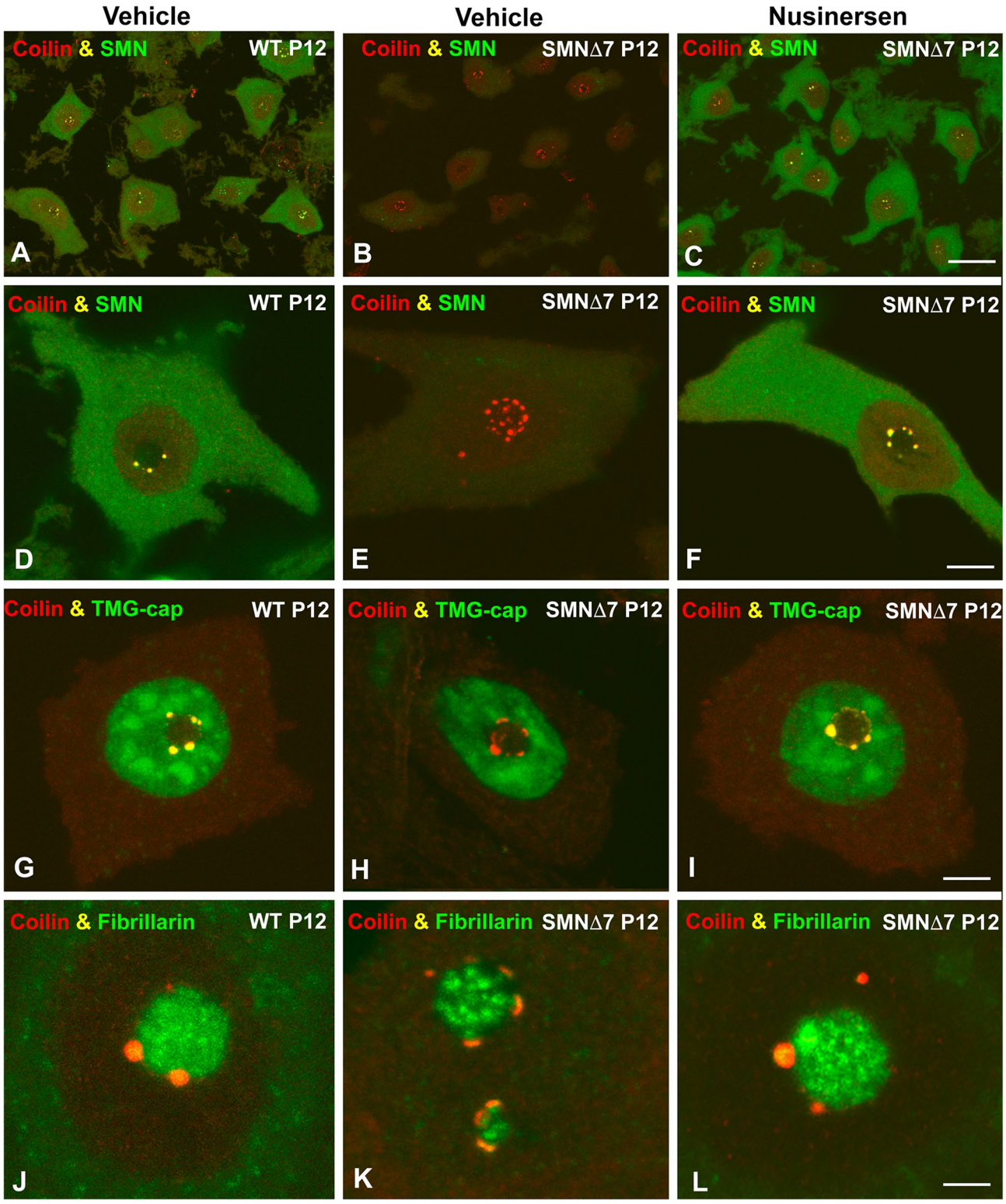

Figure 2. (**A**–**F**) Confocal images of dissociated αMNs from WT (**A**,**D**), SMNΔ7 (**B**,**E**) and nusinersen-treated SMNΔ7 mice (**C**,**F**) double immunolabeled for coilin (red) and SMN (green). Note that coilin and SMN colocalize in canonical CBs from WT and nusinersen-SMNΔ7 αMNs (**D**,**F**), whereas coilin-positive and SMN-negative perinucleolar caps are detected in αMNs from the vehicle-treated SMNΔ7 mouse. (**G**–**L**) Double immunolabeling for coilin and TMG-cap (**G**–**I**) or fibrillarin (**J**–**L**) in αMNs from WT, SMNΔ7 and nusinersen-treated SMNΔ7 mice. Coilin colocalizes with both TMG-cap and fibrillarin in canonical CBs from WT and nusinersen-treated SMNΔ7 αMNs (**G**,**I**,**J**,**L**). In contrast, the perinucleolar caps of SMNΔ7 αMNs are free from the splicing factor marker TMG-cap (**H**) and exhibit a weak fibrillarin signal (**K**). Scale bars: 20 µm (**A**–**C**), 5 µm (**D**–**I**) and 2.5 µm (**J**–**L**).

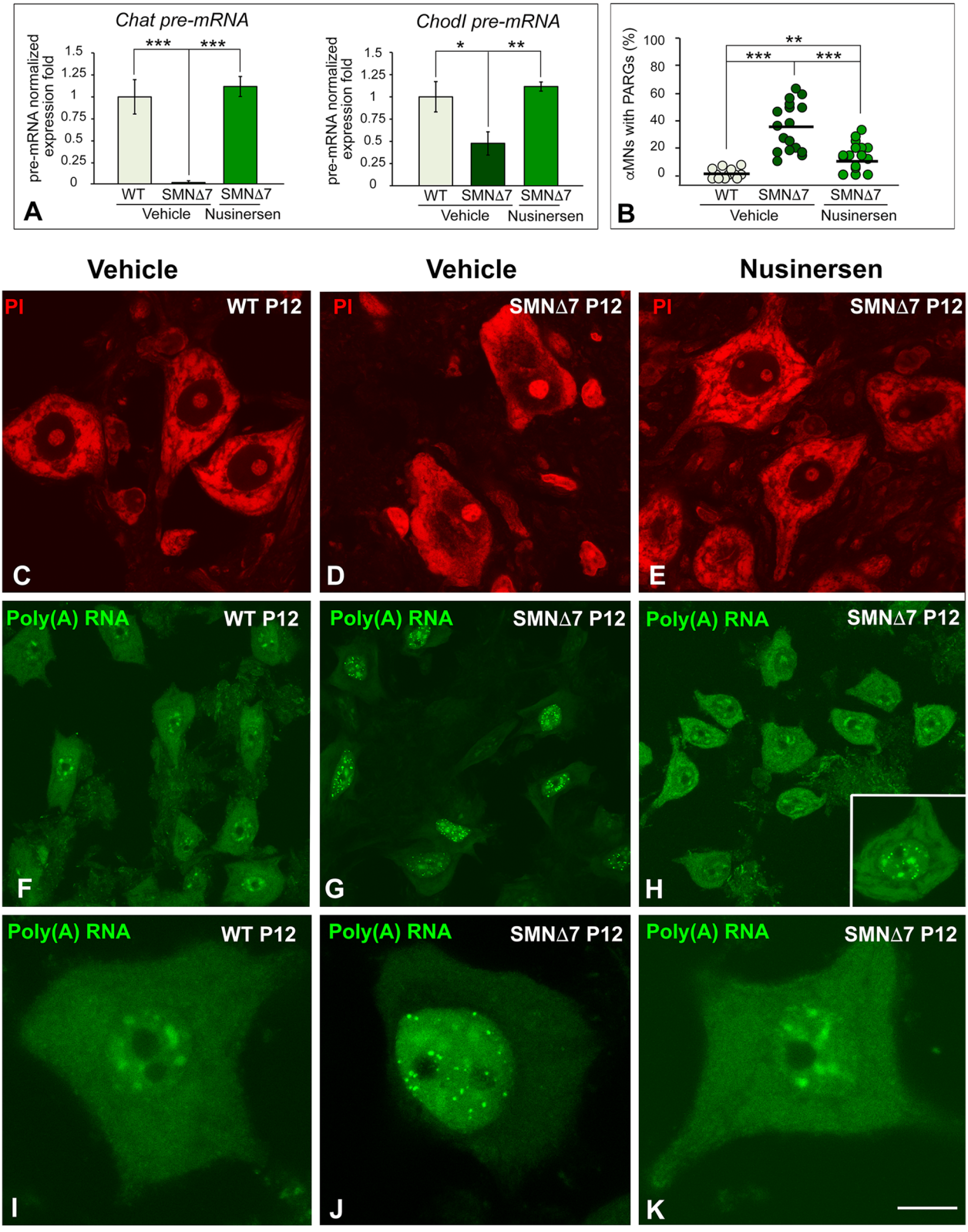

Figure 3. (**A**) RT-PCR analysis of the expression of *Chodl* and *ChAT* pre-mRNAs in whole spinal cord RNA extracts from WT, SMNΔ7 and nusinersen-treated SMNΔ7 mice at P12. Bars represent the mean ± SD, $^{*}p < 0.05$ and $^{***}p < 0.0005$ (n = 4 mice per group, Student's *t* test analysis was performed using GraphPad). (**B**) The mean percentages of αMNs with PARGs were 1.38% in WT mice and 35.73% in SMNΔ7 mice. Nusinersen treatment in SMNΔ7 mice significantly reduced the proportion of αMNs with PARGs to 12.04%. *p* values of WT vs. SMNΔ7 αMNs: 1.78×10^{-6} ($^{***}p < 0.0005$); SMNΔ7 vs. nusinersen-treated αMNs: 2.8×10^{-6} ($^{***}p < 0.0005$); and WT vs. nusinersen-treated SMNΔ7: 0.0046 ($^{**}p < 0.005$) (Student's *t* test analysis was performed using GraphPad). (**C**–**E**) Dissociated spinal cord αMNs from WT, SMNΔ7 and nusinersen-treated SMNΔ7 mice

at P12 stained with propidium iodide (PI) to demonstrate the RNA-rich nucleolus and protein synthesis machinery (Nissl substance). Note the rescue of prominent Nissl bodies in nusinersen-treated SMNΔ7 αMNs (**E**) and the central chromatolysis in untreated SMNΔ7 αMNs (**D**). (**F**–**H**) FISH for poly(A) RNAs in WT, SMNΔ7 and nusinersen-treated SMNΔ7 αMNs at P12. A similar pattern of poly(A) RNA hybridization signal was observed in WT and nusinersen-treated SMNΔ7 αMNs: diffuse in the nucleus, excluding the nucleolus, concentrated in nuclear speckles of splicing factors and diffuse in the cytoplasm (**F**,**H**,**I**,**K**). Note the abundance of nuclear poly(A) RNA-positive granules (PARGs) in numerous SMNΔ7 αMNs, which was accompanied by a substantial reduction of the hybridization signal in the cytoplasm (**G**,**J**). PARGs were occasionally found in nusinersen-treated SMNΔ7 αMNs (**H**, inset). Scale bars: 15 µm (**C**–**E**), 25 µm (**F**–**H**) and 5 µm (**I**–**K**).

Discussion

It is well established that αMNs are the main physiopathological cellular targets of SMA, although increasing evidence has revealed the primary importance of other peripheral tissues[41,57,58]. Degeneration of αMNs leads to severe muscular atrophy by denervation, muscle paralysis and premature death by respiratory failure in type I SMA, the most severe form of the disease.

In our previous studies in the SMNΔ7 mouse model of SMA, we observed that SMN depletion in αMNs during the symptomatic postnatal stage severely impacts nuclear compartments involved in pre-rRNA and pre-mRNA processing[26]. Moreover, polyadenylated mRNAs are aggregated in PARGs, reflecting an alteration of mRNA splicing with increased intron retention, abnormal accumulation of incorrectly processed mRNAs and inhibition of the nuclear export of mature mRNAs[27]. This neuronal dysfunction leads to a neurodegenerative process, which is characterized by reduced availability of mature mRNAs for translation, progressive disruption of the protein synthesis machinery and, ultimately, neuronal death[26,27,53].

In this study, we demonstrate that the therapeutic outcome of the ICV administration of nusinersen (Spinraza) in the SMNΔ7 mouse model of type I SMA is mediated by the selective restoration of SMN levels in the spinal cord but not in muscle. Nusinersen treatment in neonatal SMNΔ7 mice normalizes the growth curve and improves motor function at the late symptomatic stage (P12). These effects are mediated by preserving the normal population of αMNs, as well as the nuclear organization of mRNA processing compartments and the protein synthesis machinery. Consistent with these findings, previous studies in mouse SMA models have demonstrated that nusinersen, when administered directly into the CSF, prolongs animal survival and prevents αMN and skeletal muscle pathology[31,36,37]. However, a recent study using the systemic administration of ASO10-27 in SMA mice supports that peripheral tissues play an essential role in SMA pathology[41]. The authors indicate that the increase in SMN exclusively in peripheral tissues compensates for its deficiency in the spinal cord and preserves αMNs. In our study, the improvements in body weight, motor function and survival in SMNΔ7 mice treated with nusinersen were associated with a notable increase in SMN levels in the spinal cord but not in the TA muscle, which exhibited reduced SMN levels, similar to those detected in untreated SMNΔ7 mice. Although a fraction of nusinersen injected into cerebral ventricles may be cleared with CSF into the blood and influence peripheral tissues, our results and those from other authors[59] support that the increase in SMN in the spinal cord is required for the rescue of αMN and skeletal myofiber homeostasis. In fact, we observed that both the skeletal myofiber size distribution and the SDH oxidative staining pattern of myofibers are rescued, despite having reduced SMN levels in muscle. However, the relative importance of SMN restoration in spinal cord versus peripheral tissues in the therapeutic outcome reported in separate studies may be notably influenced by differences in transgenic mouse models of SMA and treatment protocols with ASO.

Consistent with the essential role of nusinersen in the splicing regulation of the *SMN2* gene, promoting the inclusion of exon 7 in the *SMN2* mRNAs and their translation in full-length SMN protein[30–32,34,60], we detected a recovery in the number and molecular composition of CBs. This neuroprotective mechanism, mediated by the increased expression of SMN in αMNs, can promote the molecular assembly of canonical CBs, which are enriched in coilin, SMN and spliceosomal snRNPs[15,16,43]. CBs are transcription-dependent nuclear organelles involved in spliceosomal snRNP biogenesis required for pre-mRNA splicing[15,16,61]. Depletion of CBs and coilin relocation in the form of perinucleolar caps or within the nucleolus are reliable early signs of neuronal dysfunction in many neurodegenerative disorders, including SMA[18,25,26,62]. It is noteworthy that snRNPs are essential components of the spliceosome, the macromolecular machine for pre-mRNA splicing[14], and their biogenesis is considerably more efficient in CBs than in the nucleoplasm[63]. In fact, depletion of CBs in cells derived from SMA patients correlates with reduced U4/U6-U5 tri-snRNP assembly, a key maturation step of spliceosomal snRNPs, and with splicing alterations[47,64]. A recent study reported an increase in the number of Gems (SMN-positive and coilin- and snRNP-negative nuclear bodies of unknown function[45,46]) in αMNs following the subcutaneous administration of ASO10-27 in a mouse model of SMA[41]. However, in our study, we have never observed Gems but canonical CBs induced by nusinersen treatment in SMA mice.

In nusinersen-treated SMNΔ7 mice, the transcription rate activation of *Chodl* and *ChAT*, two genes dysregulated in SMA that are essential for αMN survival[38,52], is consistent with the increase in CBs, whose numbers must be accommodated to the neuronal demand for pre-mRNA processing[44]. In this context, it was also noteworthy that nusinersen treatment in SMNΔ7 mice also rescued the normal organization of the protein synthesis machinery (Nissl bodies) and substantially recovered the nuclear and cytoplasmic compartmentalization of polyadenylated mRNAs. It is well established that all mRNAs, except for histone mRNAs, are polyadenylated in the nucleus, and the poly(A) tail is necessary for efficient mRNA export and translation[65]. The regulation of the nuclear and cytoplasmic compartmented transcriptomes is essential for cell homeostasis. Indeed, in this study and previously[27], we have demonstrated the nuclear accumulation of polyadenylated RNAs into PARGs, which is

associated with intron retention. Nuclear retention of polyadenylated mRNAs may prevent the nuclear export of unspliced or inappropriately expressed transcripts and attenuate translation and energy consumption to maintain energy homeostasis under stress conditions[27,66]. Moreover, nuclear retention of polyadenylated mRNAs may be linked to defective snRNP biogenesis in CBs. In this sense, a recent study[67] reported that the inhibition of U4 snRNP biogenesis, a key component for U4/U6-U5 tri-snRNP assembly in CBs[68], results in the abnormal nuclear accumulation of polyadenylated mRNAs. Importantly, the ICV administration of nusinersen in SMNΔ7 mice substantially reduced the formation of PARGs and restored the nuclear and cytoplasmic compartmentalization of polyadenylated mRNAs in αMNs. This neuronal response is consistent with a substantial recovery of CB number and pre-mRNA processing and export of mature polyadenylated mRNAs for their translation.

In conclusion, the nusinersen (Spinraza)-dependent rescue of the (i) molecular assembly of canonical CBs, (ii) expression of *Chodl* and *ChAT* primary transcripts, (iii) nuclear and cytoplasmic distribution of polyadenylated mRNAs, and (iv) organization of protein synthesis machinery in αMNs of the SMNΔ7 mouse appears to be essential for maintaining neuronal homeostasis and survival. The increase in SMN expression in the spinal cord partially prevents the severe SMA myopathy induced by αMN degeneration. We suggest that the incomplete recovery of neuromuscular performance in nusinersen-treated SMNΔ7 mice with moderate hindlimb paresis may result from reduced SMN expression in muscle. Further studies will be addressed to investigate the potential role of nusinersen treatment on skeletal myofibers, particularly on the focal disruption of the sarcomere architecture and actin dynamics observed in the SMNΔ7 mice (our unpublished results). In this vein, the combined use of subcutaneous and ICV administration of nusinersen may improve the therapeutic effects of this drug in SMA myopathy[41].

Materials and methods

Animals. *Smn*$^{+/-}$;*SMN2*$^{+/+}$;*SMNΔ7*$^{+/+}$, heterozygous knockouts for mouse *Smn* (FVB. Cg-Tg[SMN2*delta7]4299Ahmb Tg[SMN2]89Ahmb Smn1tm1Msd/J, stock number 005025), which were purchased from the Jackson Laboratory (Sacramento, USA), were crossed to generate *Smn*$^{-/-}$;*SMN2*$^{+/+}$;*SMNΔ7*$^{+/+}$ (SMNΔ7) mice and *Smn*$^{+/+}$;*SMN2*$^{+/+}$;*SMNΔ7*$^{+/+}$ mice that were wild-type for *Smn* (WT). SMNΔ7 mice exhibit a severe postnatal SMA phenotype with a mean lifespan of approximately 2 weeks[69,70]. Animal care and handling were performed in accordance with the Spanish legislation (Spanish Royal Decree 53/2013 BOE) and the guidelines of the European Commission for the Accommodation and Care of Laboratory Animals (revised in Appendix A of the Council Directive 2010/63/UE). The experimental plan was approved by the Ethics Committee of the University of Cantabria and the Committee for Animal Care and Use of the University of Lleida. On P0, the identification of WT and SMNΔ7 mice performed by genotyping with PCR. DNA was extracted from the tail, as previously described[69]. Age-matched WT littermates of mutant animals were used as controls.

To investigate the effects of nusinersen (Spinraza) treatment in the αMNs of SMNΔ7 mice, we used 32 animals (16 WT mice and 16 SMNΔ7 mice) that were divided into four groups. WT and SMNΔ7 mice were treated with 10 µl of Spinraza (Biogen) at a dose of 6.5 mg/kg (nusinersen group), or with 10 µl of a 0.9% saline solution (vehicle group). Spinraza or the vehicle was injected at the day of birth (P0) via ICV at the precise point indicated in Fig. 1A using a 10-µl syringe and a custom 33-gauge needle (Hamilton), as described previously[41]. All mice were sacrificed at the late symptomatic neurodegenerative stage (P12)[26,27].

Motor righting reflex test. To analyze the effect of nusinersen treatment on motor functions, we used the surface righting test (righting reflex), according to the protocol of Feather-Schussler and Ferguson[39]. Briefly, this test assesses the motor capacity such that a mouse pup can stand up from a supine position. The average age for the rodent straightening reflex to appear is P5. As this test is a reflex, there is no learning component, and it can be repeated throughout the period of experimentation. This test consists of placing the pups face up on a cotton sheet or bench pad and keeping them in this position for 5 s. The pups are then released, and the time it takes to return to the prone position is recorded, as well as the direction of the correction (left or right). A total of 1 min is given for each test, if necessary. The test is repeated for a total of three trials.

Succinate dehydrogenase (SDH) assay. To investigate the effect of the ICV administration of nusinersen on the phenotype type of TA muscle myofibers in the SMNΔ7 mouse, we used the histochemical SDH assay, a specific mitochondrial marker of myofiber oxidative activity. Thus, most SDH-positive myofibers correspond to small type 1 myofibers, which have slow contraction and high aerobic metabolism. Less SDH-positive myofibers of type 2X of greater caliber are associated with faster contraction and more anaerobic muscle. Finally, type 2A myofibers have an intermediate signal and activity between type 1 and 2X myofibers[71]. Briefly, transverse cryosections were incubated in an SDH reaction mixture (1.5 mM nitroblue tetrazolium, 5 mM EDTA, 48 mM succinic acid, 0.75 mM sodium azide, 30 mM methyl-phenylmethyl sulfate, and phosphate buffered pH 7). During the electron transfer from succinic acid to nitroblue tetrazolium by SDH, a color change occurs, the rate of which represents SDH activity. As controls, we used cryosections incubated in a medium lacking succinic acid. Then, the samples were air-dried and mounted, and images were captured with a microscope (Zeiss, Axioscop Plus) using 40× or 63× oil objectives. The morphometric analysis of myofiber diameter was performed on transversal cryosections of the TA muscle stained with the histochemical SDH assay. The measurement of the diameter of each myofiber in the field was performed on randomly collected microscope images using a 40× objective and ImageJ software (National Institutes of Health). At least 100 myofibers per animal (n = 3, WT; n = 3, SMNΔ7; and n = 3, nusinersen-treated SMNΔ7 mice) were measured.

Immunofluorescence and confocal microscopy. For immunofluorescence analysis of αMNs at P12, 4 mice per group (WT, SMNΔ7 and nusinersen-treated SMNΔ7 mice) were fixed by perfusion with 3.7% para-

formaldehyde (freshly prepared) in phosphate-buffered saline (PBS) under deep anesthesia with pentobarbital (50 mg/kg). The spinal cords were rapidly dissected, removed, postfixed for 6 h and washed in PBS. Transverse sections (160-µm thick) of the spinal cord were obtained with a vibratome, and small tissue fragments from the anterior horn were dissected out. The samples were transferred to a drop of PBS on a positively charged slide (Superfrost Plus, Thermo Scientific, Germany), and squash preparations of dissociated MNs were generated following the previously reported procedure[43].

For muscle, tissue fragments of the TA were pinned to cork, immersed in ice-cold relaxing buffer (100 mM NaCl, 2 mM KCl, 2 mM $MgCl_2$, 6 mM K_3PO_4, 1 mM EGTA, and 0.1% glucose; pH 7.0) and relaxed at 4 °C until fixed in 3.7% paraformaldehyde[72]. Muscle fragments were cryoprotected in 15% and 30% sucrose in PBS (phosphate saline buffer: 137 mM NaCl, 2.7 mM KCl, 8 mM Na_2HPO_4, and 2 mM KH_2PO_4; pH 7.4) until they sank, embedded in Tissue-Tek OCT Compound (Sakura FineTek USA), and frozen on a chilled metal block in dry ice. Cryosections measuring 8 µm in thickness were mounted on SuperFrost slides and stored at − 80 °C until use.

For immunofluorescence, all samples were processed as described in Pena et al.[43]. Briefly, samples were treated with 0.5% Triton X-100 for 45 min and incubated for 3 h with the primary antibody containing at room temperature. Specific secondary antibody conjugated with FITC, Texas Red or Cy3, or Cy5 (diluted 1:75, Jackson, USA) were used. Some samples were counterstained with propidium iodide (PI) or Phalloidin-FITC. The slides were mounted with ProLong Anti-Fading Medium (Invitrogen).

We used an LSM510 (Zeiss, Germany) laser scanning microscope using a 63 × oil (1.4 NA) objective. To avoid overlapping signals, images were obtained by sequential excitation at 488 nm and 543 nm. The fluorescence profiles of confocal intensity signals across a line shown in Fig. S2 were generated using confocal images of double immunolabeled samples. Images were processed using Adobe Photoshop CS6 software.

The following primary antibodies were used for immunofluorescence: mouse monoclonal anti-SMN (diluted 1:100, catalog no. 610646, BD Transduction Laboratories, USA); mouse monoclonal anti-TMG-cap (NA02A, Oncogene, USA); mouse monoclonal anti-fibrillarin (diluted 1:100, catalog no. ab4566, Abcam, USA); rabbit polyclonal anti-coilin (1:500, 204.10, Prof. A. Lamond, Dundee, UK); and goat polyclonal anti-choline acetyltransferase (ChAT) (1:200, AB144P, Millipore, MA, USA).

In situ hybridization and quantification. Fluorescence in situ hybridization (FISH) was performed according to the protocol described by Narcís et al.[27]. Preparations of MNs were permeabilized with TBS-E-SDS for 15 min at 37 °C, washed three times in 6 × SSPE-0.1% Tween 20 for 15 min, and incubated with the probe containing tRNA for 3 h at 42 °C in a humidified chamber. An oligo$(dT)_{(50)}$-mer, 5′-end-labeled with biotin (MWG-Biotech, Germany), was used as a probe for fluorescence in situ hybridization (FISH) to poly(A) RNA. The hybridization mixture contained 80 ng of oligo dT(50), 2 × SSC, 1 mg/ml tRNA, 10% dextran sulfate and 25% formamide. After hybridization, preparations of MNs were washed in 6 × SSC for 15 min and then washed in 4 × SSC-0.1% Tween 20 for 15 min at room temperature. The hybridization signal was detected with FITC-avidin for 30 min. All samples were mounted with Vectashield (Vector, USA).

The quantitative analysis of the proportion of SMNΔ7 αMNs containing PARGs was performed in squash preparations processed for FISH with the poly(dT) probe. The proportion of neurons containing these granules was estimated by direct examination of the different focal planes throughout neuronal nuclei using a 40 × objective. Quantification was performed on at least 100 αMNs from WT (n = 4), SMNΔ7 (n = 4) and nusinersen-treated SMNΔ7 (n = 4) mice.

qRT-PCR for relative gene expression analysis. For qRT-PCR, we used WT (n = 4), SMNΔ7 (n = 4) and nusinersen-treated SMNΔ7 (n = 4) mice. Mice were decapitated after being anesthetized, and the lumbar spinal cord was quickly removed and frozen in liquid nitrogen. RNA was isolated with TRIzol following the manufacturer's instructions (Invitrogen, Carlsbad) and purified with the RNeasy kit (Qiagen, Hilden, Germany).

According to our laboratory protocols[27], 1 µg of RNA was reverse-transcribed to first-strand cDNA utilizing a High Capacity cDNA Reverse Transcription Kit (Life Technologies) using random hexamers as primers. The expression of the mRNA candidates *ChAT* and *Chodl* was determined by qRT-PCR using gene-specific SYBR Green-based primers (Invitrogen). The threshold cycle (Ct) for each well was determined and the results were normalized to *Gapdh* mRNA. Relative gene expression was calculated according to the 2-(ΔΔCt) equation[73]. Each value in this work represents the mean ± SD of independent samples obtained under the same conditions and compared to two replicated qRT-PCR analyses. The SYBR Green-based specific primers for murine pre-RNAs analyzed were as follows: for the pre-mRNA of *ChAT* 5′-CTTGGGGCCAGTCTGATAGC-3′ and 5′-GGACAC ATGGCTAGAAGGGG-3′ and for the pre-mRNA of *Chodl* 5′-GCTGTTGTCTCCCGCATCTT-3′ and 5′-AAG TGGAAGCGTTTGGGATT-3′.

SDS-PAGE and immunoblotting. Analysis of the level of SMN protein were performed according to the protocol described by Narcís et al. [27]. Briefly, spinal cords and skeletal TA muscle samples from WT (n = 3), SMNΔ7 (n = 3) and nusinersen-treated SMNΔ7 (n = 4) mice were lysed at 4 °C in a buffer containing 50 mM Tris (pH 8), 150 mM NaCl, 2% Nonidet NP-40, 1 mM $MgCl_2$, 1 mM dithiothreitol, and 10% glycerol and supplemented with EDTA-free complete protease inhibitor cocktail and PhosphoSTOP (Roche). Samples were sonicated and cleared by centrifugation at 14,000 rpm for 10 min at 4 °C. The proteins were separated on 4–20% NuPage TG SDS–PAGE gels (Invitrogen) and transferred to nitrocellulose membranes using standard procedures. Mouse monoclonal anti-SMN (diluted 1:500) and rabbit polyclonal anti-Lamin A/C (diluted 1:1,000, generously donated by Prof. Gerace) were used. Protein bands were detected with an Odyssey Infrared-Imaging System (Li-Cor Biosciences) according to the Odyssey Western-Blotting Protocol. For the quantitative analysis

of the blots, ImageJ software was used (U.S. National Institutes of Health, Bethesda, Maryland, USA, https://imagej.nih.gov/ij).

Statistical analysis. For comparisons among the experimental groups, data were analyzed using GraphPad Prism 7 software and PASW Statistics 22 (SPSS, Inc.) packages. Data are expressed as mean ± SD. The statistical analysis was assessed by one-way ANOVA or mixed-design two-way ANOVA (Split-Plot ANOVA), followed by the Bonferroni post hoc test (SPSS) or Student's *t* test (GraphPad). In all cases, differences were considered to be statistically significant if $p < 0.05$.

Received: 27 February 2020; Accepted: 8 June 2020
Published online: 01 July 2020

References

1. Lefebvre, S. *et al.* Identification and characterization of a spinal muscular atrophy-determining gene. *Cell* **80**, 155–165 (1995).
2. Lefebvre, S. *et al.* Correlation between severity and SMN protein level in spinal muscular atrophy. *Nat. Genet.* **16**, 265–269. https://doi.org/10.1038/ng0797-265 (1997).
3. Burghes, A. H. M. & Beattie, C. E. Spinal muscular atrophy: why do low levels of survival motor neuron protein make motor neurons sick?. *Nat. Rev. Neurosci.* **10**, 597–609. https://doi.org/10.1038/nrn2670 (2009).
4. Monani, U. R. *et al.* A single nucleotide difference that alters splicing patterns distinguishes the SMA gene SMN1 from the copy gene SMN2. *Hum. Mol. Genet.* **8**, 1177–1183. https://doi.org/10.1093/hmg/8.7.1177 (1999).
5. Monani, U. R. *et al.* The human centromeric survival motor neuron gene (SMN2) rescues embryonic lethality in Smn(−/−) mice and results in a mouse with spinal muscular atrophy. *Hum. Mol. Genet.* **9**, 333–339 (2000).
6. Lorson, C. L. *et al.* SMN oligomerization defect correlates with spinal muscular atrophy severity. *Nat. Genet.* **19**, 63–66. https://doi.org/10.1038/ng0598-63 (1998).
7. Cho, S. & Dreyfuss, G. A degron created by SMN2 exon 7 skipping is a principal contributor to spinal muscular atrophy severity. *Genes Dev.* **24**, 438–442. https://doi.org/10.1101/gad.1884910 (2010).
8. Feldkötter, M. *et al.* Quantitative analyses of SMN1 and SMN2 based on real-time lightCycler PCR: fast and highly reliable carrier testing and prediction of severity of spinal muscular atrophy. *Am. J. Hum. Genet.* **70**, 358–368. https://doi.org/10.1086/338627 (2002).
9. Cuscó, I. *et al.* SMN2 copy number predicts acute or chronic spinal muscular atrophy but does not account for intrafamilial variability in siblings. *J. Neurol.* **253**, 21–25. https://doi.org/10.1007/s00415-005-0912-y (2006).
10. Wirth, B. *et al.* Quantitative analysis of survival motor neuron copies: identification of subtle SMN1 mutations in patients with spinal muscular atrophy, genotype-phenotype correlation, and implications for genetic counseling. *Am. J. Hum. Genet.* **64**, 1340–1356. https://doi.org/10.1086/302369 (1999).
11. Wirth, B. *et al.* Mildly affected patients with spinal muscular atrophy are partially protected by an increased SMN2 copy number. *Hum. Genet.* **119**, 422–428. https://doi.org/10.1007/s00439-006-0156-7 (2006).
12. Pellizzoni, L., Yong, J. & Dreyfuss, G. Essential role for the SMN complex in the specificity of snRNP assembly. *Science* **298**, 1775–1779. https://doi.org/10.1126/science.1074962 (2002).
13. Meister, G. *et al.* A multiprotein complex mediates the ATP-dependent assembly of spliceosomal U snRNPs. *Nat. Cell Biol.* **3**, 945–949. https://doi.org/10.1038/ncb1101-945 (2001).
14. Matera, A. G. & Wang, Z. A day in the life of the spliceosome. *Nat. Rev. Mol. Cell Biol.* **15**, 108–121. https://doi.org/10.1038/nrm3742 (2014).
15. Gall, J. G. Cajal bodies: the first 100 years. *Annu. Rev. Cell Dev. Biol.* **16**, 273–300. https://doi.org/10.1146/annurev.cellbio.16.1.273 (2000).
16. Machyna, M., Heyn, P. & Neugebauer, K. M. Cajal bodies: where form meets function. *Wiley Interdiscip. Rev. RNA* **4**, 17–34. https://doi.org/10.1002/wrna.1139 (2013).
17. Sawyer, I. A., Hager, G. L. & Dundr, M. Specific genomic cues regulate Cajal body assembly. *RNA Biol.* https://doi.org/10.1080/15476286.2016.1243648 (2016).
18. Lafarga, M., Casafont, I., Bengoechea, R., Tapia, O. & Berciano, M. T. Cajal's contribution to the knowledge of the neuronal cell nucleus. *Chromosoma* **118**, 437–443 (2009).
19. Frey, M. R. & Matera, A. G. RNA-mediated interaction of Cajal bodies and U2 snRNA genes. *J. Cell Biol.* **154**, 499–509. https://doi.org/10.1083/jcb.200105084 (2001).
20. Schul, W., van Driel, R. & de Jong, L. Coiled bodies and U2 snRNA genes adjacent to coiled bodies are enriched in factors required for snRNA transcription. *Mol. Biol. Cell* **9**, 1025–1036. https://doi.org/10.1091/mbc.9.5.1025 (1998).
21. Wang, Q. *et al.* Cajal bodies are linked to genome conformation. *Nat. Commun.* **7**, 10966. https://doi.org/10.1038/ncomms10966 (2016).
22. Raska, I. *et al.* Association between the nucleolus and the coiled body. *J. Struct. Biol.* **104**, 120–127 (1990).
23. Machyna, M. *et al.* The coilin interactome identifies hundreds of small noncoding RNAs that traffic through Cajal bodies. *Mol. Cell* **56**, 389–399. https://doi.org/10.1016/j.molcel.2014.10.004 (2014).
24. Trinkle-Mulcahy, L. & Sleeman, J. E. The Cajal body and the nucleolus: "In a relationship" or "It's complicated"?. *RNA Biol.* https://doi.org/10.1080/15476286.2016.1236169 (2016).
25. Tapia, O. *et al.* Reorganization of Cajal bodies and nucleolar targeting of coilin in motor neurons of type I spinal muscular atrophy. *Histochem. Cell Biol.* **137**, 657–667. https://doi.org/10.1007/s00418-012-0921-8 (2012).
26. Tapia, O. *et al.* Cellular bases of the RNA metabolism dysfunction in motor neurons of a murine model of spinal muscular atrophy: Role of Cajal bodies and the nucleolus. *Neurobiol. Dis.* **108**, 83–99. https://doi.org/10.1016/j.nbd.2017.08.004 (2017).
27. Narcís, J. O. *et al.* Accumulation of poly(A) RNA in nuclear granules enriched in Sam68 in motor neurons from the SMNΔ7 mouse model of SMA. *Sci. Rep.* **8**, 9646. https://doi.org/10.1038/s41598-018-27821-3 (2018).
28. Caillet-Boudin, M.-L. *et al.* Brain pathology in myotonic dystrophy: when tauopathy meets spliceopathy and RNAopathy. *Front. Mol. Neurosci.* **6**, 57. https://doi.org/10.3389/fnmol.2013.00057 (2014).
29. Singh, N. K., Singh, N. N., Androphy, E. J. & Singh, R. N. Splicing of a critical exon of human survival motor neuron is regulated by a unique silencer element located in the last intron. *Mol. Cell Biol.* **26**, 1333–1346. https://doi.org/10.1128/MCB.26.4.1333-1346.2006 (2006).
30. Hua, Y. *et al.* Antisense masking of an hnRNP A1/A2 intronic splicing silencer corrects SMN2 splicing in transgenic mice. *Am. J. Hum. Genet.* **82**, 834–848. https://doi.org/10.1016/j.ajhg.2008.01.014 (2008).
31. Hua, Y. *et al.* Antisense correction of SMN2 splicing in the CNS rescues necrosis in a type III SMA mouse model. *Genes Dev.* **24**, 1634–1644. https://doi.org/10.1101/gad.1941310 (2010).

32. Rigo, F. *et al.* Pharmacology of a central nervous system delivered 2′-*O*-methoxyethyl-modified survival of motor neuron splicing oligonucleotide in mice and nonhuman primates. *J. Pharmacol. Exp. Ther.* **350**, 46–55. https://doi.org/10.1124/jpet.113.212407 (2014).
33. Talbot, K. & Tizzano, E. F. The clinical landscape for SMA in a new therapeutic era. *Gene Ther.* https://doi.org/10.1038/gt.2017.52 (2017).
34. Bennett, C. F., Krainer, A. R. & Cleveland, D. W. Antisense oligonucleotide therapies for neurodegenerative diseases. *Annu. Rev. Neurosci.* **42**, 385–406. https://doi.org/10.1146/annurev-neuro-070918-050501 (2019).
35. Wood-Allum, C. & Shaw, P. J. Motor neurone disease: a practical update on diagnosis and management. *Clin. Med.* **10**, 252–258 (2010).
36. Passini, M. A. *et al.* Antisense oligonucleotides delivered to the mouse CNS ameliorate symptoms of severe spinal muscular atrophy. *Sci. Transl. Med.* **3**, 72ra18. https://doi.org/10.1126/scitranslmed.3001777 (2011).
37. Sahashi, K. *et al.* TSUNAMI: an antisense method to phenocopy splicing-associated diseases in animals. *Genes Dev.* **26**, 1874–1884. https://doi.org/10.1101/gad.197418.112 (2012).
38. Sleigh, J. N. *et al.* Chondrolectin affects cell survival and neuronal outgrowth in in vitro and in vivo models of spinal muscular atrophy. *Hum. Mol. Genet.* **23**, 855–869. https://doi.org/10.1093/hmg/ddt477 (2014).
39. Feather-Schussler, D. N. & Ferguson, T. S. A battery of motor tests in a neonatal mouse model of cerebral palsy. *J. Vis. Exp.* https://doi.org/10.3791/53569 (2016).
40. Dubowitz, V. & Sewry, C. *Muscle Biopsy: A Practical Approach* (Elsevier, Philadelphia, 2007).
41. Hua, Y. *et al.* Motor neuron cell-nonautonomous rescue of spinal muscular atrophy phenotypes in mild and severe transgenic mouse models. *Genes Dev.* **29**, 288–297. https://doi.org/10.1101/gad.256644.114 (2015).
42. Jablonka, S. *et al.* Reduced survival motor neuron (Smn) gene dose in mice leads to motor neuron degeneration: an animal model for spinal muscular atrophy type III. *Hum. Mol. Genet.* **9**, 341–346. https://doi.org/10.1093/hmg/9.3.341 (2000).
43. Pena, E. *et al.* Neuronal body size correlates with the number of nucleoli and Cajal bodies, and with the organization of the splicing machinery in rat trigeminal ganglion neurons. *J. Comp. Neurol.* **430**, 250–263 (2001).
44. Lafarga, M., Tapia, O., Romero, A. M. & Berciano, M. T. Cajal bodies in neurons. *RNA Biol.* https://doi.org/10.1080/15476286.2016.1231360 (2017).
45. Liu, Q. & Dreyfuss, G. A novel nuclear structure containing the survival of motor neurons protein. *EMBO J.* **15**, 3555–3565 (1996).
46. Navascues, J. *et al.* Targeting SMN to Cajal bodies and nuclear gems during neuritogenesis. *Chromosoma* **112**, 398–409. https://doi.org/10.1007/s00412-004-0285-5 (2004).
47. Zhang, Z. *et al.* SMN deficiency causes tissue-specific perturbations in the repertoire of snRNAs and widespread defects in splicing. *Cell* **133**, 585–600. https://doi.org/10.1016/j.cell.2008.03.031 (2008).
48. Bäumer, D. *et al.* Alternative splicing events are a late feature of pathology in a mouse model of spinal muscular atrophy. *PLoS Genet.* **5**, e1000773. https://doi.org/10.1371/journal.pgen.1000773 (2009).
49. Lotti, F. *et al.* An SMN-dependent U12 splicing event essential for motor circuit function. *Cell* **151**, 440–454. https://doi.org/10.1016/j.cell.2012.09.012 (2012).
50. Doktor, T. K. *et al.* RNA-sequencing of a mouse-model of spinal muscular atrophy reveals tissue-wide changes in splicing of U12-dependent introns. *Nucleic Acids Res.* **45**, 395–416. https://doi.org/10.1093/nar/gkw731 (2017).
51. Jangi, M. *et al.* SMN deficiency in severe models of spinal muscular atrophy causes widespread intron retention and DNA damage. *Proc. Natl. Acad. Sci.* **114**, E2347–E2356. https://doi.org/10.1073/pnas.1613181114 (2017).
52. Zhong, Z. *et al.* Chondrolectin mediates growth cone interactions of motor axons with an intermediate target. *J. Neurosci.* **32**, 4426–4439. https://doi.org/10.1523/JNEUROSCI.5179-11.2012 (2012).
53. Bernabò, P. *et al.* In vivo translatome profiling in spinal muscular atrophy reveals a role for SMN protein in ribosome biology. *Cell Rep.* **21**, 953–965. https://doi.org/10.1016/j.celrep.2017.10.010 (2017).
54. Peters, A., Palay, S. L. & deF Webster, H. *The Fine Structure of the Nervous System: Neurons and Their Supporting Cells* 3rd edn. (Oxford University Press, New York, 1991).
55. Casafont, I., Berciano, M. T. & Lafarga, M. Bortezomib induces the formation of nuclear poly(A) RNA granules enriched in Sam68 and PABPN1 in sensory ganglia neurons. *Neurotox. Res.* **17**, 167–178 (2010).
56. Palanca, A., Casafont, I., Berciano, M. T. & Lafarga, M. Proteasome inhibition induces DNA damage and reorganizes nuclear architecture and protein synthesis machinery in sensory ganglion neurons. *Cell Mol. Life Sci.* **71**, 1961–1975. https://doi.org/10.1007/s00018-013-1474-2 (2014).
57. Hamilton, G. & Gillingwater, T. H. Spinal muscular atrophy: going beyond the motor neuron. *Trends Mol. Med.* **19**, 40–50. https://doi.org/10.1016/j.molmed.2012.11.002 (2013).
58. Chaytow, H., Huang, Y. T., Gillingwater, T. H. & Faller, K. M. E. The role of survival motor neuron protein (SMN) in protein homeostasis. *Cell Mol. Life Sci.* https://doi.org/10.1007/s00018-018-2849-1 (2018).
59. Porensky, P. N. *et al.* A single administration of morpholino antisense oligomer rescues spinal muscular atrophy in mouse. *Hum. Mol. Genet.* **21**, 1625–1638. https://doi.org/10.1093/hmg/ddr600 (2012).
60. Kole, R., Krainer, A. R. & Altman, S. RNA therapeutics: beyond RNA interference and antisense oligonucleotides. *Nat. Rev. Drug Discov.* **11**, 125–140. https://doi.org/10.1038/nrd3625 (2012).
61. Lafarga, M., Andres, M. A., Berciano, M. T. & Maquiera, E. Organization of nucleoli and nuclear bodies in osmotically stimulated supraoptic neurons of the rat. *J. Comp. Neurol.* **308**, 329–339. https://doi.org/10.1002/cne.903080302 (1991).
62. Baltanás, F. C. *et al.* Purkinje cell degeneration in pcd mice reveals large scale chromatin reorganization and gene silencing linked to defective DNA repair. *J. Biol. Chem.* **286**, 28287–28302. https://doi.org/10.1074/jbc.M111.246041 (2011).
63. Klingauf, M., Stanek, D. & Neugebauer, K. M. Enhancement of U4/U6 small nuclear ribonucleoprotein particle association in Cajal bodies predicted by mathematical modeling. *Mol. Biol. Cell* **17**, 4972–4981. https://doi.org/10.1091/mbc.E06-06-0513 (2006).
64. Novotný, I. *et al.* In vivo kinetics of U4/U6·U5 tri-snRNP formation in Cajal bodies. *Mol. Biol. Cell* **22**, 513–523. https://doi.org/10.1091/mbc.E10-07-0560 (2011).
65. Kühn, U. & Wahle, E. Structure and function of poly(A) binding proteins. *Biochim. Biophys. Acta* **1678**, 67–84. https://doi.org/10.1016/j.bbaexp.2004.03.008 (2004).
66. Shan, P. *et al.* SIRT1 functions as a negative regulator of eukaryotic poly(A)RNA transport. *Curr. Biol.* **27**, 2271-2284.e5. https://doi.org/10.1016/j.cub.2017.06.040 (2017).
67. Hett, A. & West, S. Inhibition of U4 snRNA in human cells causes the stable retention of polyadenylated pre-mRNA in the nucleus. *PLoS ONE* **9**, e96174. https://doi.org/10.1371/journal.pone.0096174 (2014).
68. Novotný, I. *et al.* SART3-dependent accumulation of incomplete spliceosomal snRNPs in Cajal bodies. *Cell Rep.* https://doi.org/10.1016/j.celrep.2014.12.030 (2015).
69. Tarabal, O. *et al.* Mechanisms involved in spinal cord central synapse loss in a mouse model of spinal muscular atrophy. *J. Neuropathol. Exp. Neurol.* **73**, 519–535. https://doi.org/10.1097/NEN.0000000000000074 (2014).
70. Le, T. T. *et al.* SMNDelta7, the major product of the centromeric survival motor neuron (SMN2) gene, extends survival in mice with spinal muscular atrophy and associates with full-length SMN. *Hum. Mol. Genet.* **14**, 845–857. https://doi.org/10.1093/hmg/ddi078 (2005).
71. Talbot, J. & Maves, L. Skeletal muscle fiber type: using insights from muscle developmental biology to dissect targets for susceptibility and resistance to muscle disease. *Wiley Interdiscip. Rev. Dev. Biol.* **5**, 518–534. https://doi.org/10.1002/wdev.230 (2016).

72. Gokhin, D. S. *et al.* Tropomodulin isoforms regulate thin filament pointed-end capping and skeletal muscle physiology. *J. Cell Biol.* **189**, 95–109. https://doi.org/10.1083/jcb.201001125 (2010).
73. Livak, K. J. & Schmittgen, T. D. Analysis of relative gene expression data using real-time quantitative PCR and the 2−ΔΔCT method. *Methods* **25**, 402–408. https://doi.org/10.1006/meth.2001.1262 (2001).

Acknowledgements

The authors wish to thank Raquel García-Ceballos for technical assistance and Alfonso Nieva for video editing. We are also grateful to Prof. A. I. Lamond (University of Dundee, UK) for anti-coilin antibody (204.10) and Prof. Larry Gerace (The Scripps Research Institute, La Jolla, USA) for anti-LaminA/C antibody. The authors are also indebted to Prof. Josep E. Esquerda for critical reading of the manuscript and helpful suggestions. This work was supported by the following grants: *Centro de Investigación Biomédica en Red sobre Enfermedades Neurodegenerativas* (CIBERNED, CB06/05/0037) Spain; *Instituto de Investigación Sanitaria Valdecilla* (IDIVAL, Next-Val 17/22), Santander, Spain; and Spanish *Ministerio de Ciencia, Innovación y Universidades* cofinanced by *Fondo Europeo de Desarrollo Regional* (FEDER) (RTI2018-099278-B-I00).

Author contributions

O.T., M.L., M.T.B. and J.C. conceived and designed the experiments. M.T.B., A.P.B., A.M.S., O.T., M.L., and J.C. performed the experiments and analyzed the data. O.T., M.L., M.T.B. and J.C.R.R. wrote the paper.

Competing interests

The authors declare no competing interests.

Additional information

Supplementary information is available for this paper at https://doi.org/10.1038/s41598-020-67569-3.

Correspondence and requests for materials should be addressed to O.T.

Reprints and permissions information is available at www.nature.com/reprints.

Publisher's note Springer Nature remains neutral with regard to jurisdictional claims in published maps and institutional affiliations.